

Abstract

Enhanced Loading of a Lithium 7 Magneto Optical Trap using Transverse Cooling and Frequency Spread Light

Fabio Mibielli Peixoto

2002

Using a frequency spread light and a zigzag beam configuration we have transversely cooled and compressed an atomic beam of ^7Li in two dimensions (2D). The loading rate of the Magneto-Optical Trap (MOT) increased by a factor of 10 capturing 2×10^9 atoms. We have studied the loading rate dependence on the 2D beam intensity and on the number of reflections. A phenomenological model that explains our results is proposed.

Evaporative cooling of ^7Li was observed in a Quadrupole and in a Time Orbiting Potential trap (TOP). The phase-space density (PSD) of the cloud in the Quadrupole increased by a factor of 10. In the TOP we observed evaporation through the “circle of death”. Some limitations for evaporative cooling of ^7Li in the TOP were discovered. They are related to the impossibility of laser cooling the atoms inside the trap.

Enhanced Loading of a Lithium 7 Magneto Optical Trap using
Transverse Cooling and Frequency Spread Light

A Dissertation
Presented to the Faculty of the Graduate School
of
Yale University
in Candidacy for the Degree of
Doctor of Philosophy

by
Fabio Mibielli Peixoto

Dissertation Director: Prof. Mark Kasevich

December, 2002

© 2003 by Fabio Mibielli Peixoto.

All rights reserved.

For my parents,
Sérgio “Cachorrão” and Márcia Regina.

Contents

List of Figures	4
List of Tables	7
Acknowledgements	8
1 Introduction	9
1.1 Format of this Thesis	11
2 Atom Cooling and Trapping	12
2.1 History	12
2.2 Laser Cooling	14
2.2.1 Doppler Cooling	16
2.2.2 Sub-Doppler Cooling	19
2.3 Trapping Neutral Atoms	22
2.3.1 Quadrupole trap	22
2.3.2 Magneto Optical Trap (MOT)	25
2.3.3 Time Orbiting Potential (TOP)	28
2.3.4 Ioffe-Pritchard trap	31
2.3.5 Optical Dipole Trap	32
2.4 Evaporative Cooling	34
2.4.1 Cold Collisions	35
2.4.2 Elastic Collision Rate	36
2.4.3 Adiabatic Compression	37

2.4.4	Forced Evaporation	39
3	MOT Loading Techniques	41
3.1	Frequency Chirping	43
3.2	Zeeman Slower	43
3.3	Vapor Cell	45
3.4	Frequency Spread Light	46
4	Cooling and Trapping ^7Li	48
4.1	Laser Spectrum	48
4.2	MOT configuration	50
4.3	Optical Molasses Cooling	55
4.4	Number of Atoms and Temperature Measurement	56
4.5	Transfer to a Magnetic Trap	60
4.5.1	Optical Pumping	61
4.5.2	Trapped State	61
4.5.3	Mode Matching	64
4.5.4	Transfer to the Quadrupole Trap	64
4.5.5	Transfer to the TOP Trap	68
5	Transverse Cooling	73
5.1	Overview	73
5.2	Experimental Setup and Results	75
5.3	Doppler Theory applied to Transverse Cooling	80
5.4	Phenomenological Model	83
6	Evaporative Cooling of ^7Li	87
6.1	RF Evaporative Cooling	87
6.2	Measurements using RF Cuts	89
6.3	Evaporation Results	93
6.3.1	MOT Temperature	94
6.3.2	Lifetime in the Quadrupole and the TOP	95

6.3.3	Evaporative Cooling in the Quadrupole	98
6.3.4	Evaporative Cooling in the TOP	101
6.3.5	What is the problem with the TOP?	111
7	Conclusion	115
A	^7Li and ^6Li Cooling Properties	117
B	^7Li Hyperfine Structure	118
C	Scattering Length	119
	Bibliography	120

List of Figures

2.1	Doppler force on a two-level atom	17
2.2	Sisyphus effect and polarization gradient	21
2.3	Quadrupole trap	22
2.4	Quadrupole potential	24
2.5	Energy level in a 1D MOT	26
2.6	TOP trap potential	29
2.7	Ioffe-Pritchard trap	31
2.8	Adiabatic compression	38
3.1	Optical pumping	42
3.2	Zeeman slower	44
3.3	Vapor cell	46
4.1	Optical components for cooling and trapping ^7Li	49
4.2	Comb and molasses beam spectrum	51
4.3	Experimental apparatus for the MOT	52
4.4	Trapping chamber	53
4.5	Chamber measurements	54
4.6	Acceleration versus velocity of an atom in the MOT	55
4.7	Number of atoms and density dependence on the optical molasses detuning	56
4.8	Atom loss during laser cooling	57
4.9	MOT temperature measured with free expansion	60
4.10	Ground state hyperfine levels of ^7Li versus magnetic field	62

4.11	Timing sequence to load the MOT and transfer to a Quadrupole trap	63
4.12	Boost circuit for the Quadrupole trap	65
4.13	Transfer efficiency to a Quadrupole versus the magnetic field radial gradient	66
4.14	TOP coils on the chamber	68
4.15	Circuit between the audio amplifier and the TOP coils	69
4.16	Magnetic field attenuation by the chamber	70
4.17	Transfer efficiency as a function of TOP field	72
5.1	New MOT setup with transverse cooling	75
5.2	Picture of the oven, below and cube	76
5.3	Optical components to split the 2D cooling light	77
5.4	Schematics of the transverse cooling showing the 2D beams trajectory	78
5.5	Picture of the atomic beam with 2D cooling	79
5.6	Graph of loading rate versus 2D beam intensity	81
5.7	Graph of loading rate versus number of 2D beam reflections on the mirrors	82
6.1	Evaporation transition versus magnetic field	88
6.2	RF spectroscopy of atoms in a TOP with (168 G/cm, 35 G)	90
6.3	Temperature with free expansion in a MOT with 2×10^9 atoms	94
6.4	Quadrupole trap lifetime	95
6.5	Old Quadrupole trap lifetime	96
6.6	TOP trap lifetime	97
6.7	Old TOP trap lifetime	98
6.8	RF cut in a Quadrupole trap with $B'_r = 88$ G/cm	99
6.9	Timing sequence for evaporation in a Quadrupole without compression	101
6.10	Change in size, density and PSD during evaporation in a Quadrupole with no compression	102
6.11	Timing sequence for evaporation in a Quadrupole with compression	103
6.12	Change of size, density and PSD during evaporation in a Quadrupole with compression	104
6.13	Transfer efficiency from the MOT to the TOP at different radial gradients .	105

6.14	Fraction of atoms below the “circle of death” for different radial gradients.. .	106
6.15	Reduction in the number of atoms in the TOP and cloud size due to evaporation of hot atoms	107
6.16	Temperature measurement in a TOP with RF cuts	108
6.17	Number of atoms in the TOP as a function of (B'_r, B_T)	110
6.18	Temperature in the TOP as a function of (B'_r, B_T)	110
6.19	Density of atoms in the TOP as a function of (B'_r, B_T)	112
6.20	Elastic collision rate in the TOP as a function of (B'_r, B_T)	112
6.21	Phase-space density in the TOP as a function of (B'_r, B_T)	113
B.1	^7Li hyperfine structure	118

List of Tables

6.1	Physical parameters calculated for the MOT → TOP mode matching.	109
6.2	Number of atoms at each experimental step of trapping and cooling ^7Li . . .	111
A.1	Important physical properties of ^7Li and ^6Li for laser cooling.	117
C.1	Triplet and singlet scattering lengths for alkalies	119

Acknowledgements

First I would like to thank Prof. Mark Kasevich for inviting me to work in his group. I have learned a lot from his vision, intelligence and hard work.

Along these four years many people have contributed to make this experiment happen. I would like to thank Wayne Rowlands for helping me in the first two years when I was still a rookie in the lab. Special thanks to Gilles Nogues for his dedication and enthusiasm. His contribution was fundamental for the implementation and success of the transverse cooling. I would also like to thank Julianne Gabelli who helped us during the setup of the experiment. At last I thank my labmates Ruquan Wang and Francesco Minardi for their ideas and invaluable help.

I am specially grateful for my parents, my brother, my sister and my friends who always believed in me. I would also like to thank Patricia and Elaine who, with their love and support, made my life much better during the Ph.D years.

Chapter 1

Introduction

Since 1980 there has been an enormous development in our ability to manipulate the atom. Using lasers and magnetic fields, researchers have developed a series of techniques in the last 20 years that allow them to trap and cool atoms to extremely low temperatures. An interesting consequence of this research has been the development of a whole new field in atomic physics called Atom Optics [1]. It consists on the study of the wave properties of neutral atoms and their applications. It is the ultimate realization of de Broglie's proposal in 1923 that particles can sometimes behave as waves [2]. Experiments of diffraction and interference using matter waves have become routine recently and they could become a better alternative than electromagnetic waves in many applications. Another consequence of these new techniques is the possibility of studying macroscopic coherent states. Bose-Einstein condensates (BEC) are a prime example [3, 4, 5].

Since the first cooling experiments in the 1980s, physicists had a desire to achieve quantum degeneracy in a bosonic gas. Their main reason is because BEC is a unique phase transition. Its origin is purely statistical. Even if the atoms do not interact among themselves, they still condense [6]. After the transition there is a macroscopic number of atoms in the ground state of the system and having such a large coherent sample of atoms opens up many new possibilities to observe macroscopic quantum behavior. It is interesting to note that BEC was first thought to be only a mathematical curiosity by A. Einstein [7, 8].

In 1995 BEC was obtained for the first time in alkali gases: ^{87}Rb [4], ^{23}Na [3] and ^7Li [5]. Previously the major efforts to achieve quantum degeneracy were concentrated on polarized

hydrogen [9, 10]. Evaporative cooling was used to cool them, a technique developed in 1986 [11, 12]. However it was not very efficient in hydrogen due to its small scattering length (see appendix C) and large inelastic losses. D. Pritchard was one of the first to predict correctly that the ratio of elastic and inelastic collision rates would be much larger for alkalies than for hydrogen [13]. The combination of laser cooling and magnetic trapping with evaporative cooling was the breakthrough necessary to achieve BEC in the alkalies.

Evaporative cooling is the most efficient technique to achieve very low temperatures ($T \sim 100$ nK) and high phase-space density ($PSD \sim 1$). The price you have to pay is that a lot of atoms are lost during this process. Hence it is important to start with a large number of atoms in your trap. In our experiment we have used a MOT to trap and cool ^7Li atoms coming from an oven. The trapping beams were frequency spread in order that we could trap more atoms from the low-velocity tail of the Maxwell-Boltzmann distribution. In this case it was unnecessary to pre-cool the atoms with a laser beam. A transverse 2D cooling technique was used to increase the brightness of the atomic beam. Other groups have already used similar methods with atoms like Cs [14], He [15, 16], Na [17, 18], Rb [19, 20, 21] and Ne [22]. In our experiment we have used frequency spread light in the 2D cooling and a zigzag beam configuration to increase the interaction length. This technique increased the atomic beam density, raising the MOT loading rate by a factor of 10 to 2×10^8 atoms/s. At the end 2×10^9 atoms were captured in the MOT.

The first sign of efficient evaporation was obtained in the Quadrupole trap. Using adiabatic compression and RF evaporation, we were able to increase the PSD of the cloud by a factor of 10. The start of evaporation has also been observed in a TOP trap. However it could not be sustained when we tried forced evaporation due to the excess loss of hot atoms through the “circle of death”.

The final goal of our experiment is to reach BEC in ^7Li . My work concentrated in setting up the right initial conditions to obtain efficient evaporation, a necessary step to reach degeneracy. Once obtained, there are many interesting experiments that can be done. The second order correlation function of the atoms could be measured, similar to the work Hanbury-Brown and Twiss did in 1957 using photons [23, 24]. In the atomic case the disappearance of the bunching effect could be used as a signature of the transition from a

thermal cloud to a condensate. A major advantage of using lithium is the existence of a stable, fermionic isotope ^6Li . Using cold atoms of ^7Li we could sympathetically cool ^6Li to reach degeneracy. A very cold sample of fermions has its own set of interesting properties. The possibility of the creation of a superfluid state due to the appearance of Cooper pairs is one of the most exciting ones [25, 26, 27].

1.1 Format of this Thesis

This thesis presents our main achievements in cooling and trapping ^7Li in the last 5 years. The chapters are divided as following: chapter 2 consists of a brief history and theory of laser cooling and trapping of neutral atoms. The most popular traps are discussed in particular the MOT, the Quadrupole and the TOP. I also talk about evaporative cooling and adiabatic compression, showing how the two are related. In chapter 3 the most popular methods used to load a MOT are presented. They can be divided in cooling and non-cooling schemes. The Zeeman slower is an example of a cooling scheme while the frequency spread light fits in the second category. Chapter 4 talks about how we cooled and trapped ^7Li . The laser spectrum and the table optics configuration are shown and how we measured the temperature and the number of atoms is explained. I also talk about the transfer to the Quadrupole trap and to the TOP in mode matching condition. Chapter 5 presents our transverse 2D cooling technique. I discuss the optics and beam configuration, the changes made to the system, the results and a theoretical analysis using Doppler cooling theory. In chapter 6 I present our first evaporative cooling results. First I talk about the subtleties of doing RF evaporation in a TOP trap and how we can estimate the temperature using RF cuts. I present our data in the Quadrupole and in the TOP and what we have learned regarding evaporation of ^7Li in a TOP trap. Chapter 7 contains my conclusion remarks.

Chapter 2

Atom Cooling and Trapping

In this chapter I present the major techniques developed in the last twenty years to cool and trap neutral atoms. It begins with a brief historical overview, an introduction to the foundation of laser cooling, a description of the most important traps for neutral atoms, and then it is explained what evaporative cooling is and how it works.

2.1 History

Since James Clerk Maxwell wrote his classical treatise in electromagnetism in 1873 [28], it is well known that light can exert force on matter. The physical origin is the interaction of the atomic charges with the propagating electric and magnetic fields. The first experiments came around the beginning of the 20th century [29, 30, 31] and by 1933 R. Frisch showed that a beam of sodium atoms could be deflected by light [32]. However the light sources at that time were neither bright nor monochromatic enough to generate a significant change on the atomic motion and so these experiments did not have any major application. Only with the advent of the laser in the late 1950s this started to change. Especially important was the development of tunable dye lasers with frequency ranges close to the optical transitions of some alkalis. In 1970 A. Ashkin noticed that near resonant lasers could be used to exert a significant force in atoms [33]. In 1975 T. Hänsch and A. Schawlow proposed the use of a near resonant laser to cool a gas of neutral atoms [34]. At the same time D. Wineland and H. Dehmelt suggested a similar scheme to cool ions [35]. Their ideas sparked a great

interest in the subject and a series of experiments followed. In a few years there was the first observation of laser cooling of ions [36, 37] and neutral atoms [38, 39, 40]. At the same time people started thinking about how to trap them. Some scientists had already proposed in the past using either magnetic fields [41, 42] or light [43]. However, because such traps are very energetic shallow in practice (a depth of a few kelvin at most), they only became feasible after the advent of laser cooling. In 1985 the group of W.D. Phillips trapped for the first time neutral atoms using a magnetic trap (a spherical Quadrupole) [44], soon followed by other groups [45, 46, 47]. One year later the group of S. Chu trapped atoms using an optical dipole trap for the first time, following a proposal made by A. Ashkin [48, 49]. There were some early proposals to make an optical trap using only the scattering force [50, 51]. But later on it was thought to be impossible due to a theorem proved by A. Ashkin and J.P. Gordon in 1983, properly named the optical Earnshaw's theorem [52]. It says that traps based on the scattering force are unstable, similar to the electrostatic theorem that shows that it is impossible to obtain a stable electrostatic trap. However in 1986 D.E. Pritchard and others argued that if we consider the atomic internal degrees of freedom, this theorem is not valid anymore [53]. This was the seed for the creation, one year later, of the Magneto Optical Trap (MOT) [54]. It combined a spherical Quadrupole magnetic field with the scattering force of three orthogonal, counter-propagating laser beams. The MOT became one of the most popular traps and it still plays a major role nowadays. The reason is that it is a very robust trap and it is relatively simple to assemble. It cools and traps at the same time, simplifying the capture of a large sample of cold atoms. We use it in our experiment and one of the biggest challenges is how to load it with a large number of atoms. As we will discuss in chapter 3, there are many different ways. Our approach was using transverse cooling and frequency spread light.

Many other magnetic and optical traps have been developed in the last 15 years, in particular the Time Orbiting Potential (TOP) [55], the Cloverleaf [56], the QUIC trap [57], the QUEST [58], and the Microtrap [59]. They all have its advantages and disadvantages and your choice should depend on which atom you are using, what kind of experiment you want to do, and what experimental setup you have. In our experiment we have used the MOT, the Quadrupole and the TOP. In the following chapters we will analyze each one of

them and how effective they are when cooling and trapping ^7Li .

Together cooling and trapping of neutral atoms made possible a series of experiments that are not only important for fundamental physics, but also could have significant applications in the future. Some of them are atom interferometry [60, 61, 62, 63], precision spectroscopy [64], atom lithography [65, 66, 67, 68] and Bose-Einstein condensation [3, 4, 5]. The last 20 years have been exciting times for atomic physicists and a nice historical overview was given by W.D. Phillips on the occasion of his Nobel prize award in 1997 [69]. A very good review of the physics of cooling and trapping is given in [70, 71].

2.2 Laser Cooling

The fundamental physics process behind laser cooling is the dissipative force that near resonant light exerts on atoms. Suppose a two-level atom interacts with a monochromatic field. We can show that the time average force in the atomic steady state is given by [1, 72]:

$$\vec{F} = \vec{F}_{sc} + \vec{F}_{dip}, \quad (2.1)$$

$$\vec{F}_{sc}(\vec{r}, \vec{v}) = \frac{\hbar\Gamma}{2} \frac{(\Omega^2/2)\nabla\phi(\vec{r})}{\Gamma^2/4 + \Omega^2/2 + \Delta^2(\vec{v})}, \quad (2.2)$$

$$\vec{F}_{dip}(\vec{r}, \vec{v}) = -\frac{\hbar\Delta(\vec{v})}{2} \frac{\Omega \nabla\Omega(\vec{r})}{\Gamma^2/4 + \Omega^2/2 + \Delta^2(\vec{v})}, \quad (2.3)$$

where

$$\Delta(\vec{v}) = \omega_L - \omega_0 - \vec{k} \cdot \vec{v}, \quad (2.4)$$

$$\Omega(\vec{r}) = -\vec{d} \cdot \vec{E}_0(\vec{r})/\hbar, \quad (2.5)$$

$$\vec{E}(\vec{r}, t) = \vec{E}_0(\vec{r}) \cos[\phi(\vec{r}) - \omega_L t]. \quad (2.6)$$

In the equations above Γ is the spontaneous decay rate (1/lifetime), $\Omega(\vec{r})$ is the Rabi frequency, $\Delta(\vec{v})$ is the Doppler shifted detuning, \vec{k} is the field wave vector, \vec{v} is the atom velocity, ω_L is the light frequency, ω_0 is the atomic transition frequency, \vec{d} is the electric dipole moment, $\vec{E}(\vec{r}, t)$ is the light electric field, and $\phi(\vec{r})$ is the phase of the light. The force given by Eq. (2.2) has its physical origin in the absorption-spontaneous decay cycle. It is called the scattering force. The component (2.3) is known as the dipole force. It arises from the redistribution of photons within the light field from the absorption-stimulated emission

cycle. Depending on the experiment, both forces might be important or not. For cooling purposes the scattering force is the most important one because at low velocities it behaves as a viscous force ($\vec{F} \propto -\vec{v}$). The dipole force is predominant when you have large detuning as in the case of dipole traps. For now let us concentrate on the scattering force. Consider a propagating plane wave interacts with a two-level atom. The phase of the light is given by $\phi(\vec{r}) = \vec{k} \cdot \vec{r}$ and the field amplitude $\vec{E}_0(\vec{r})$ is uniform. That means that $\nabla\phi(\vec{r}) = \vec{k}$ and $\nabla\Omega(\vec{r}) = 0$. We can also write the Rabi frequency as $\Omega = \Gamma\sqrt{I/2I_s}$, where I is the light intensity and I_s is the saturation intensity [1]. Using these in (2.2) and (2.3) we get for the total force on the atom:

$$\vec{F} = \vec{F}_{sc} = \frac{\hbar\Gamma\vec{k}}{2} \frac{S}{1+S}, \quad (2.7)$$

$$S = \frac{I/I_s}{1 + 4\Delta^2(\vec{v})/\Gamma^2}, \quad (2.8)$$

where S is the saturation parameter. So in a plane wave an atom only feels the scattering force. From Eq. (2.7) one important feature can be observed: the force saturates at $\hbar\Gamma k/2$ for $S \gg 1$. That means that in practice we only need $I \cong I_s$, when close to resonance, to maximize it. Also notice that it acts in the direction of the incident photon. That happens because the atom spontaneously decays in random directions and so the total momentum recoil averages to zero. To be more precise, the atom does a random walk in momentum space due to the stochastic behavior of the spontaneous emission. This is similar to the Brownian motion and in analogy the momentum variance $\langle p^2(t) \rangle$ of an atom interacting with a plane wave increases linearly with time [72, 73]:

$$\langle p^2(t) \rangle = 2D_p t, \quad (2.9)$$

$$D_p = \hbar^2 k^2 \gamma, \quad (2.10)$$

where D_p is the momentum diffusion constant and γ is the total photon scattering rate ($\gamma = (\Gamma/2)S/(1+S)$ when interacting with one plane wave). This drift in momentum space is a source of heating [72] and, as we will see in the next section, it imposes a limit on the final temperature achieved by Doppler cooling.

A Fokker-Planck equation can be obtained for the atomic momentum

distribution ρ [74, 73, 75]:

$$\frac{\partial \rho}{\partial t}(v, t) = \frac{\partial}{\partial v} \left[\frac{D_p}{m^2} \frac{\partial \rho}{\partial v} - \frac{\rho}{m} F(v) \right], \quad (2.11)$$

where m is the atomic mass and F is the velocity-dependent light force. It can be shown that if D_p is independent of velocity and $F(v) \propto -v$, an initial Gaussian distribution in one dimension remains Gaussian [76, 77]. This is the theoretical foundation for the definition of temperature in a laser cooled gas [78].

The simplest laser cooling scheme is to shine a near resonant laser beam on atoms leaving a hot oven. However there are two problems with this method: first we can see from Eq. (2.8) that only atoms with velocities in the range $\Delta(\vec{v}) \sim \Gamma$ will be slowed down. This is a very small fraction of atoms in the Maxwell-Boltzmann distribution. The second problem is that atoms are multi-level and as a consequence they can be optically pumped into a state outside the cooling cycle, not feeling the force anymore. The first problem can be solved in different ways. The frequency of the laser, in order to keep it on resonance with the atoms, can be changed (frequency chirping) [79, 80, 81, 82], a magnetic field gradient can be used to change the atomic resonance, the so called Zeeman slower [83, 84, 85, 86], or we can shine a multi-frequency beam instead of a monochromatic one [87, 88]. The second problem can be solved using a so called repumping beam. Either add a weak beam with the right frequency to bring the atoms back into the cooling cycle or add a sideband on the cooling beam with the proper frequency using an optical modulator [82]. Another way also is to use a circular polarized light with a bias magnetic field to keep the atom in a closed swing state due to the selection rules [83, 84]. We will discuss in details these methods in chapter 3.

2.2.1 Doppler Cooling

T. Hänsch and A. Schawlow's cooling proposal in 1975 [34] was to shine a gas with a red-detuned ($\delta \equiv \omega_L - \omega_0 < 0$) laser from all directions. When the atom moves towards a laser it sees its frequency shifted up by the Doppler effect (2.4) and shifted down when it moves away, so it will scatter more photons from the incoming light, damping its motion wherever it goes. Since the Doppler shift plays such an important role, this technique became known as Doppler cooling.

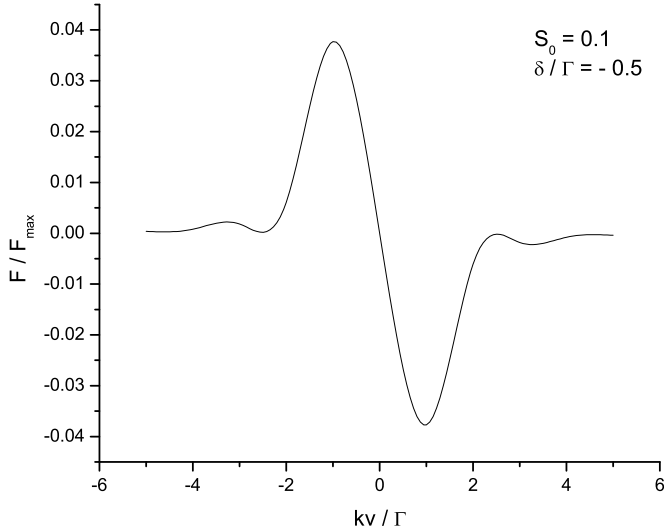


Figure 2.1: Total force on an atom from two counterpropagating , red-detuned plane waves. Notice that the force peaks around $|kv| \sim |\delta|$ and it has a viscous behavior at low velocities.

Suppose there are two counterpropagating plane waves. Consider the low intensity limit ($I/I_s < 1$) such that interference among the beams and coherence effects from the atomic interaction with the light can be ignored. Then, considering that each beam acts independently on the atom and using (2.7) and (2.8), the total force is given by:

$$\vec{F} = \frac{\hbar\Gamma S_0 \vec{k}}{2} \left[\frac{1}{1 + S_0 + 4(\delta - \vec{k} \cdot \vec{v})^2/\Gamma^2} - \frac{1}{1 + S_0 + 4(\delta + \vec{k} \cdot \vec{v})^2/\Gamma^2} \right], \quad (2.12)$$

$$\delta = \omega_L - \omega_0, \quad (2.13)$$

$$S_0 = I/I_s. \quad (2.14)$$

Figure 2.1 is a plot of (2.12) in one dimension. It has two important features: it acts as a viscous force at low velocities ($F \propto -v$) and it peaks around $v_p \sim |\delta|/k$. The first property is what makes it useful for cooling a gas. The second one is the reason for developing ingenious ways to make the light resonant with the maximum number of atoms in a beam.

In the case of ${}^7\text{Li}$ for example, the cooling transition ($2S_{1/2}, F = 2 \leftrightarrow 2P_{3/2}, F = 3$) has $\Gamma = 2\pi \times 5.9$ MHz and $\lambda = 671$ nm. If $|\delta| = \Gamma$, then $v_p = |\delta|/k = 4$ m/s. Compared to the average thermal velocity of 1000 m/s, notice that if a near-resonant monochromatic beam is applied to an oven, only a very small fraction of atoms would be cooled. That is why it is necessary to change the laser frequency, use a Zeeman slower or a multi-frequency light to cool effectively an atomic beam. The range of velocities Δv around the peak that can be cooled is given by the linewidth $k\Delta v \sim \Gamma$.

A linear approximation of Eq.(2.12) can be obtained if we assume $|kv| \ll |\delta|, \Gamma$ [78]:

$$\vec{F} = \alpha \vec{v}, \quad (2.15)$$

$$\alpha = 4\hbar k^2 S_0 \frac{2\delta/\Gamma}{[1 + S_0 + (2\delta/\Gamma)^2]^2}. \quad (2.16)$$

From Eq.(2.16) we can see that if the light is red-detuned ($\delta < 0$), then Eq.(2.15) becomes a viscous force. It seems from Eq.(2.15) that the atomic velocity would decay exponentially to zero. However remember from section 2.2 that there is also a heating process due to the stochastic behavior of the absorption and spontaneous emission. So in reality the atoms reach an equilibrium at a non-zero speed v_d called the Doppler speed. The corresponding temperature is the lowest one that can be achieved through this process and it is called the Doppler temperature. Its expression is obtained considering that in equilibrium the cooling and heating rates should be equal [78]:

$$\left(\frac{dE}{dt} \right)_{cool} = \vec{F} \cdot \vec{v} = -|\alpha|v^2, \quad (2.17)$$

$$\left(\frac{dE}{dt} \right)_{heat} = \frac{D_p}{m}. \quad (2.18)$$

In equilibrium we must have $(2.17)+(2.18) = 0$, giving an ensemble of atoms a mean square velocity:

$$\langle v_d^2 \rangle = \frac{\hbar^2 k^2}{m} \frac{\gamma}{|\alpha|}, \quad (2.19)$$

where we used (2.10). The total scattering rate γ is given by $\Gamma S/(1 + S)$, because there are two beams. Using this value and (2.16) in (2.19):

$$\langle v_d^2 \rangle = \frac{\hbar\Gamma}{4m} \frac{1 + S_0 + (2\delta/\Gamma)^2}{2|\delta|/\Gamma}. \quad (2.20)$$

Using the equipartition theorem, the Doppler temperature can be defined as:

$$\frac{k_B T_D}{2} = \frac{m \langle v_d^2 \rangle}{2}. \quad (2.21)$$

Applying (2.20) in (2.21):

$$k_B T_D = \frac{\hbar\Gamma}{4} \frac{1 + S_0 + (2\delta/\Gamma)^2}{2|\delta|/\Gamma}. \quad (2.22)$$

Assuming $S_0 \ll 1$, the minimum Doppler temperature obtained from (2.22) is for $\delta = -\Gamma/2$:

$$k_B T_D^{min} = \frac{\hbar\Gamma}{2}. \quad (2.23)$$

This is also known as the Doppler limit and it is only a function of the cooling transition linewidth. In the beginning it was thought that this was the lowest temperature that could be achieved through laser cooling. Later on it was shown that this is not true as we will see in the next section.

The first observation of 3D Doppler cooling was obtained by the group of S. Chu in 1985 [89]. They cooled sodium atoms using six counterpropagating, red-detuned laser beams. Due to the viscous environment created by the light, they nicknamed this configuration an “optical molasses”. The temperature measured was $200_{-60}^{+200} \mu\text{K}$, close to the Doppler limit of $240 \mu\text{K}$ for Na and at that time it was considered a success of the Doppler cooling theory. Lithium 7 was first cooled and trapped in 1991 by Z. Lin *et. al.* [90]. Its measured temperature was $350 \pm 40 \mu\text{K}$, roughly twice the Doppler limit of $140 \mu\text{K}$. Their explanation was that, since the excited hyperfine states can not be resolved, the effective Γ in (2.23) is much larger than expected, increasing T_D^{min} .

2.2.2 Sub-Doppler Cooling

The first experiments with optical molasses [89] agreed very well with the theory of Doppler cooling. So it was with some surprise that in 1987 the NIST group announced a series of measurements that did not agree at all with the theory [91]. Not only the lifetime of the optical molasses and the temperature dependence with detuning did not agree, but the temperature measured for Na was only $43 \pm 20 \mu\text{K}$, much lower than the expected Doppler limit of $240 \mu\text{K}$ [92]. Other experiments followed soon using Na, Cs and Rb and all of

them confirmed the violation of the Doppler theory [93, 94, 95, 96, 97]. In some of these experiments they had noticed that the temperature depended on the polarization of the molasses beam and also on the existence of external magnetic fields. This was not expected in the old theory and it was a clue on how to change it.

Two groups independently presented an explanation for this sub-Doppler cooling [94, 98]. The idea was to take into consideration the polarization gradient of the light and the multi-level structure of the atom, characteristics that were previously ignored in the Doppler theory. The physical explanation for the cooling depends on the polarization gradient that you have. Let us consider the two most common situations. In the case of two counterpropagating beams with orthogonal linear polarization, the total polarization will vary spatially from linear to elliptical and to circular with a period of $\lambda/2$ (Fig. 2.2a). This change causes a spatial modulation of the atomic dressed state eigenvalue (Dressed state is the eigenstate of the atom + field hamiltonian). An atom with velocity $v\tau_p \sim \lambda$, where τ_p is the relaxation time for the optical pumping between the ground state sublevels, will on average be optically pumped when it is on the top of the potential hill to the bottom (see Fig. 2.2b). This process is known as the Sisyphus effect (a reference to the Greek myth of Sisyphus) and it extracts kinetic energy of the atom, cooling it below the Doppler limit [99]. If instead the beams have opposite circular polarization, the physical process is different. As shown in Fig. 2.2c, the total polarization is linear and rotates around the propagation axis with a pitch of $\lambda/2$. Since the polarization does not change, the dressed states eigenvalues do not vary spatially. That means that there is no Sisyphus effect in this case. The atoms cool below the Doppler limit because the rotation of the polarization induces a population difference between the ground state sublevels. This difference forces the atom to scatter more light from the counterpropagating beam than the copropagating one, damping its velocity [99]. It is similar to the Doppler cooling process, but the physical origin is different.

This sub-Doppler cooling has the characteristic that the final temperature is proportional to the light intensity, while in the Doppler theory it is independent (2.23). The sub-Doppler limit is given by the temperature equivalent to the recoil momentum of the atom ($k_B T_R = \hbar^2 k^2 / m$). It is possible to cool atoms below this limit [100, 101], however it

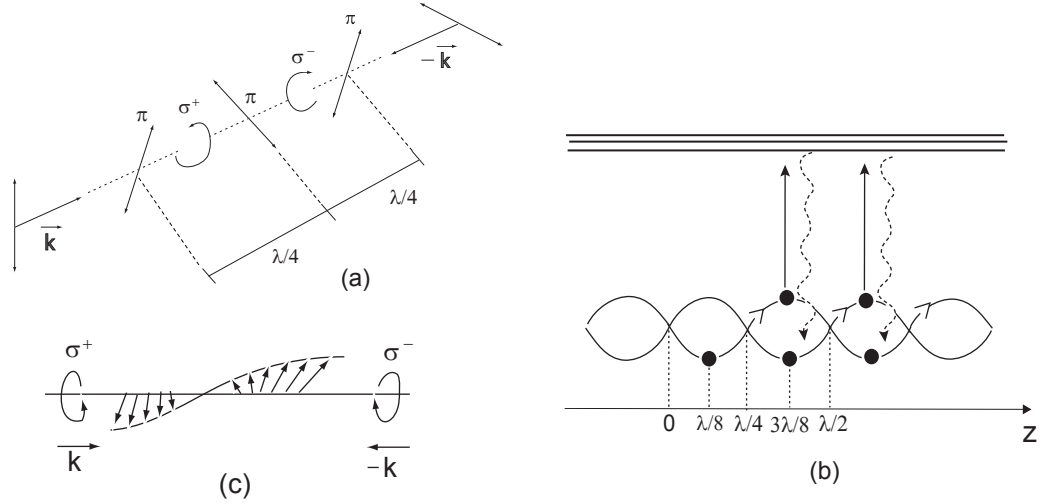


Figure 2.2: a) Two orthogonal, linear polarized beams generate a polarization gradient with a periodicity of $\lambda/2$. The polarization alternates between linear and circular. b) Due to the polarization gradient, the dressed states eigenvalues also oscillate with a period $\lambda/2$. On average the atoms are optically pumped from the top of the potential hill to the bottom. This process, also known as Sisyphus effect, extracts kinetic energy from the atom, cooling it down. c) Two beams with opposite circular polarization generate a gradient equivalent to a spatially, rotating linear polarization.

turned out not to be a practical way to reach lower temperatures in quantum degeneracy experiments. The method of evaporative cooling was much more successful (see section 2.4).

In experiments using ^7Li , sub-Doppler cooling has never been observed [90, 102]. The reason is that the excited hyperfine levels have a separation comparable to the linewidth, so the optical pumping is not as efficient as in other alkalies. However, using adiabatic cooling in a 1D optical lattice, the group of R.G. Hulet was able to cool ^7Li atoms close to the recoil limit of $6 \mu\text{K}$ [103].

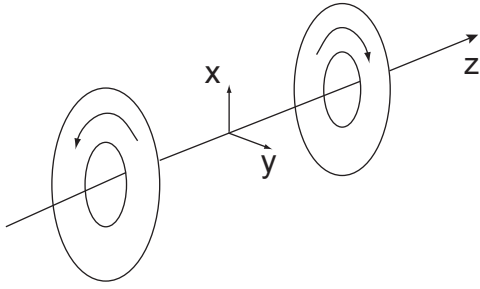


Figure 2.3: The Quadrupole trap consists of two coils in an anti-Helmholtz configuration. The arrows on the coils indicate the direction of the current.

2.3 Trapping Neutral Atoms

The development of atomic traps was a natural consequence of laser cooling. After slowing down the atoms you would like to study and manipulate them for as long as possible. Since the first observation of trapped neutral atoms in 1985 [44], there have been several proposals of different traps using magnetic fields, the optical dipole force (2.3) and the radiation pressure (2.2). I will analyze some of the most important traps used in the last 15 years, among them the ones used in our experiment.

2.3.1 Quadrupole trap

The Quadrupole trap was the first one ever used to trap neutral atoms [44]. It consists of two coils with current flowing in opposite directions, in the so called anti-Helmholtz configuration (Fig. 2.3). The magnetic field is zero at the center and it is approximately linear in its neighborhood:

$$\vec{B}_{\text{quad}}(\text{center}) \cong B'_r x \hat{x} + B'_r y \hat{y} - 2B'_r z \hat{z}, \quad (2.24)$$

where B'_r is the radial gradient. In (2.24) we have used the cylindrical symmetry of the trap ($B'_x = B'_y$) and the fact that $\nabla \cdot \vec{B} = 0$ implies $B'_z = -2B'_r$. Magnetic traps are particularly useful for alkalis because they have a strong magnetic dipole due to their unpaired electron. The potential energy of a dipole $\vec{\mu}$ is $U(\vec{r}) = -\vec{\mu} \cdot \vec{B}(\vec{r})$. If we assume that $\vec{\mu}$ adiabatically

follows the field direction $\vec{B}/|\vec{B}|$ we can write the energy equation as:

$$U(\vec{r}) = -\mu|\vec{B}|, \quad (2.25)$$

$$\mu \equiv \vec{\mu} \cdot \vec{B}/|\vec{B}| = constant. \quad (2.26)$$

The adiabatic condition is valid if:

$$\omega_l > \frac{1}{|\vec{B}|} \frac{\partial |\vec{B}|}{\partial t}, \quad (2.27)$$

where $\omega_l = \vec{\mu} \cdot \vec{B}/\hbar$ is the Larmor frequency. Violations of (2.27) happen in regions of low field or large variations of direction and it induces non-adiabatic state transitions on the atom, the so called Majorana transitions [104, 105, 106, 107]. In Quantum Mechanics the factor (2.26) is defined as $\mu = -m_F g_F \mu_B$ where g_F is the Landé g-factor of the atomic hyperfine state, m_F is the magnetic sublevel, and μ_B is the Bohr magneton. The atomic energy (2.25) is then expressed as:

$$U(\vec{r}) = m_F g_F \mu_B |\vec{B}(\vec{r})|. \quad (2.28)$$

Depending on the atomic state, the product $m_F g_F$ is either positive or negative. In the first case the atom is in a low-field seeking state, otherwise it is in a high-field seeking state. Since Maxwell's equations require that in an open, free-source region a magnetic (or electric) field can only have a local minimum [108], we can only trap atoms in low-field seeking states ($m_F g_F > 0$). Using (2.24) in (2.28), the Quadrupole potential in cylindrical coordinates is given by:

$$U_{Quad}(\rho, z) = m_F g_F \mu_B B'_r \sqrt{\rho^2 + 4z^2}, \quad (2.29)$$

where $\rho^2 = x^2 + y^2$. It has a linear shape in the axial and radial directions as shown in Fig. 2.4. This behavior is what makes the Quadrupole a very tight trap.

The advantages of a Quadrupole trap are that it offers good optical access, it is easy to build and it has a very strong confinement due to its linear potential close to the center. By this last statement we mean that, for a given energy, the atoms in this trap are confined to a smaller volume when compared to other traps with similar field strength. A strong confinement increases the atomic density and that is important in the process of achieving

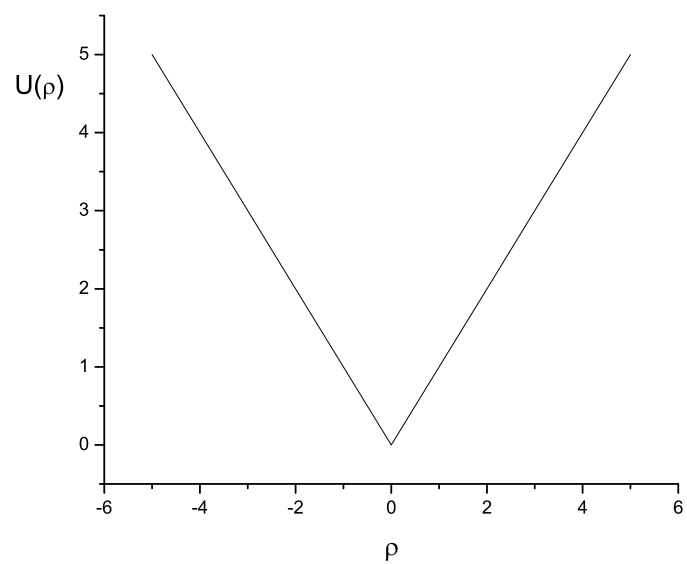


Figure 2.4: The Quadrupole potential in the radial direction at $z = 0$. It has the same linear behavior in the axial direction.

efficient evaporative cooling (see section 2.4). The main disadvantage is that the minimum is zero at the center. Atoms passing close to this region can suffer Majorana transitions to high-field seeking states, being ejected from the trap. This gets worse when the cloud gets colder and more atoms move closer to $\vec{B} = 0$. This is the reason why traps with $|\vec{B}|_{min} \neq 0$ had to be developed in order to obtain BEC.

2.3.2 Magneto Optical Trap (MOT)

Following an idea suggested by J. Dalibard, the group of S. Chu obtained in 1987 the first atomic trap based on the scattering force [54]. In order to avoid the optical Earnshaw's theorem [52] they applied a weak magnetic field using a Quadrupole trap. The Zeeman shift makes the light force position dependent, violating the theorem condition that the force should depend only on the light intensity. The trap consists of three counter-propagating laser beams with opposite circular polarizations. The light is also red-detuned to generate an optical molasses to cool the atoms. The way the trap works is very simple. Let us suppose a one-dimensional, linear magnetic field, similar to what we find at the center of a Quadrupole trap (see Fig. 2.5). If the atom moves away from the center, the Zeeman shift brings the atomic levels closer to resonance with the opposing light beam. This effect creates a restoring force, trapping the atoms at the center of the MOT. It is important that the beams have the correct polarization to make them resonant with the magnetic sublevel.

Considering that the detuning is dependent on position $\delta = \delta(\vec{r})$, we can expand the expression (2.12) around the origin and get for the force on a slow moving atom at the center of the MOT [109]:

$$\vec{F}_{MOT}(\vec{r}, \vec{v}) = -\overleftrightarrow{k} \cdot \vec{r} - \overleftrightarrow{\alpha} \cdot \vec{v}, \quad (2.30)$$

where \overleftrightarrow{k} and $\overleftrightarrow{\alpha}$ are the spring and friction tensors. Hence for small displacements close to the origin the atom behaves as a damped harmonic oscillator. The MOT not only traps but it also cools the atoms. This is one of the main reasons for its popularity. Another advantage is that it is a very robust trap, not depending critically on beam alignment and polarization.

The number of atoms trapped in a MOT is determined by the loading rate, the background pressure and the two-body collision rate. It is given by the following rate equa-

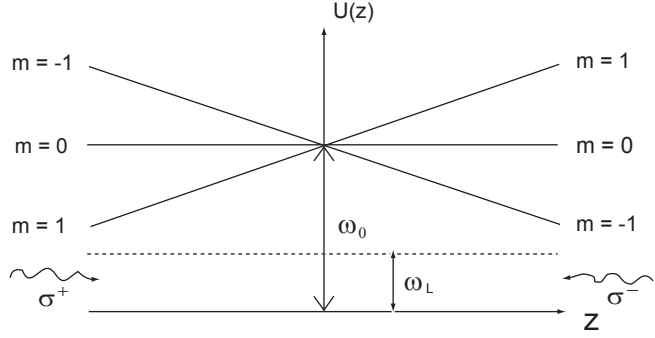


Figure 2.5: Atomic energy level in a 1D MOT ($B(z) = B'_z z$). The polarization of the beams is chosen in order to generate a restoring scattering force. The laser frequency ω_L is red-detuned to provide cooling ($\delta = \omega_L - \omega_0 < 0$).

tion [109]:

$$\frac{dN(t)}{dt} = R - \frac{N(t)}{\tau} - \beta \frac{N^2}{V}, \quad (2.31)$$

where R is the loading rate, τ is the 1/e decay time due to background gases, β is the two-body collision rate, and V is the trap volume. Experimentally the best way to increase the number of trapped atoms is by maximizing R and having a good vacuum ($P \lesssim 10^{-11}$ Torr, $\tau \gtrsim 60$ s). And because having a large initial sample of cold atoms is very important for many experiments, especially BEC, better and new ways to increase R have been developed. In chapter 3 I will discuss the most popular methods used and in chapter 5 I will present the technique developed in this work using transverse cooling with frequency spread light. The two-body collision rate β was measured for ${}^7\text{Li}$ and it is of the order of $10^{-13}\text{cm}^3/\text{s}$ [110]. The physical origin of this loss is radiative distribution where an excited atom emits a red-detuned photon due to a collision, gaining enough kinetic energy to leave the trap.

The MOT is a complex system whose characteristics can change dramatically depending on the number of atoms trapped. An atom in a MOT is subjected to three forces: a trapping force, an attenuation force and a radiation trapping force [111]. The first one is due to the

light interaction (2.30). The other two are interatomic forces that only become important when the number of atoms trapped is larger than $\sim 10^4$. The attenuation force happens because of an imbalance between the trapping beam intensities when going through a thick cloud. This results in an attractive force that can be expressed as [109]:

$$\vec{F}_A = -\frac{I\sigma_L^2}{4\pi c r^2} \hat{r}, \quad (2.32)$$

where I is the beam intensity, σ_L is the absorption cross-section for photons from the laser, c is the speed of light and r is the interatomic distance. The radiation trapping force is due to absorption and re-emission of scattered photons within the cloud. The exchange of a photon between two atoms increases their relative momentum by $2\hbar k$, meaning that this is a repulsive force. It can be expressed as [109]:

$$\vec{F}_R = \frac{I\sigma_L\sigma_R}{4\pi c r^2} \hat{r}, \quad (2.33)$$

where σ_R is the absorption cross-section for re-scattered photons.

In the regime of large number of atoms ($N \geq 10^4$) the radiation force (2.33) overcomes the two other forces (2.30) and (2.32). As a consequence the atomic density reaches a limit, becoming uniform with a maximum value around 10^{11} atoms/cm³ [109, 112]. Above this value the radius of the cloud increases with the number of atoms as $r \propto N^{1/3}$ [113]. In order to overcome this limitation, W. Ketterle *et. al.* proposed the so called “dark SPOT” [114]. It is a modified MOT where the atoms are trapped in a dark hyperfine level, avoiding the multiple scattering force. This is accomplished by creating a region at the center of the trap beams where there is no repumping frequency. As a consequence the atoms are optically pumped into the dark state at the center of the MOT, not participating in the re-scattering of the light. Using this method they were able to achieve densities of the order of 10^{12} atoms/cm³ with more than 10^{10} atoms trapped.

The temperature is also affected by the number of atoms in the MOT. In the temperature limited regime (low density) its value is the same as in an optical molasses with the same detuning and intensity [97]. In this regime the Sisyphus cooling becomes important and the temperature can reach sub-Doppler values. In the constant density regime the multiple re-scattering of photons enhances the momentum diffusion, increasing the MOT temperature

[97, 115]. The fraction of photons re-scattered before leaving the cloud can be expressed as [115]:

$$f \cong n\sigma_R l, \quad (2.34)$$

where n is the atomic density and l is the cloud size. The temperature is given by:

$$T = T_{mol}(1 + \xi f), \quad (2.35)$$

where ξ is a function of the momentum diffusion constant. In the constant density regime we have $l \sim N^{1/3}$. Using this expression in (2.34) and (2.35) we get:

$$T - T_{mol} \propto N^{1/3}. \quad (2.36)$$

The relation above represents a major trade-off in the MOT: more atoms you trap, the hotter your cloud is.

2.3.3 Time Orbiting Potential (TOP)

On the race to obtain BEC back in 1995, one of the main problems was the Majorana losses. They are caused by non-adiabatic transitions to high-field seeking states, when the atoms get close to a region with zero magnetic field. Quadrupole traps are easy to make and have great confinement, but as soon as the cloud starts to get colder, the losses through “the hole” (region around $\vec{B} = 0$) begin to increase dramatically. So you either have to use a different trap with a non-zero minimum or you have to modify the Quadrupole trap. The group of E. Cornell in JILA followed the second option and they added a rotating, radial magnetic field to the Quadrupole that shifts the zero off-center (see Fig. 2.6a) [55]. The rotation frequency is smaller than the Larmor frequency to keep the adiabaticity of the atomic motion, but higher than the atomic oscillation, in order that the atoms see only a time average potential. This time-average gives a parabolic potential with a non-zero minimum. Cold atoms can be stored for a long time at the bottom of this trap and it has been used by the JILA group and others to reach BEC in rubidium 87 [4, 116]. It is important to note that Majorana transitions can still happen close to a circumference on the xy plane with a radius $R_D = B_T/B'_r$, where B_T is the TOP field magnitude and B'_r is the Quadrupole radial gradient. This is the so called “circle of death”. Only the hotter atoms

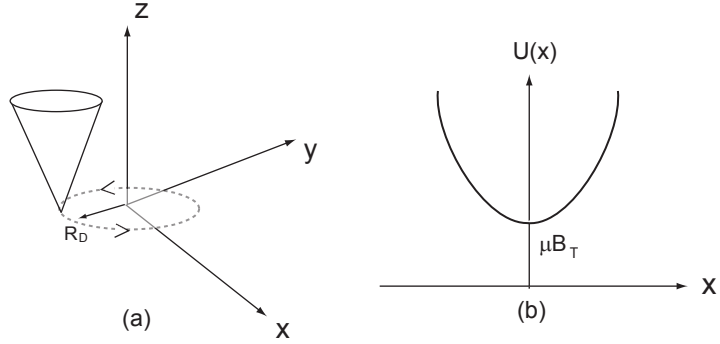


Figure 2.6: In figure (a) we see a representation of the instantaneous TOP potential. The zero magnetic field rotates on the xy plane with a frequency ω_T and a radius R_D , the so called “circle of death”. In figure (b) we have the time-average potential with a non-zero minimum. It is approximately harmonic for $r \ll R_D$.

will reach this circle and that means that the TOP has a built-in evaporation process. This is good in one way because hot atoms can be evaporated without any external intervention (an RF field for example), but on the other hand it limits the trap depth.

Let us now study in more details the properties of the TOP. The total magnetic field is given by:

$$\vec{B}_{TOP}(\vec{r}, t) = (B_T \cos \omega_T t + B'_r x) \hat{x} + (B_T \sin \omega_T t + B'_r y) \hat{y} - 2B'_r z \hat{z}, \quad (2.37)$$

where ω_T is the TOP frequency. The magnitude of the total TOP field in cylindrical coordinates (ρ, ϕ, z) is:

$$|\vec{B}_{TOP}(\rho, \phi, z, t)| = B_T \sqrt{1 + \frac{\rho^2 + 4z^2}{R_D^2} + 2 \frac{\rho}{R_D} \cos(\phi - \omega_T t)}, \quad (2.38)$$

$$R_D = B_T / B'_r, \quad (2.39)$$

where $\rho = \sqrt{x^2 + y^2}$, $\phi = \arctan(y/x)$ and R_D is the “circle of death” radius. Using the expansion $\sqrt{1+u} = 1 + u/2 - u^2/8 + O(3)$ in (2.38) and averaging over a TOP rotation

period $\zeta = 2\pi/\omega_T$, we get:

$$\left\langle |\vec{B}_{TOP}(\rho, \phi, z)| \right\rangle_\zeta = B_T \left[1 + \frac{1}{4} \frac{(\rho^2 + 8z^2)}{R_D^2} \right], \quad (2.40)$$

where we have ignored terms higher than the second order in ρ/R_D . From Eq.(2.40) we see that the time-average potential near the center is harmonic:

$$U_{TOP}(\rho, z) - |\mu|B_T = \frac{1}{2} m \omega_r^2 \rho^2 + \frac{1}{2} m \omega_z^2 z^2, \quad (2.41)$$

$$\omega_r^2 = \frac{|\mu|(B'_r)^2}{2mB_T}, \quad (2.42)$$

$$\omega_z^2 = \frac{4|\mu|(B'_r)^2}{mB_T} = 8\omega_r^2, \quad (2.43)$$

where μ is the atomic magnetic moment and m is the atomic mass. The trap curvature is given by:

$$B''_r = \frac{(B'_r)^2}{2B_T}, \quad (2.44)$$

$$B''_z = \frac{4(B'_r)^2}{B_T}. \quad (2.45)$$

From Eqs.(2.44) and (2.45) we see that the confinement is 8 times larger in the axial direction. This means that a small cloud in equilibrium in a TOP should be shaped as an ellipsoid with dimensions $r_x = r_y = \sqrt{8}r_z$.

The trap depth is limited by the “circle of death”. Using (2.39), (2.42) and (2.43) in (2.41) we can get its value:

$$\Delta U_{TOP} = U_{TOP}(R_D, 0) - |\mu|B_T = \frac{|\mu|B_T}{4}. \quad (2.46)$$

Using $|\mu| = |m_F g| \mu_B$ in (2.46) and the fact that $\mu_B/k_B \cong 67 \text{ } \mu\text{K/G}$, we can write the trap depth in temperature units:

$$T_{Depth} \equiv \frac{\Delta U_{TOP}}{\eta k_B} = |m_F g_F| \frac{67}{4\eta} B_T (\mu\text{K/G}). \quad (2.47)$$

As an example if we want $\Delta U_{TOP} = 5k_B T$ ($\eta = 5$) for $T = 200 \text{ } \mu\text{K}$ and $|m_F g| = 1$, according to (2.47) we would need $B_T \cong 60 \text{ G}$. This is an easy field to produce in a laboratory, however the TOP is a shallow trap when compared to other magnetic ones. This is a disadvantage specially if the atoms are too hot when transferred from the MOT.

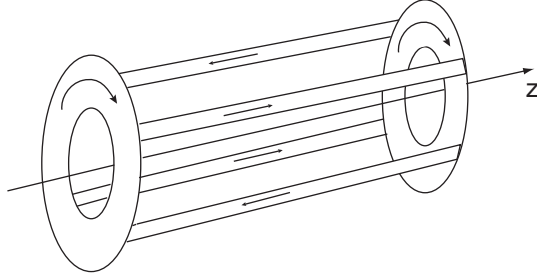


Figure 2.7: This is the simplest model for an Ioffe-Pritchard trap. The pinch coils generate the bias field and the axial curvature, while the bars provide the transverse gradient. The arrows indicate the direction of the current. An additional pair of Helmholtz coils can be used to lower the bias field B_0 .

2.3.4 Ioffe-Pritchard trap

A more popular trap that also has a non-zero minimum are the ones called Ioffe-Pritchard traps (IP traps). Its design was first proposed for plasma confinement experiments in the 1960s [117] and it was later applied to atoms by D. Pritchard [45, 118]. In its simplest form it consists on a pair of Helmholtz coils (pinch coils) and four parallel straight bars with opposing current (Ioffe bars. See Fig. 2.7). The pinch coils provide the bias field B_0 and the curvature B_z'' ($B_z'' \equiv \frac{\partial^2 B_z}{\partial z^2}(\text{origin})$) while the bars generate the transverse gradient B_r' ($B_r' \equiv \frac{\partial B_x}{\partial x}(\text{origin})$). An axial symmetric IP trap has the following magnetic field in cylindrical coordinates [119, 120]:

$$\vec{B}_{IP}(\rho, \phi, z) = \left[B_r' \rho \cos 2\phi - \frac{B_z''}{2} \rho z \right] \hat{\rho} - B_r' \rho \sin 2\phi \hat{\phi} + \left[B_0 + \frac{B_z''}{2} (z^2 - \frac{\rho^2}{2}) \right] \hat{z}, \quad (2.48)$$

$$|\vec{B}_{IP}| = B_0 \sqrt{1 + \left[\left(\frac{B_r'}{B_0} \right)^2 - \frac{B_z''}{2B_0} \right] \rho^2 + \frac{B_z''}{B_0} z^2 - \frac{B_r' B_z''}{B_0^2} \rho^2 z \cos 2\phi + \left(\frac{B_z''}{2B_0} \right)^2 \left(z^4 + \frac{\rho^4}{4} \right)}. \quad (2.49)$$

Using Eq. (2.49) the potential close to the center can be approximated, up to the second

order, as an anisotropic harmonic oscillator [120]:

$$U_{IP}(\rho, z) = \frac{\mu}{2}(B_r''\rho^2 + B_z''z^2), \quad (2.50)$$

$$B_r'' = \frac{(B_r')^2}{B_0} - \frac{B_z''}{2}. \quad (2.51)$$

The bias field B_0 has to be only large enough to avoid Majorana transitions ($B_0 \sim 1\text{G}$), and a small value is desired to maximize B_r'' . In order to fine tune B_0 , an additional pair of Helmholtz coils can be used to counterbalance the pinch coils. The radial confinement is much stronger than the axial in an IP trap.

When compared to the TOP, the IP trap has some advantages. Its effective radial curvature (2.51) is close to double the value of the TOP (2.44), it only employs DC fields and it is a much deeper trap since it does not have a “circle of death”. A disadvantage is that it has a smaller optical access due to the Ioffe bars and it is more complicated to assemble. A lot of experiments have adopted IP traps. The absence of Majorana losses and its tight confinement are important features when trying to obtain BEC. It is interesting to note that there are many different configurations that can generate a field like (2.48). It can either be built using the traditional design [121, 122] or in a “cloverleaf” configuration [56], using three coils (QUIC trap) [57, 123] or a 4D coil trap [124]. The choice usually depends on how much optical access you need and the geometry of your experimental apparatus.

2.3.5 Optical Dipole Trap

In 1970 A. Ashkin made some interesting experiments where he trapped microscopic particles using only lasers [33, 125]. The so called “optical tweezers” have become a useful tool to probe DNA molecules and proteins [126] and in experiments in soft condensed matter [127]. In 1978 he extended this concept by proposing an atomic trap using only lasers [49]. Contrary to the MOT, in such a trap the dipole force (2.3) is the most important one. In the case of a red-detuned beam ($\Delta < 0$), equation (2.3) shows that the atom is attracted to a maximum of intensity. Ashkin’s proposal as a stable 3D trap was a tightly focused laser beam.

A serious limitation with any optical trap is that they are very shallow (depth below 1mK), being able to trap only pre-cooled atoms. Another problem are the fluctuations

in the dipole force and the stochastic behavior of the spontaneous emission. Those become a source of heating, turning the trap unstable. For this reason only after laser cooling was developed did this trap became feasible. The first successful attempt was made by the group of S. Chu in 1986. They trapped around 500 sodium atoms in a single, focused, red-detuned laser beam [48]. The atoms were previously cooled in an optical molasses and they were kept cold by turning off periodically the trap and applying the cooling beams.

In an optical dipole trap the detuning is very large $|\Delta|/\Gamma \gg 1$. From Eqs. (2.2) and (2.3) we have:

$$\frac{|F_{dip}|}{|F_{sc}|} = \frac{2}{k} \frac{|\Delta|}{\Gamma} \frac{|\nabla\Omega|}{\Omega}. \quad (2.52)$$

From Eq.(2.52) the large detuning condition indicates that $|F_{dip}| \gg |F_{sc}|$ and so the scattering force can be ignored most of the time. The dipole force (2.3) can also be written as the gradient of a pseudo-potential [1]:

$$\vec{F}_{dip}(\vec{r}, \vec{v}) = -\nabla U_{dip}(\vec{r}, \vec{v}), \quad (2.53)$$

$$U_{dip}(\vec{r}, \vec{v}) = \frac{\hbar\Delta(\vec{v})}{2} \ln(1 + S), \quad (2.54)$$

where S is given by (2.8) and $\Delta(\vec{v})$ by (2.4). In the large detuning regime ($\delta/\Gamma \gg 1$), we have $\Delta(\vec{v}) \cong \delta$, $S \cong \Gamma^2 I / (4\delta^2 I_s) \ll 1$, $\ln(1 + S) \cong S$, and a good approximation of (2.54) is:

$$U_{dip}(\vec{r}, \vec{v}) \cong \frac{\hbar\Gamma^2}{8\delta} \frac{I}{I_s}. \quad (2.55)$$

The scattering rate is related to the potential through the following formula:

$$\hbar\gamma_{sc} = \left(\frac{\Gamma}{\delta}\right) U_{dip}. \quad (2.56)$$

Equations (2.55) and (2.56) reveal some important characteristics of the dipole trap. First if $\delta < 0$ (red-detuned light) the optical potential is attractive while if $\delta > 0$ (blue-detuned light) is repulsive. Second $U_{dip} \propto I/\delta$ and $\gamma_{sc} \propto I/\delta^2$, so it is interesting to have large intensities to obtain a deep trap and large detuning to minimize heating. An application of this principle is the Quasi-Electrostatic trap (QUEST) where the laser frequency is in the infrared region ($\omega \ll \omega_0$) and $\gamma_{sc} \lesssim 10^{-3} s^{-1}$, meaning that it is basically a conservative trap [58, 128].

Now let us analyze the simple dipole trap proposed by Ashkin and used in Chu's experiment: a single, focused, gaussian laser beam. Assuming that the laser propagates along the z direction, the intensity is given in cylindrical coordinates by:

$$I(\rho, z) = \frac{2P}{\pi w^2(z)} e^{-2\rho^2/w^2(z)}, \quad (2.57)$$

$$w(z) = w_0 \sqrt{1 + (z/z_R)^2}, \quad (2.58)$$

where w_0 is the beam waist, P is the laser power, and $z_R = \pi w_0^2/\lambda$ is the Rayleigh length [129]. Using (2.57) in (2.55) and defining the trap depth as $\Delta U_{dip} \equiv |U_{dip}(0, 0)|$:

$$U_{dip}(\rho, z) = \frac{\Delta U_{dip}}{1 + (z/z_R)^2} \frac{|\delta|}{\delta} e^{-2\rho^2/w^2(z)}, \quad (2.59)$$

$$\Delta U_{dip} = \frac{\hbar \Gamma^2 P}{4|\delta| \pi w_0^2 I_s}. \quad (2.60)$$

In a cold sample $k_B T \ll \Delta U_{dip}$ and the cloud will be close to the center meaning that $z/z_R, \rho/w_0 \ll 1$. Expanding Eq. (2.59) to the second order:

$$U_{dip}(\rho, z) \cong \Delta U_{dip} \frac{|\delta|}{\delta} \left[1 - 2 \left(\frac{\rho}{w_0} \right)^2 - \left(\frac{z}{z_R} \right)^2 \right]. \quad (2.61)$$

From Eq. (2.61) we see that cold atoms in a focused gaussian beam can be approximated as trapped in a harmonic potential.

The main advantages of an optical dipole trap are the possibility of trapping atoms in different spin states, high confinement, and simpler setup (no need to build "fancy" coils). The possibility of trapping atoms in different states is one of its most useful characteristics because it allows the study of a heterogeneous cloud. However there are some disadvantages. The two main problems are the energy shallowness of the trap, with depths usually around $100 \mu\text{K}$, and the small trap volume. This reflects in a very small transfer of atoms from the MOT ($\lesssim 10\%$). Despite those limitations M.D. Barrett *et. al.* have achieved BEC in ^{87}Rb using a QUEST trap formed by two crossing beams [130].

2.4 Evaporative Cooling

Sub-Doppler cooling make possible the achievement of temperatures of a few microkelvin in atomic gases. However, to study quantum degeneracy, it is also necessary to achieve very

high densities. Actually the physical parameter that should be maximized is the phase-space density (PSD): a measure of how many atoms per quantum state there are in the system. It is given by the following formula:

$$PSD = n_{av} \lambda_{dB}^3, \quad (2.62)$$

$$\lambda_{dB} = \sqrt{\frac{2\pi\hbar^2}{mk_B T}}, \quad (2.63)$$

where n_{av} is the average atomic density and λ_{dB} is the thermal de Broglie wavelength.

The transition to BEC in a non-interacting bosonic gas happens when $PSD \geq 2.612$ [6]. At this point the de Broglie wavelength is comparable to the interatomic distance; the particles begin to behave coherently as a single matter wave. This is a very interesting state of matter where macroscopic quantum effects can be observed. No wonder it has been sought after since the beginning of laser cooling. Unfortunately the maximum PSD that can be achieved in an optical molasses is of the order of 10^{-6} . The main limitation is the increase in light-induced losses when the cloud reaches high densities $\sim 10^{12} \text{ cm}^{-3}$.

A different cooling process is necessary to gain the remaining six orders of magnitude in PSD. Evaporative cooling is the solution [131]. It is a very simple physical process applicable to any bounded system of particles. If hot particles leave the system, the remaining ones will be colder after re-thermalization. This is how a hot cup of coffee gets cold and the same principle can be applied to trapped atoms. Actually what is used is forced evaporative cooling, where the binding energy of the system is gradually decreased. This way hot atoms are continuously expelled from the trap, cooling the cloud. This method was first proposed by H. Hess in 1985 as an efficient way to cool trapped atoms to reach BEC [132, 11]. Initially it was applied to trapped, polarized hydrogen [12], but BEC was first obtained when evaporation was used with laser cooled alkalies [55, 133]. Since then every single experiment that achieved quantum degeneracy used forced evaporative cooling.

2.4.1 Cold Collisions

Cold collisions play an important role during evaporation. Atoms trapped in a magnetic trap are submitted to two kinds of collision: elastic and inelastic. At low temperatures, the elastic collisions consist mainly of s-wave scattering and they are very important in re-thermalizing

the sample. Inelastic collisions consist mainly of collisions with background gas, hyperfine state changing collisions and three-body recombination. They usually lead to trap losses and it is important to minimize them in order to maximize our trap lifetime. Background collisions are one of our main concerns because they are always present, independently of the temperature and density. They can be minimized by creating an ultra-high vacuum environment with $P \lesssim 10^{-11}$ Torr. In our experiment the chamber where the atoms are trapped is isolated from the oven through a skimmer. This is a thin, long cylinder, similar to a straw, that creates a differential pumping between two chambers. Inside the trapping cell the pressure obtained was $P \sim 10^{-11}$ Torr, giving a 60 s trap lifetime.

Hyperfine state changing collisions are ground state collisions where either one or both atoms change its hyperfine state. If the new state is a high-field seeking one or if the kinetic energy gained by the pair is larger than the trap depth, the atoms are lost. They can be either spin exchange or dipolar relaxation. For doubly spin polarized atoms ($F = 2$, $m = 2$), spin exchange is forbidden due to angular momentum conservation. Our sample is prepared in this state, so we do not have to worry about this type of loss. Dipolar relaxation is the most important loss mechanism for ${}^7\text{Li}$ after background collisions. The loss rate per trapped atom can be expressed as [134]:

$$\frac{\dot{N}}{N} = -G_1 - 2G_2 n_{av} - \frac{8}{\sqrt{3}} G_3 n_{av}^2, \quad (2.64)$$

where G_1 is the background loss rate constant, G_2 is for the dipolar loss, and G_3 is for the three-body recombination. The Hulet group has measured $G_2 = (1.05 \pm 0.10) \times 10^{-14} \text{ cm}^3/\text{s}$ and $G_3 \leq 10^{-27} \text{ cm}^6/\text{s}$ for doubly spin polarized ${}^7\text{Li}$ atoms in a magnetic field of 1000 G [134]. Both loss mechanism only become relevant at high densities ($n \gtrsim 10^{12} \text{ cm}^{-3}$).

2.4.2 Elastic Collision Rate

From the previous discussion we can see that elastic collisions are good for evaporative cooling, while inelastic ones are bad. A critical parameter is the ratio between elastic and inelastic collision rates Γ_{el}/Γ_{in} . Since background collisions are the most important inelastic process at low densities, we can write $1/\Gamma_{in} = \tau$, where τ is the trap lifetime. At low temperatures (hundreds of microkelvin), it can be shown that only s-wave scattering is

relevant. In this case Γ_{el} is given by:

$$\Gamma_{el} = \sqrt{2} n_{av} \sigma v_{th}, \quad (2.65)$$

$$\sigma = 8\pi a^2, \quad (2.66)$$

$$v_{th} = \sqrt{\frac{8k_B T}{\pi m}}, \quad (2.67)$$

where σ is the elastic cross section between two identical bosons, a is the s-wave scattering length, v_{th} is the average thermal velocity and the factor $\sqrt{2}$ takes into account that what is important is the relative velocity between the two colliding atoms. A high value for the elastic collision rate ($\Gamma_{el} \geq 5 \text{ s}^{-1}$) is necessary to have an efficient evaporative cooling during forced evaporation. Otherwise the remaining atoms in the trap can not re-thermalize fast enough and atoms are only lost without any real gain in PSD. The product $\Gamma_{el}\tau$ corresponds to the number of elastic collisions during a trap lifetime. In order to reach degeneracy, we want $\Gamma_{el}\tau$ as large as possible. That means that a really good vacuum is necessary and the density has to be maximized at the start of the evaporation process. As an example it has been estimated that, in order to achieve BEC with 1% of the atoms left, we need $\Gamma_{el}\tau \sim 500$ [131].

2.4.3 Adiabatic Compression

There is a simple technique that can help to increase the elastic collision rate just before evaporation. It is called adiabatic compression and it consists in ramping up adiabatically the trapping potential. The phase-space density remains constant [135], while the density and the temperature increase. We can derive the scaling laws for this process. Suppose that the potential in d-dimensions $U(r) \propto r^{d/\delta}$ is raised by a factor α :

$$U' = \alpha U, \quad (2.68)$$

where the prime sign means the parameter in the compressed state. From the fact that the PSD (2.62) does not change and using Eq. (2.63), we obtain:

$$\frac{n'}{n} = \left(\frac{T'}{T} \right)^{3/2}. \quad (2.69)$$

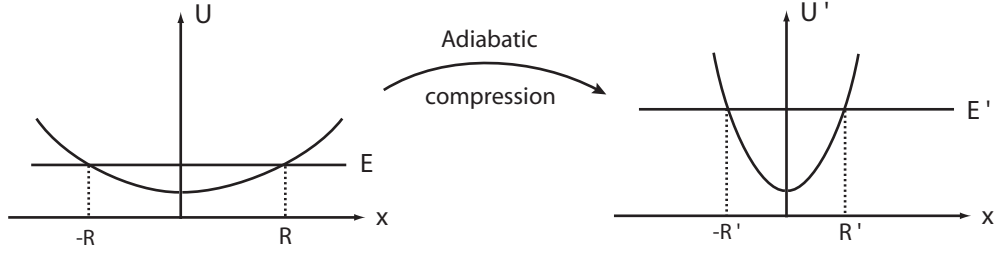


Figure 2.8: Trapping potential before and after an adiabatic compression. Notice that the total energy of the system increases.

Observing figure 2.8 we can obtain the following relation for the total energy:

$$\frac{E'}{E} = \alpha \left(\frac{R'}{R} \right)^{d/\delta}. \quad (2.70)$$

We know that $E'/E = T'/T$ from the equipartition theorem and $(R'/R)^d = V'/V = n/n'$ from the definition of density. Applying these relations in (2.70):

$$\frac{T'}{T} = \alpha \left(\frac{n}{n'} \right)^{1/\delta}. \quad (2.71)$$

From Eqs. (2.69) and (2.71) we can get the following scaling laws:

$$n' = \alpha^{\frac{3\delta}{2\delta+3}} n, \quad (2.72)$$

$$T' = \alpha^{\frac{2\delta}{2\delta+3}} T. \quad (2.73)$$

Using (2.72), (2.73) and (2.67) in (2.65):

$$\Gamma'_{el} = \alpha^{\frac{4\delta}{2\delta+3}} \Gamma_{el}. \quad (2.74)$$

For the Quadrupole (linear potential) $U(r) \propto r$, $d = 3$ and $\delta = 3$. The scaling laws are:

$$n' = \alpha n, \quad (2.75)$$

$$T' = \alpha^{2/3} T, \quad (2.76)$$

$$\Gamma'_{el} = \alpha^{4/3} \Gamma_{el}. \quad (2.77)$$

For the TOP (harmonic potential) $U(r) \propto r^2$, $d = 3$ and $\delta = 3/2$. The scaling laws are:

$$n' = \alpha^{3/4} n , \quad (2.78)$$

$$T' = \alpha^{1/2} T , \quad (2.79)$$

$$\Gamma'_{el} = \alpha \Gamma_{el} . \quad (2.80)$$

2.4.4 Forced Evaporation

Forced evaporation is done by gradually lowering the trap depth. The ramp down has to be at the right speed: neither too fast, otherwise the remaining atoms do not have time to re-thermalize, nor too slow, where more atoms are lost than necessary due to inelastic collisions. The right timing is defined by the elastic collision rate and it has been calculated that the number of elastic collisions necessary for thermalization is 2.7 [131, 136].

The two most common methods to lower the trap depth are by decreasing the trap strength or by radio frequency (RF) induced evaporation. The first method is more important for optical dipole traps where RF evaporation is not possible. It has the disadvantage that the confinement decreases, but it has already been used successfully in achieving BEC for the first time in an optical trap [130]. In a magnetic trap RF evaporation is the most popular method. By choosing the right frequency an RF source can be tuned with a transition to a high-field seeking state. Atoms that are flipped into this state are kicked out from the trap. The resonance frequency is proportional to the potential energy, and as a consequence the hottest atoms are eliminated first. The frequency necessary to flip the atoms between states (F', m'_F) and (F, m_F) is:

$$h\nu_{RF} = (m'_F g'_F - m_F g_F) \mu_B B(\vec{r}) + h\nu_0, \quad (2.81)$$

where $h\nu_0$ is the spacing between the hyperfine states at $B = 0$.

The potential energy of an atom in a magnetic trap is $U(\vec{r}) = m'_F g'_F \mu_B B(\vec{r})$, hence the condition that an atom is kicked out is that its total energy obeys:

$$\frac{E}{h} \geq \frac{m'_F g'_F}{m'_F g'_F - m_F g_F} (\nu_{RF} - \nu_0), \quad (2.82)$$

The depth of the trap is now defined by (2.82) and if we lower ν_{RF} at the right pace, we should be able to gradually cool the cloud.

There can only be a gain in phase-space density if the loss in the number of atoms is compensated by a sufficient decrease in temperature. This only happens if $\Gamma_{el}\tau$ is large enough at the start of the evaporation. A good start is around $\Gamma_{el}\tau \geq 100$. In practice what it is needed is a large lifetime $\tau \geq 60$ s and a large density in the magnetic trap. This is why it is important to capture a large number of atoms in the MOT ($N \geq 10^8$). We have implemented the transverse cooling with the objective of having enough atoms in the MOT to generate an efficient evaporation.

Chapter 3

MOT Loading Techniques

Since the MOT can only capture atoms up to the capture velocity v_c , that is much smaller in general than the average thermal velocity of the atoms, it is necessary to choose an appropriate means to load the trap. The methods available can be split in two categories depending if they change or not the velocity distribution of the atoms. Cooling methods like frequency chirping and Zeeman slower use a counter-propagating laser beam that narrows and cools the velocity distribution. As a consequence the number of atoms below v_c increases, improving the MOT loading. Non-cooling methods are represented by the vapor cell and the frequency spread light (a.k.a. white light). In this case the laser beam is spread in frequency space and the atoms captured are from the low-velocity tail of the Maxwell-Boltzmann distribution. The other technique that helps improving the loading of the MOT is transverse cooling. Its main contribution is by increasing the density of the atomic beam. This method was very important in our experiment and it will be discussed in detail in chapter 5. What mainly differentiate these techniques is how they deal with two common problems when cooling atoms. These problems were identified since the first experiments with laser cooling [69]. They are the optical pumping to dark states and the Doppler shift.

Since no atom is a perfect two-level system, after a few cooling cycles it can be optically pumped to a hyperfine state that is off-resonance with the cooling light. As we can see in Fig. 3.1a, even if the laser frequency is in resonance with the transition ($F = 2 \leftrightarrow F' = 3$) and the light is σ^+ polarized such as that it can only decay back to $F = 2$, the separation of

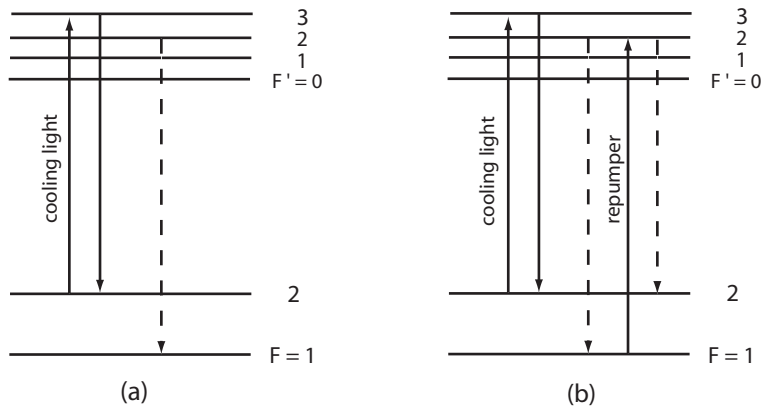


Figure 3.1: In figure (a) the atom is optically pumped to $F = 1$, not being able to interact with the cooling light anymore. In figure (b) a repumper has been added bringing the atom back to the cooling cycle.

the excited hyperfine states can be comparable to the natural linewidth (see appendix B for the case of ${}^7\text{Li}$), making it possible a transition to $F = 1$. In such a case the atom would be cooled only for a very short time; the average time it takes to be optically pumped to $F = 1$. The easiest solution is to add a weak, repumping beam that can excite the atoms back from this state. This way the atom stays in the cooling cycle for as long as the repumping light is on.

The Doppler shift also limits the cooling because initially only the fraction of atoms with the right velocity will be on resonance with the cooling light. To make things worse, when the atoms are decelerated, their Doppler shift changes and they get off-resonance, not being cooled anymore. So even if we have a repumper, the atom will eventually become off-resonance with the light and the cooling efficiency is again compromised.

In the following sections I will analyze in more detail how each technique deals with these problems and also comment on the advantages and disadvantages of each one of them.

3.1 Frequency Chirping

The easiest way to cool a beam of atoms is by using a counter-propagating, red-detuned laser beam. However when the velocity decreases by $\Delta v \sim \Gamma/k$, where Γ is the natural linewidth and k is the wave-vector magnitude, the atoms begin to get out of resonance due to the Doppler shift and their interaction with the light decreases. Already in 1976 V. Letokhov *et. al.* noticed this problem [137] and proposed that the laser frequency should vary in order to keep in resonance with the atoms. Using Eq. (2.4) we can find a relation that the frequency has to obey for this to happen [138]:

$$\omega_L(t) = \omega_0 + \Delta + \vec{k} \cdot \vec{v}(t), \quad (3.1)$$

$$\frac{d\omega_L}{dt} = \vec{k} \cdot \frac{d\vec{v}}{dt} = \frac{\vec{k} \cdot \vec{F}}{m}, \quad (3.2)$$

where we have imposed Δ to be constant and $\vec{F}(\vec{v})$ is given by (2.15) in the low velocity limit. The maximum scan rate is imposed by $F_{max} = \hbar k \Gamma / 2$ and for ${}^7\text{Li}$ it is $\dot{\nu}_{max} = 4.70 \text{ GHz/ms}$. The optical pumping problem is solved by adding a repumper beam that is also chirped.

The main advantages of this method are that it can generate a large velocity compression and it does not require any additional fields. Its main disadvantages are that it can only produce pulsed beams of cold atoms and it can be technologically challenging to scan the laser frequency at the right rate.

3.2 Zeeman Slower

This technique, first developed by W. Phillips and H. Metcalf [40], is similar in principle to frequency chirping. Instead of changing the light frequency, we change the atomic frequency by using a magnetic field. A counter-propagating laser beam to cool the atoms is still used, but now there is an inhomogeneous magnetic field $B(z)$ that keeps the atoms on resonance (see Fig. 3.2). The detuning is given by:

$$\Delta = \omega_L - \omega_0 + kv(z) - \eta B(z), \quad (3.3)$$

where the term $\eta B(z)$ is the linear Zeeman shift. The resonance condition is satisfied if:

$$\eta B(z) = kv(z). \quad (3.4)$$

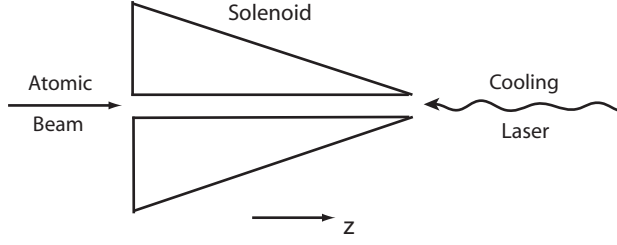


Figure 3.2: Schematics of the Zeeman slower. The solenoid has more turns at the entrance to have a higher field at that point. The solenoid length depends on the final velocity chosen for the atoms.

If the atom has an initial speed v_0 and a uniform deceleration a , $v(z)$ is given by:

$$v(z) = \sqrt{v_0^2 - 2az} = v_0 \sqrt{1 - 2az/v_0}. \quad (3.5)$$

Using (3.5) in (3.4) we have the formula for the magnetic field:

$$B(z) = B_0 \sqrt{1 - x}, \quad (3.6)$$

$$x = 2az/v_0, \quad (3.7)$$

where B_0 is the field necessary to keep the atoms with $v = v_0$ on resonance. All the atoms with $v \leq v_0$ will be slowed down to a final velocity determined by the solenoid length and field gradient.

The existence of a maximum acceleration during the cooling also imposes a limit on the Zeeman slower similar to the scan rate limit (3.2) in frequency chirping. Writing (3.3) as $\Delta = \nu_L - \nu(z) + v(z)/\lambda$ and taking its derivative with respect to t ($d\Delta/dt = 0$), we have:

$$\frac{d\nu}{dB} \frac{dB}{dz} v = \frac{a}{\lambda} \leq \frac{a_{max}}{\lambda}, \quad (3.8)$$

where $a_{max} = F_{max}/m$. The condition (3.8) imposes a limit on the maximum gradient dB/dz that we can have at each point in the solenoid.

In the case of the Zeeman slower the optical pumping problem is avoided by making use of the strong bias magnetic field. The hyperfine states are well separated due to the Zeeman shift and by using a circularly polarized cooling beam the selection rules keep the atom oscillating in a closed 2-level state ($F = 2$, $m = 2 \leftrightarrow F = 3$, $m = 3$).

Atoms in the Zeeman slower are not only compressed in velocity space, but also spatially. This is because faster atoms are decelerated more, being bunched together with slower atoms. This generates a continuous flow of cold and compressed atoms. Another advantage is the necessity of only one frequency to keep the atoms in the cooling cycle. However the existence of the magnetic field can be a disadvantage because stray fields might be a source of error for some experiments.

3.3 Vapor Cell

The concept of a vapor cell was first proposed by the group of C. Wieman [139, 140] and it is based on the fact that there are enough atoms in the low-velocity range of a room-temperature atomic distribution to load a MOT without cooling. For example, considering a MOT capture velocity of 15 m/s and a cesium vapor at a temperature of 300 K, one atom in 10^4 is slow enough to be captured [139].

The way it works is very simple. A glass cell has a “cold finger” attached to it and filled up with the material that we want to trap. By varying the temperature of the “cold finger”, the vapor pressure in the cell can be changed. A common value for loading the MOT is 10^{-8} Torr. After adjusting the pressure we just have to turn on the MOT to load it (see Fig. 3.3). Later on the pressure can be decreased to increase the trap lifetime and an optical molasses can be used to cool the cloud. The optical pumping problem is dealt with by using a repumper beam or an additional frequency sideband in the MOT beams.

The total number of atoms loaded in the MOT is determined by the equilibrium between the capture rate and losses due to collisions with the background gas. It is interesting to note that the steady-state value is independent of the pressure and is given by [140]:

$$N_{MOT} = 0.1 \frac{A}{\sigma} \left(\frac{v_c}{v_{th}} \right)^4, \quad (3.9)$$

where A is the surface area of the trap volume, σ is the elastic cross-section between the

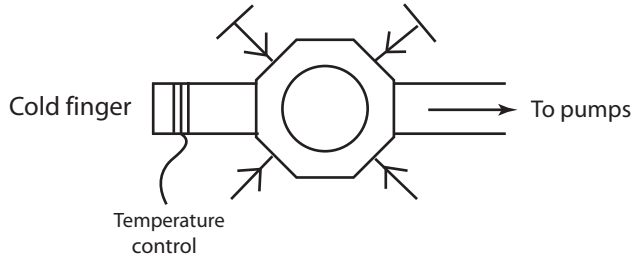


Figure 3.3: Design of a vapor cell. The “cold finger” temperature can be controlled using a thermocouple cooler. The MOT coils are not shown in this picture.

atoms being trapped (2.66) and v_{th} is the average thermal velocity (2.67).

The main advantage of the vapor cell is its simplicity. There is no need to use an additional cooling beam or to build a solenoid. Just by using the usual MOT configuration we are able to trap atoms. The disadvantage is that there is a trade-off between the loading time and trap lifetime. A higher vapor pressure not only decreases the loading time but also the trap lifetime and this is not good for evaporative cooling. Hence it is necessary to optimize the vapor pressure (by modulating it for example) in order to have a reasonable repetition rate for the experiment and a trap lifetime long enough to evaporate.

3.4 Frequency Spread Light

This is a similar method to the vapor cell, where atoms are also captured from the low-velocity range without any previous cooling. The crucial difference is that now the light is frequency spread (also called a comb beam). In this case the light is on resonance with a larger number of atoms, increasing the capture velocity and the loading rate.

The loading rate can be expressed as $R \propto v_c^4 d^2$, where d is the comb beam diameter [88]. The capture velocity is proportional to the beam power, therefore a comb beam with a large diameter and high power is desirable in order to capture a large number of atoms in the MOT. It is also important to have a large intensity ($I > 20 \text{ mW/cm}^2$ in the case of ${}^7\text{Li}$) to

recapture atoms lost due to fine-structure changing collisions that can be induced by the near-resonant light [88]. If the intensity is not high enough, the comb light might actually induce a trap loss, decreasing the loading rate.

In our experiment we have used frequency spread light to load the MOT. The comb beam has a waist of 7.4 mm and a maximum power of 300 mW. This gives a peak intensity of 350 mW/cm², high enough to recapture any atom lost due to fine-structure changing collisions. The frequency spread is generated by double passing the beam in an Electro Optic Modulator (EOM) at 11.7 MHz. This frequency was chosen because it is close to twice the natural linewidth (5.9 MHz) in order that the atoms see a continuous frequency band. The frequency ranges from 10 MHz to 127 MHz below the cooling frequency. We have also added a sideband at 816 MHz using an EOM to avoid the problem of optical pumping to the F = 1 hyperfine state. More details regarding the comb will be given in section 4.1.

This method has an advantage over the vapor cell. It does not require keeping a partial vapor pressure in the cell to load the MOT. This condition not only limits the trap lifetime, but it can also be difficult to implement for elements like lithium that require high temperatures to vaporize ($T \sim 300^{\circ}\text{C}$ for Li). The frequency spread has the same advantages as the vapor cell when compared to frequency chirping and Zeeman slower. It has no necessity for an additional cooling beam or magnetic field. The configuration is the same as a traditional MOT with the addition of frequency spread beams. The main disadvantage is that high power beams are necessary in order to have a good loading rate. In our experiment, for example, we had to use dye lasers, that are less stable and reliable than diode lasers, because we needed over 500 mW at the laser output to trap enough atoms in our MOT (around 10^8).

Chapter 4

Cooling and Trapping ^7Li

A standard MOT was used to cool and trap ^7Li . The loading method employed frequency spread light to capture atoms in the low velocity tail of the Maxwell-Boltzmann distribution. Using this process 2×10^8 atoms were trapped with a temperature of $\sim 300 \mu\text{K}$. In the following sections I will analyze in details the spectrum of the laser light, the MOT parameters, how we measured the number of atoms and the temperature and the process of transferring atoms from the MOT to the magnetic traps.

4.1 Laser Spectrum

The energy level diagram for ^7Li is shown in appendix B. The cooling transition is $F_1 = 2 \leftrightarrow F_3 = 3$ at 670.962 nm and its natural linewidth $\Gamma/2\pi$ is 5.9 MHz. The excited state has a lifetime of 27.2 ns. Notice that the separation between the excited hyperfine states is comparable to the linewidth. During cooling and trapping a sideband close to 803.5 MHz is necessary to avoid optical pumping to $F_1 = 1$.

The laser is generated using a Coherent dye laser model 899. It is locked at the $F_1 = 2 \leftrightarrow F_3 = 3$ transition ($\lambda = 670.96$ nm) using a standard saturated absorption cell. Figure 4.1 shows the main optical components before the laser goes to the MOT. First a small fraction ($\sim 0.1\%$) goes to the lock cell, then an EOM at 816 MHz generates the re-pumping sideband. The optimal power ratio that maximizes the number of atoms trapped is 57% in the carrier and 21.5% in each sideband (+ 816 MHz and - 816 MHz). A beam

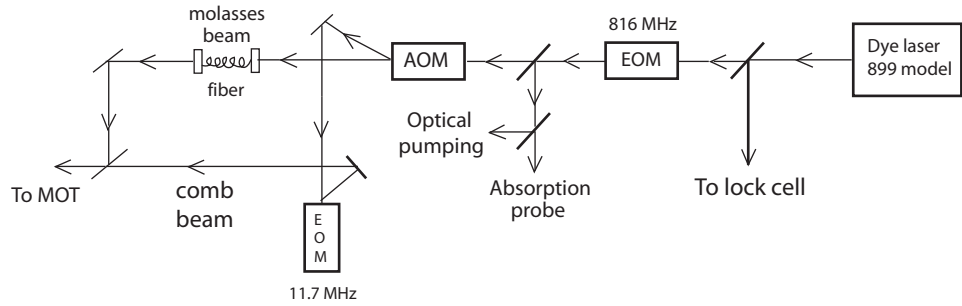


Figure 4.1: Main optical components on the laser preparation for trapping and cooling in the MOT

splitter (BS) reflects $\sim 1\%$ of the power to be used as an optical pumping beam and absorption probe. An acoustic-optic modulator (AOM) splits the beam in two: a molasses and a comb. The power ratio between the two depends on the voltage applied to the AOM. During the MOT loading phase all the power is in the comb. This beam is frequency spread by double passing it through an EOM at 11.7 MHz. This value was chosen such that it is close to twice the natural linewidth of the cooling transition ($\sim 2 \times 5.9$ MHz). This way the atom sees a continuous spectrum of light while being cooled down. The double pass generates 5 sidebands on each side of the carrier. It is important to note that in order to maximize the capture of atoms in the MOT, it is necessary to have a large amount of power in the comb with a large diameter [88]. The usual output power of the dye laser is 650 mW and this gives around 300 mW in the comb with a waist of 7.4 mm. Any additional power does not give an increase in the number of atoms because it is already limited by light assisted losses in the MOT.

The molasses beam is used for cooling and detection. Its waist is less than half of the comb at 3.2 mm. For cooling only a small amount of power ($300 \mu\text{W}$) is needed during 5 ms at most. For detection full power in the molasses (22 mW) is used to saturate the transition. The molasses light passes through a fiber optics (50% transmission efficiency) to fix its position from day-to-day operation. The molasses and comb are rejoined on a BS just before being split into 3 beams with equal power that will form the MOT.

The molasses and the comb have different spectrum. Both have sidebands at ± 816 MHz, but the molasses is single-frequency, while the comb, as the name already says, is multi-frequency. The following equations show the relation between their spectra and the cooling frequency:

$$\nu_{mol} = \nu_0 - \Delta_{mol}, \quad (4.1)$$

$$\nu_{comb}^i = \nu_0 - \Delta_{comb}^i, \quad (4.2)$$

$$\Delta_{mol} = \delta_{lock} - \delta_{AOM} - \xi, \quad (4.3)$$

$$\Delta_{comb}^i = \delta_{lock} - \xi + i \times \delta_{EOM}, \quad i \in \{-5, -4, \dots, 4, 5\}, \quad (4.4)$$

where ν_0 is the cooling frequency, $\delta_{lock} = 76.5$ MHz is the lock AOM frequency, $\delta_{AOM} = 62.9$ MHz is the molasses-comb AOM frequency, $\xi = (8 \pm 1)$ MHz is a systematic frequency shift and $\delta_{EOM} = 11.7$ MHz is the comb EOM frequency. Using these values in (4.3) and (4.4) we get:

$$\Delta_{mol} = 5.6 \text{ MHz} \cong 1(\Gamma/2\pi), \quad (4.5)$$

$$\Delta_{comb}^i = (68.5 + i \times 11.7) \text{ MHz}, \quad i \in \{-5, -4, \dots, 4, 5\}, \quad (4.6)$$

$$\Delta_{comb} = \{1.7, 3.7, 5.7, 7.6, 9.6, 11.6, 13.6, 15.6, 17.5, 19.5, 21.5\} \text{ } (\Gamma/2\pi). \quad (4.7)$$

Figure 4.2 shows graphically the spectrum of the comb and the molasses. Notice that both are red-detuned relative to the cooling transition and that the highest frequency component of the comb is very close to the molasses. It is important to make sure that this term is not blue-detuned, otherwise it would heat up the atoms, making the MOT less efficient.

4.2 MOT configuration

The MOT is of the standard type following the same configuration as the first one made by S. Chu [54]. It consists on three retro-reflected, circularly polarized laser beams plus a Quadrupole field. A significant difference in our MOT is that we use frequency spread beams instead of single frequency ones. The configuration of our apparatus is shown in figure 4.3.

At room temperature lithium is a soft, silvery metal. Its melting point is at 180 °C, hence high temperatures are needed to produce a strong atomic beam. A sample of ${}^7\text{Li}$

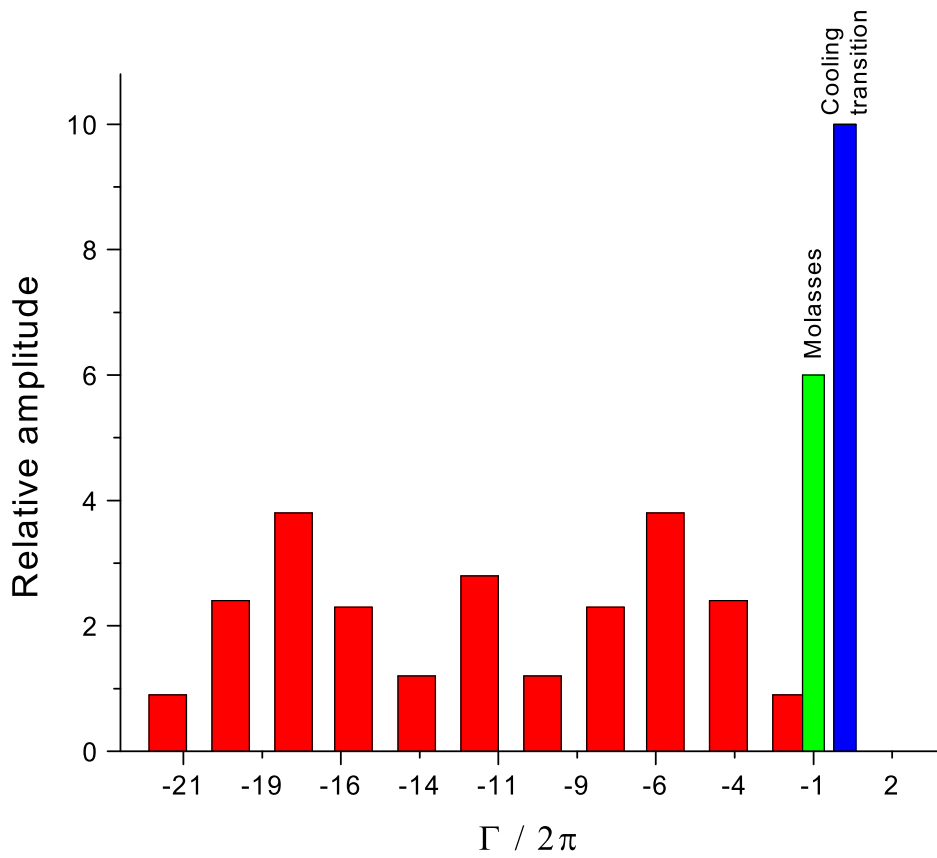


Figure 4.2: The horizontal axis shows the detuning in linewidth relative to the cooling transition. The vertical axis indicates the relative amplitudes among the comb components. The amplitude of the molasses and the cooling frequency are arbitrary.

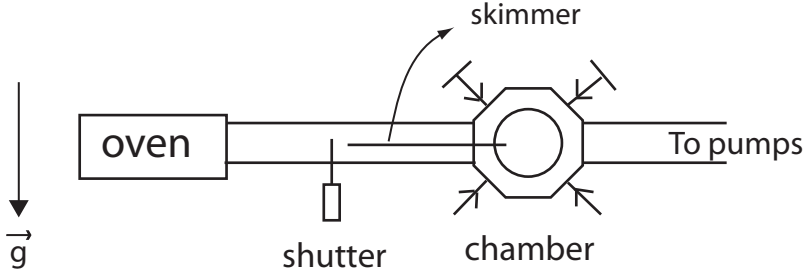


Figure 4.3: Apparatus used for the MOT. The arrow indicates the direction of gravity. The shutter is closed after loading the MOT to avoid collisions of the incoming atomic beam with the cloud.

with 99.9% purity is used and the oven is heated up to $350\text{ }^{\circ}\text{C}$ to produce a bright atomic beam. The chamber where the MOT is created is an octagon made of stainless steel (see Figs. 4.4 and 4.5). It has six windows with anti-reflecting coating. Inside the chamber it is desirable to create an ultra-high vacuum environment ($P \lesssim 10^{-11}\text{ Torr}$) to have a very long trap lifetime ($\tau \geq 60\text{ s}$). With this purpose the whole system was baked at $T \sim 200\text{ }^{\circ}\text{C}$ for 3 days and an ion pump and a titanium sublimation pump were attached to the chamber. A skimmer was placed between the oven and the chamber creating a differential pumping. At the entrance of the skimmer there is a shutter that can shut off the atomic beam, avoiding atomic collisions with the cloud after loading the MOT.

The loading of the MOT is very simple. With the shutter open and the oven at $350\text{ }^{\circ}\text{C}$, the comb beam is turned on for 20 s. The loading rate is $R \sim 1 \times 10^7\text{ s}^{-1}$ and at the end $N \sim 2 \times 10^8$ atoms are trapped in the MOT. The comb waist w is $(7.41 \pm 0.06)\text{ mm}$ and its optimal power P is 80 mW on each of the three beams, giving a peak intensity of $I_{\text{comb}} = 2P/\pi w^2 = 93\text{ mW/cm}^2$ per beam. With these parameters and assuming $I_{\text{sat}} = 7.7\text{ mW/cm}^2$, the capture velocity of the MOT was calculated as $v_c = 127\text{ m/s}$. This

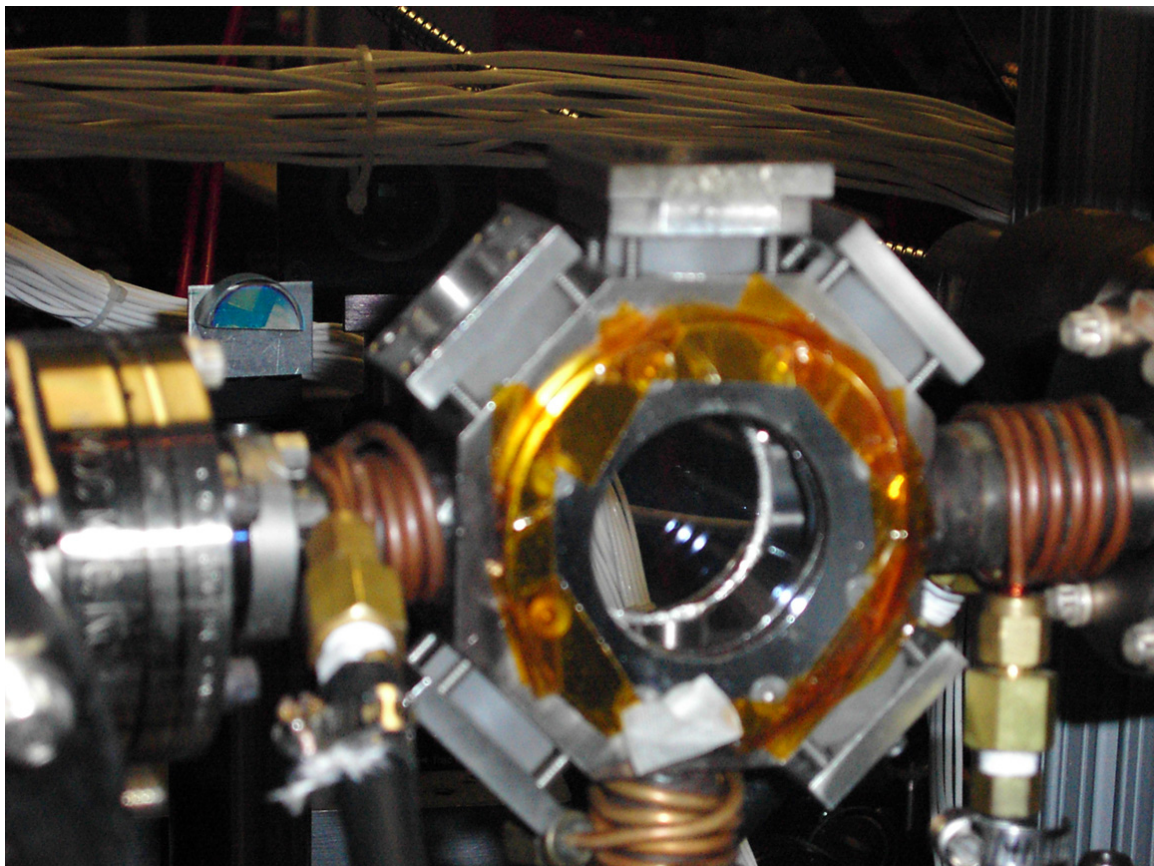


Figure 4.4: In this picture we can see the chamber with its six windows. The largest one is perpendicular to the axis of the Quadrupole coils. The coils are not shown.

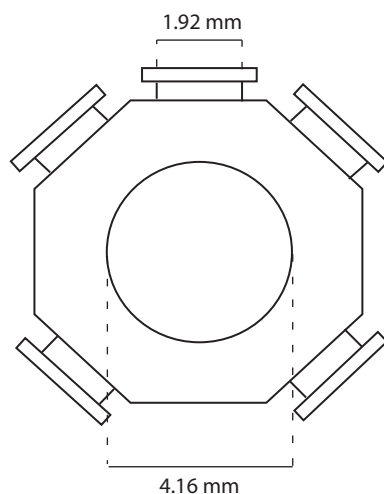


Figure 4.5: The chamber and its six windows with its respective diameters. The axial direction of the Quadrupole trap is perpendicular to the largest window.

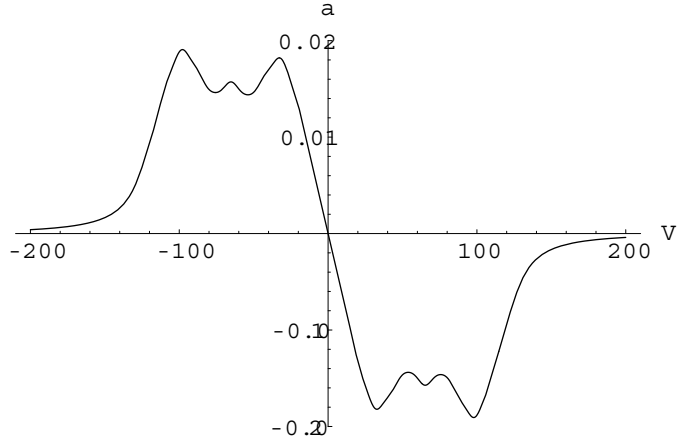


Figure 4.6: Velocity dependence on the acceleration of an atom in the MOT. The spread in velocity reflects the frequency spread of the comb light. The capture velocity is 127 m/s with the comb, compared with 4 m/s for a monochromatic beam.

is the maximum velocity an atom can have to be captured. Figure 4.6 shows how the atomic acceleration depends on its velocity. Comparing with Fig. 2.1, we can see how the comb beam spread the capture range of the scattering force, dramatically improving the loading of the MOT when compared to a single monochromatic beam. The optimal Quadrupole radial gradient for loading is 21 G/cm. The spectrum of the comb is given in Fig. 4.2.

4.3 Optical Molasses Cooling

After loading the MOT, the comb is turned off, the oven shutter is closed and the molasses beam is turned on for a short period of time. By creating an optical molasses the atoms are cooled and the cloud density increased. This will be important later on the atoms are

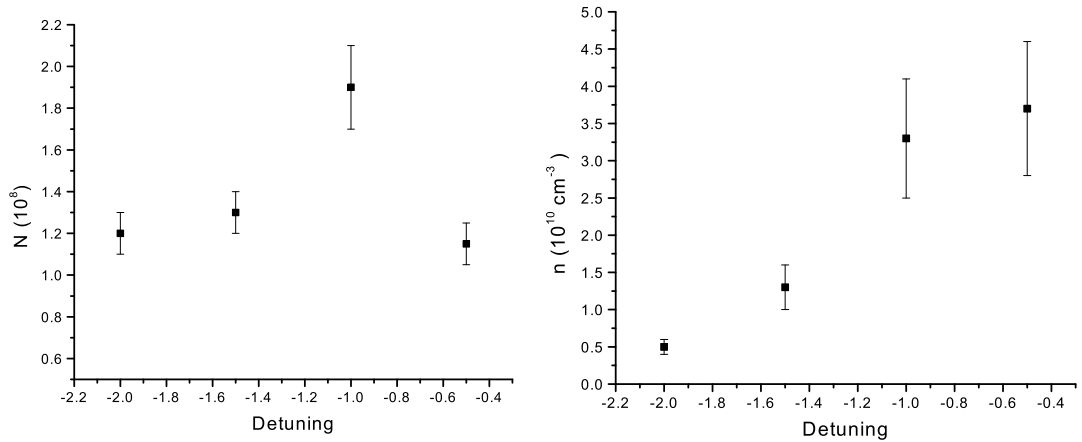


Figure 4.7: Number of atoms and density of the cloud after optical molasses cooling. A detuning closer to resonance compresses more the cloud, but decreases the number of atoms in the trap due to light-induced losses.

transferred to a magnetic trap. The molasses waist is (3.2 ± 0.1) mm and the power is only $80 \mu\text{W}$ per beam. This gives an intensity of $I_{mol} = 0.51 \text{ mW/cm}^2$ per beam. The light is red-detuned by one linewidth (see Fig. 4.2). This is the detuning that gives the best compromise between atom loss and compression as we can see in Fig. 4.7. Too close to resonance the cloud is compressed more, but loses more atoms due to light-induced losses. As we can see in Fig. 4.8, a long cooling time loses up to 60% of the atoms due to light-induced losses. A good time is 0.5 ms. One more important thing to notice is that the Quadrupole field is left on during cooling with the same value as during loading. If it is turned off some atoms drift away, while if it is left on the cooling is not affected.

4.4 Number of Atoms and Temperature Measurement

The number of atoms is measured using fluorescence. The molasses beam is turned on for an interval of time t_D , with zero magnetic field, and the number of fluorescent photons is

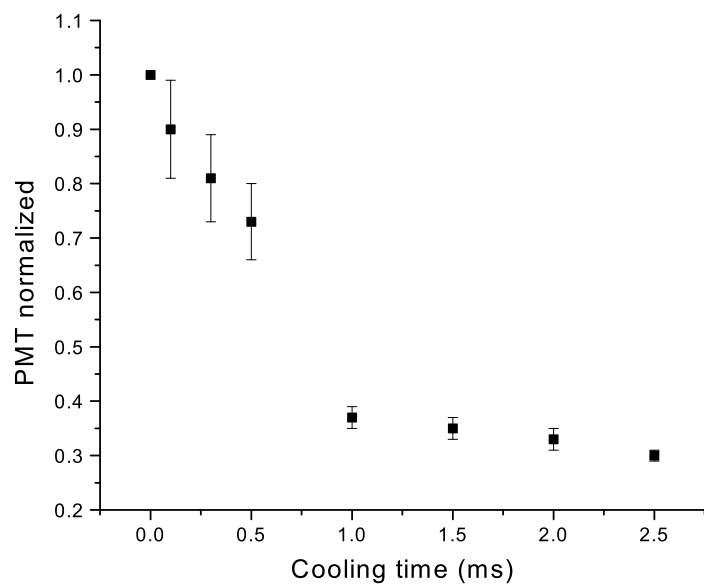


Figure 4.8: Number of atoms left in the trap after cooling. Notice that above 0.5 ms there is a sharp decrease. These atoms are lost due to light-induced losses.

measured using a CCD camera or a photomultiplier tube (PMT). The number of atoms N is directly proportional to the number of photons emitted per unit of time. This relation is expressed as:

$$\phi = \gamma N, \quad (4.8)$$

where γ is the atomic scattering rate. As we have seen in section 2.2, γ for a 2-level atom is given by:

$$\gamma = \frac{\Gamma}{2} \frac{S}{1+S}, \quad (4.9)$$

where S is the saturation parameter (2.8). If the intensity of the molasses is large enough ($I_{mol} \gg I_s$), we have $\gamma = \Gamma/2$. The parameter ϕ_{exp} is measured by the camera or PMT and it can be expressed as:

$$\phi_{exp} = \left[\frac{\Omega}{4\pi} \prod_i T_i \right] \phi, \quad (4.10)$$

where Ω is the solid angle defined by the collecting lens and T_i are the transmission coefficients of each optical element between the cloud and the detector. Using (4.8) and (4.9) in (4.10) we have an experimental formula for the number of atoms:

$$N = \frac{8\pi}{\Gamma\Omega\epsilon} \frac{\phi_{exp}}{\prod_i T_i}, \quad (4.11)$$

where $\epsilon = S/1+S \in [0, 1]$ is the degree of saturation of the transition.

In practice what is measured is the power of the light emitted. This relates to ϕ_{exp} as:

$$\phi_{exp} = \frac{P_{meas}}{hc/\lambda}, \quad (4.12)$$

where hc/λ is the energy of one photon. In this formula h is the Planck constant, c is the speed of light and λ is the wavelength. The power for the camera is given by:

$$P_{meas} = \frac{E_{meas}}{t_D}, \quad (4.13)$$

where t_D is the detection time. The energy E_{meas} is measured by the camera and it is calibrated using a power meter. For a PMT we calibrate $V_{PMT} \propto P_{meas}$, where V_{PMT} is the output voltage of the PMT. Using these relations in (4.11), the final formula for the number of atoms is obtained:

$$N = \frac{8\pi}{\Gamma\Omega\epsilon} \frac{E_{meas}}{(hc/\lambda) \prod_i T_i t_D} \text{ for the camera,} \quad (4.14)$$

$$N = \frac{8\pi}{\Gamma\Omega\epsilon} \frac{P_{meas}}{(hc/\lambda) \prod_i T_i} \text{ for the PMT,} \quad (4.15)$$

where all the terms can be measured in the laboratory. The degree of saturation ϵ is equal to 1 if we saturate the transition. The total power in all three molasses beams at detection is 30 mW. Given a waist of 3.2 mm, and the fact that 21.5% of the power is lost in a non-resonant sideband (- 816 MHz), we have $I_{mol} = 146 \text{ mW/cm}^2$ at detection. Considering an effective saturation intensity of $I_s^{eff} = 7.7 \text{ mW/cm}^2$ (see section 5.2), we have $I_{mol}/I_s^{eff} = 19 \gg 1$. So the use of $\epsilon = 1$ is justified.

The definition of temperature in a sample of laser cooled atoms is based on the fact that the atoms have a Maxwell-Boltzmann velocity distribution. The temperature is given by the spread in velocity Δv :

$$f(v)dv = \frac{1}{\sqrt{2\pi}\Delta v} e^{-v^2/2\Delta v^2} dv, \quad (4.16)$$

$$\frac{k_B T}{m} \equiv \Delta v^2, \quad (4.17)$$

where m is the atomic mass.

There are different ways to measure Δv^2 experimentally. In our case we have used ballistic expansion. It consists in releasing the atoms from the trap and observing its free expansion. The spatial profile is a Gaussian with a spread Δx that increases linearly with time:

$$g(x, t)dx = \frac{1}{\sqrt{2\pi}\Delta x(t)} e^{-x^2/2\Delta x^2(t)} dx. \quad (4.18)$$

The value of Δx is measured for different times t using the camera. By plotting Δx^2 vs. t^2 , Δv^2 can be obtained from the slope and the temperature from (4.17).

One main source of error for this type of measurement is the existence of a force acting on the atoms during the expansion. Even after the Quadrupole field is turned off, there is still a gradient due to eddy currents in the apparatus. Also there can be a background magnetic field, especially the one generated by the strong permanent magnet in the ion pump. They can affect the cloud motion, distorting the temperature measurement.

In figure 4.9 Δx^2 vs. t^2 is plot for the free expansion of 1.2×10^8 atoms released from the MOT after 5 ms molasses cooling. The molasses was red-detuned by one linewidth. From the linear fit in Fig. 4.9 we have $\Delta v_r^2 = 0.324 \text{ m}^2/\text{s}^2$ and $\Delta v_z^2 = 0.235 \text{ m}^2/\text{s}^2$, where r and z correspond to the radial and axial direction in the trap. Using these values on Eq. (4.17)

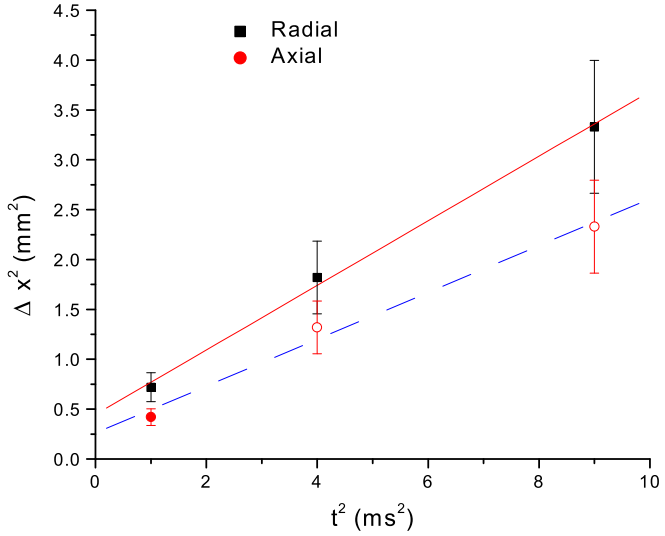


Figure 4.9: Free expansion of a cloud released from a MOT after 5 ms cooling time. The radial and axial terms correspond to directions along the Quadrupole field.

and knowing that $m_{Li}/k_B = 842 \mu K s^2/m^2$, we get:

$$T_r = 273 \mu K, \quad (4.19)$$

$$T_z = 198 \mu K. \quad (4.20)$$

Both temperatures are not equal but this is expected. As I have noticed before, measurements using free expansion are not very accurate. There are many sources of errors, especially stray magnetic field gradients from external sources (ion pump, eddy currents, etc) that can distort the expansion in one direction. The MOT temperature can be represented as being the average of (4.19) and (4.20):

$$T_{MOT} = 235 \pm 50 \mu K. \quad (4.21)$$

4.5 Transfer to a Magnetic Trap

After cooling the atoms in the MOT they are transferred into a magnetic trap. Inside a trap the cloud can reach much higher densities and lower temperatures using techniques

of evaporative cooling. In a MOT those values are limited by light-induced losses and the re-scattering of light as seen in section 2.3.2. In our experiment we have worked with two different magnetic traps: a Quadrupole and a TOP.

4.5.1 Optical Pumping

In a magnetic trap only low-field seeking states can be trapped. We can see in Fig. 4.10 that only the states ($F = 2, m = 2$), ($F = 2, m = 1$) and ($F = 1, m = -1$) have this property. It is also interesting to have a polarized sample, that means, having all the atoms in the same hyperfine state. This way inelastic losses due to collisions of atoms at different states are minimized and the number of atoms transferred to the trap is increased.

The atoms are polarized using optical pumping. Just after the molasses cooling, a beam is shined on the cloud for 0.3 ms with $200 \mu\text{W}$ (its waist is similar to the molasses). At the same time a bias magnetic field generated by a small coil is turned on ($B_{bias} \sim 15 \text{ G}$). The pumping beam has the appropriate circular polarization to optically pump the atoms to ($F = 2, m = 2$). The power on the 816 MHz sideband is also increased to its maximum value (33%) to optimize the pumping. The timing sequence from loading to transferring to the Quadrupole is shown in Fig. 4.11. The transfer efficiency is 35% to the Quadrupole trap with the optical pumping and 10% without it. The TOP has also a similar value.

4.5.2 Trapped State

The main reason why we chose to trap atoms in the ($F = 2, m = 2$) state instead of ($F = 1, m = -1$) is because of its larger scattering cross section. An elastic collision between two cold atoms is a low energy process and it can be shown that only the s-wave component of the scattering length is important. The scattering length is a measure of the interaction between two atoms. This quantity is a function of the atomic state, among other things, and it is much larger for a ${}^7\text{Li}$ atom in the ($F = 2, m = 2$) state than in the ($F = 1, m = -1$). For a doubly spin polarized atom it is $a_{2,2} = -27.6 a_0$ and for an atom in the ($F = 1, m = -1$) state it is $a_{1,-1} = 5.3 a_0$, where a_0 is the Bohr radius [141]. The elastic cross section (2.66) is $(-27.6/5.3)^2 \cong 27$ times larger for atoms in ($F = 2, m = 2$) state, so the elastic collision rate (2.65) is larger by the same amount. As a consequence it

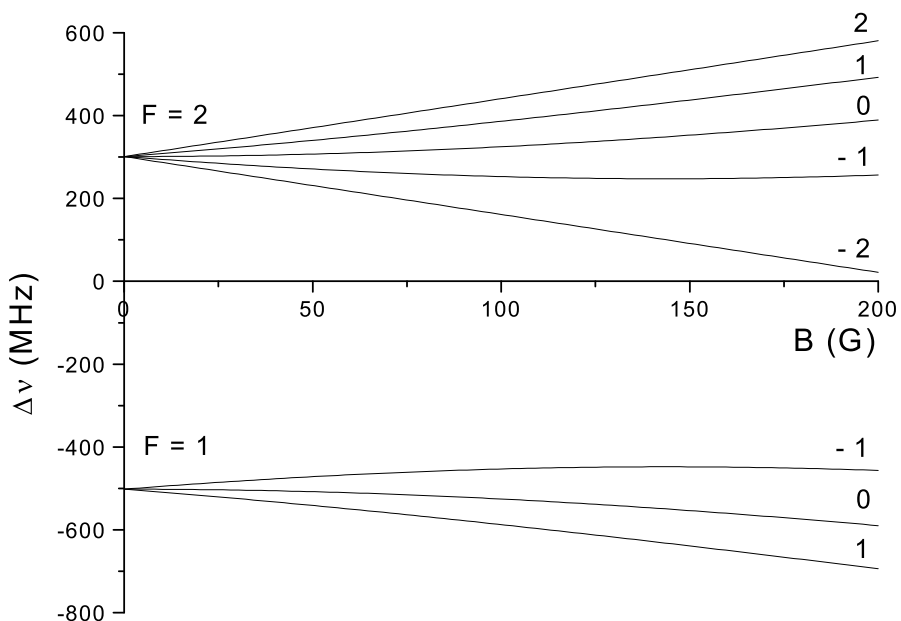


Figure 4.10: Dependence of the ground state hyperfine levels of ${}^7\text{Li}$ with the magnetic field. The vertical axis gives the energy difference in frequency units. Notice that ($F = 1, m = -1$) becomes a high-field seeking state for $B > 140$ G.

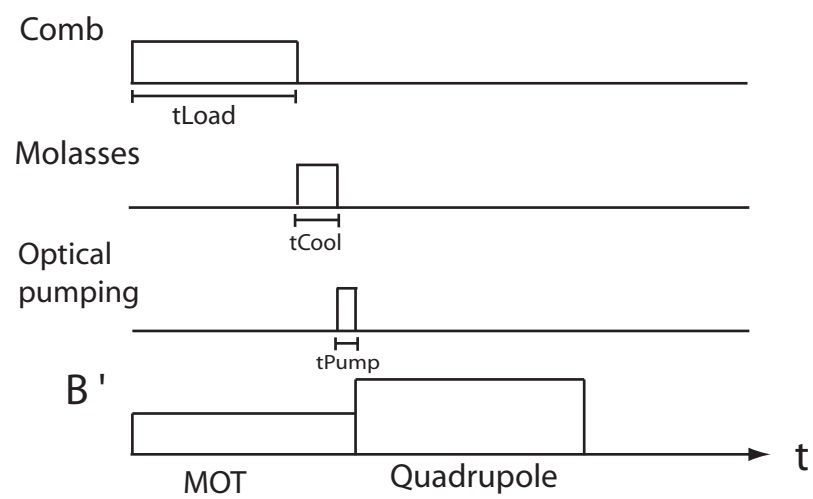


Figure 4.11: Timing sequence from loading the MOT to transferring to a Quadrupole trap.
Typical values are $t_{Load} = 20$ s, $t_{Cool} = 1$ ms, and $t_{Pump} = 0.3$ ms.

is much easier to evaporate doubly spin polarized atoms. An interesting observation is that the interaction between atoms in ($F = 2$, $m = 2$) states is attractive, as shown by the minus sign in its scattering length. This imposes a limit in the number of atoms that can condense in a BEC. Since the atoms attract each other in this state, they are in a metastable state during BEC and above a certain number of atoms the cloud collapses [142, 143]. For ${}^7\text{Li}$ this limit is around 1400 atoms [144, 145].

4.5.3 Mode Matching

Before transferring the cloud from the MOT to a magnetic trap, it has to be decided how strong the trap should be. Since we are interested in doing evaporative cooling, the mode matching condition is the most appropriate one [120]. It consists in choosing the right trap strength to maximize the elastic collision rate Γ_{el} . It can be shown that for a trap potential $U(r) \propto r^{d/\delta}$ in d-dimensions $\Gamma_{el} \propto N^{\frac{2}{\delta+3/2}} \times PSD^{\frac{\delta-1/2}{\delta+3/2}}$, where N is the number of atoms and PSD is the phase-space density [120]. In the case of a Quadrupole trap in 3D $U(r) \propto r$, $\delta = 3$, and $\Gamma_{el} \propto N^{4/9} \times PSD^{5/9}$. Hence the objective in the mode matching is to maximize N and avoid losses in PSD during the transfer. From Eqs. (2.62) and (2.63) we can see that the second condition can be satisfied if the volume and the temperature remain constant. Using this constraint and the energy equations we can predict the best value for the Quadrupole radial gradient and the TOP field.

4.5.4 Transfer to the Quadrupole Trap

When transferring the atoms to the Quadrupole trap it is desirable that the field ramps up as fast as possible to maximize the transfer efficiency. With this purpose we have built a boost circuit that allowed us to turn on the Quadrupole field with a current up to 400 A in less than 0.5 ms. Previously the coil inductance limited the rising time to 20 ms. The boost circuit gave us an improvement of a factor of 40.

In figure 4.12 it is shown the schematics of the boost circuit. The voltage V_0 represents the power supply for the coils. It consists of 4 DC power supplies connected in parallel and operating in constant voltage mode. Each one has a maximum output voltage and current of 14 V and 150 A. The coils are switched on/off by applying a variable voltage (0 to 10 V)

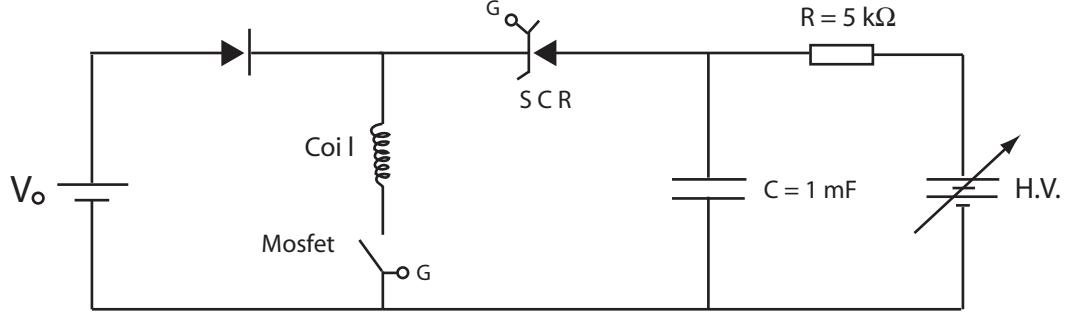


Figure 4.12: Boost circuit for the Quadrupole trap.

to the gate of a MOSFET. Using a high voltage power supply (H.V.) the boost is prepared by charging a capacitor during the MOT loading ($\tau_{boost} = RC = 5 \text{ s} < \text{Loading time}$). When the coils are switched on to full current (Gate voltage = 10 V), the silicon controlled rectifier (SCR) is also switched on by applying 10 V to its gate. The capacitor discharges very fast, ramping up the current in the coils in less than 0.5 ms.

The atomic motion in a MOT can be approximated by a damped harmonic oscillator (see (2.30)). Imposing that the MOT and the Quadrupole trap have the same volume and by writing the Quadrupole energy equation (2.29) in a harmonic format, we have:

$$\overline{U}_{MOT} = \frac{1}{2} \kappa_{MOT} \overline{\rho^2} = \frac{1}{2} \kappa_{Quad} \overline{\rho^2} = \overline{U}_{Quad}, \quad (4.22)$$

$$\therefore \kappa_{MOT} = \kappa_{Quad}, \quad (4.23)$$

$$\kappa_{Quad} \equiv \frac{2|m_F g_F| \mu_B B'_r}{\bar{\rho}}. \quad (4.24)$$

Using now the condition that the temperature is conserved $\kappa_{MOT} \overline{\rho^2}/2 = k_B T_{MOT}$ and Eqs. (4.23) and (4.24), we can calculate B'_r :

$$B'_r = \frac{k_B T_{MOT}}{|m_F g_F| \mu_B \bar{\rho}}, \quad (4.25)$$

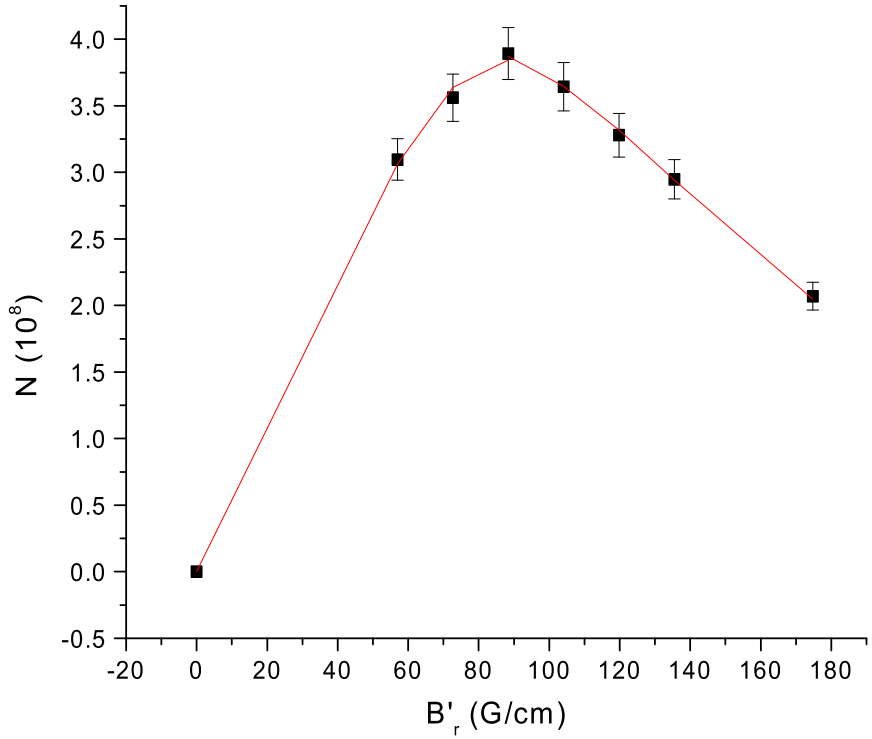


Figure 4.13: Number of atoms transferred to the Quadrupole as a function of the radial gradient.

where $\bar{\rho}$ is the average MOT radius and we assumed $\overline{\rho^2} \cong (\bar{\rho})^2$. Using $T_{MOT} = 235 \pm 50 \mu\text{K}$, $m_{FgF} = 1$ for ($F = 2$, $m = 2$), $\mu_B/k_B = 67.2 \mu\text{K/G}$ and $\bar{\rho} \sim 1 \text{ mm}$ in (4.25), we get $B'_r = 35 \pm 7 \text{ G/cm}$. This is the Quadrupole gradient that satisfies the mode matching condition on the transfer from the MOT.

The total number of atoms transferred to a Quadrupole trap versus the radial gradient was measured. The result is shown in Fig. 4.13. We can see that the largest transfer happens at $B'_r = 88 \text{ G/cm}$. This is different from the radial gradient predicted to avoid losses in PSD. However the number of atoms is also an important factor to optimize Γ_{el} and at a low gradient of 35 G/cm we lose over a factor of 2 in the number of atoms. So we have decided to avoid these losses by using $B'_r = 88 \text{ G/cm}$.

In order to fit the data a simple model was developed for the transfer. The maximum

happens when $\bar{U}_{Quad} = \bar{U}_{MOT} = \bar{E}$, where $\bar{E} = 3k_B T$ is the average total energy of the atoms in the MOT. This happens when $B'_r = B'_0$. If $B'_r \leq B'_0$ then the number of atoms transferred N is proportional to the number of atoms inside the MOT with $\rho \leq \rho_1$ and $z \leq z_1$, where ρ_1 and z_1 are such that $\bar{U}_{Quad}(\rho_1, 0) = \bar{U}_{MOT}(\rho_1, 0)$ and $\bar{U}_{Quad}(0, z_1) = \bar{U}_{MOT}(0, z_1)$. If $B'_r \geq B'_0$ then the limits change to (ρ_2, z_2) , given by $U_{Quad}(\rho_2, 0) = \bar{E}$ and $U_{Quad}(0, z_2) = \bar{E}$. These values are the following:

$$(\rho_1, z_1) = \left(\frac{2\mu_B B'_r}{m\omega_r^2}, \frac{4\mu_B B'_r}{m\omega_z^2} \right), \quad (4.26)$$

$$(\rho_2, z_2) = \left(\frac{3k_B T}{\mu_B B'_r}, \frac{3k_B T}{2\mu_B B'_r} \right). \quad (4.27)$$

The number of atoms transferred is proportional to:

$$N \propto \int_0^{\rho} \rho e^{-\rho^2/\rho_{rms}^2} d\rho \int_{-z}^z e^{-z^2/2z_{rms}^2} dz, \quad (4.28)$$

$$\rho_{rms}^2 \equiv 2k_B T/m\omega_r^2, \quad (4.29)$$

$$z_{rms}^2 \equiv k_B T/m\omega_z^2. \quad (4.30)$$

The solution of Eq. (4.28) is:

$$N \propto \left[1 - e^{-\rho^2/\rho_{rms}^2} \right] \operatorname{Erf} \left(z/\sqrt{2}z_{rms} \right), \quad (4.31)$$

where Erf is the error function. Using (4.26), (4.27) with (4.29) and (4.30) we get:

$$\rho_1^2/\rho_{rms}^2 = 3(B'_r/B'_0)^2, \quad (4.32)$$

$$z_1^2/2z_{rms}^2 = 3(B'_r/B'_0)^2, \quad (4.33)$$

$$\rho_2^2/\rho_{rms}^2 = 3(B'_0/B'_r)^2, \quad (4.34)$$

$$z_2^2/2z_{rms}^2 = 3(B'_0/B'_r)^2. \quad (4.35)$$

Applying (4.32), (4.33), (4.34) and (4.35) in (4.31), we can fit Fig. 4.13 with:

$$N = \begin{cases} a \left[1 - e^{-3(B'_r/b)^2} \right] \operatorname{Erf}(\sqrt{3}B'_r/b), & \text{for } B'_r \leq B'_0 \\ c \left[1 - e^{-3(d/B'_r)^2} \right] \operatorname{Erf}(\sqrt{3}d/B'_r), & \text{for } B'_r \geq B'_0 \end{cases} \quad (4.36)$$

where a, b, c and d are fit parameters. Their values are $a = (4 \pm 1) \times 10^8$, $b = 74 \pm 37$ G/cm, $c = (4 \pm 1) \times 10^8$ and $d = 99 \pm 32$ G/cm. The values of b and d are close to the experimental value of $B'_0 = 88$ G/cm.

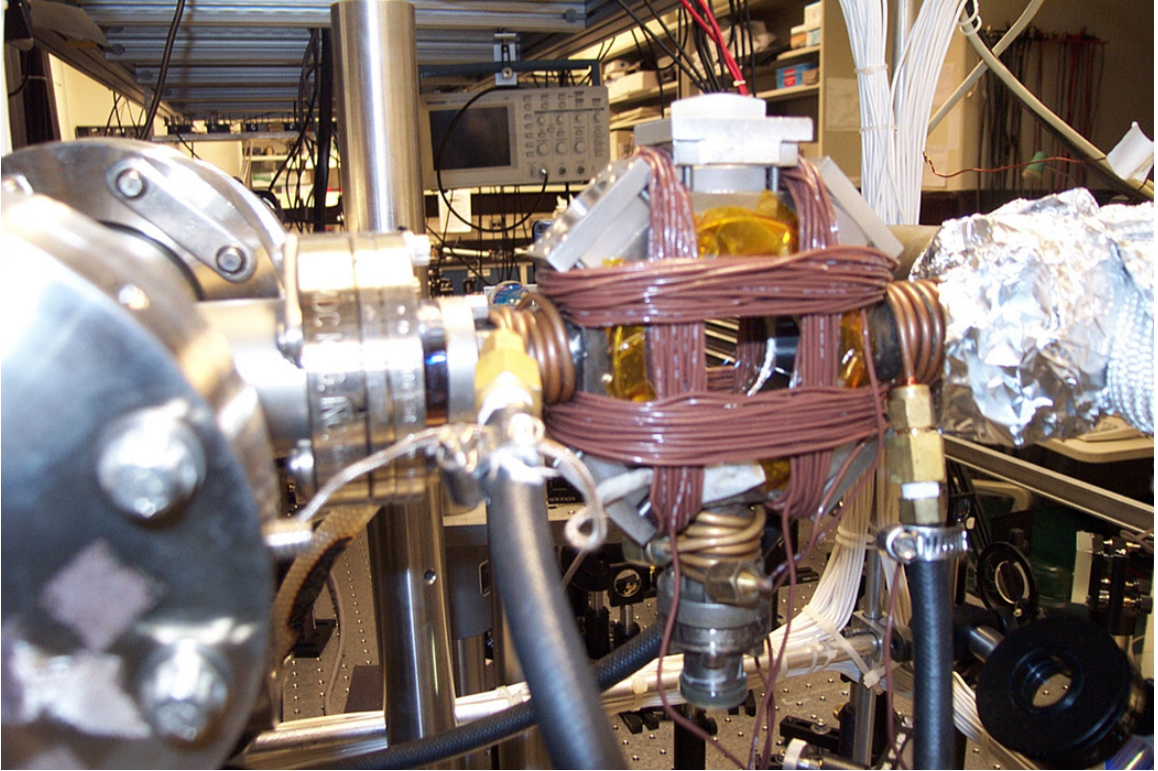


Figure 4.14: TOP coils wrapped around the chamber. Each coil has 20 turns and they are driven by a two-channel audio amplifier. The Quadrupole coils are not shown.

4.5.5 Transfer to the TOP Trap

In order to reach quantum degeneracy it is necessary to use a different trap other than the Quadrupole. This is because the colder the cloud gets, closer to the center of the trap the atoms are, and in the Quadrupole the magnetic field is zero at this point. This causes Majorana transitions to non-trapped states and this loss of atoms stops the evaporative cooling process. So we have decided to transfer to the TOP instead. The main reasons for our choice are that the TOP has a strong confinement and it could be easily implemented in our apparatus.

To generate a rotating, uniform magnetic field, we have wrapped around the chamber four coils, each pair in a Helmholtz configuration (see Fig. 4.14). They are driven by a 2-channel audio amplifier with 350 W and 10 A maximum output per channel. Using a

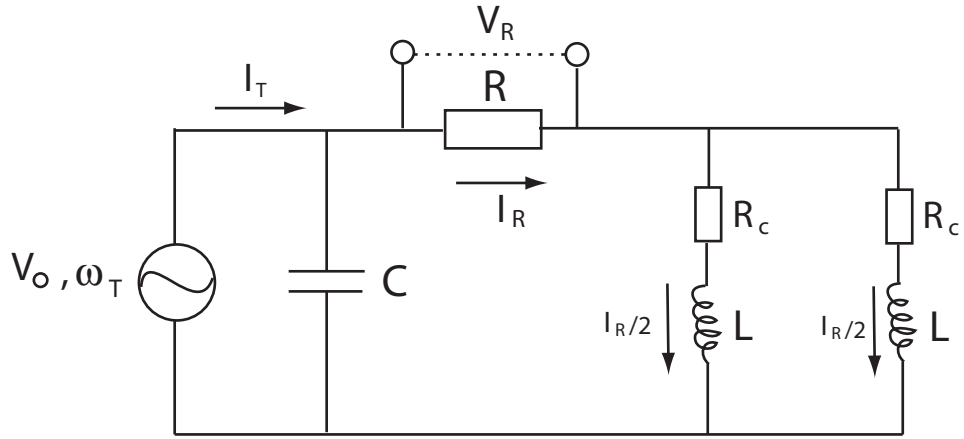


Figure 4.15: Circuit linking a channel from the audio amplifier and a pair of TOP coils.

phase-shifter circuit, one channel was shifted 90° relative to the other, making the magnetic field rotate with a frequency ω_T . The circuit for each channel is shown in Fig. 4.15. The resistor R ($10\text{ m}\Omega$) is used to measure the current I_R that goes into the coils and R_c represents the resistance of each coil. The capacitor C ($4.4\text{ }\mu\text{F}$) amplifies the current I_R relative to I_T . This is important since I_T is limited to 10 A per channel.

How was the TOP frequency ω_T chosen? An important condition on ω_T is that it has to be larger than the atomic oscillation frequency, but smaller than the Larmor frequency: $\omega_L > \omega_T > \omega_{r,z}$. The condition $\omega_T > \omega_{r,z}$ is necessary for the atoms to feel only the time-average potential (2.40) and we need $\omega_L > \omega_T$ to avoid Majorana transitions. Using the equations $\omega_L = |\mu|B_T/\hbar$ and (2.43), with $B_T^{min} = 1\text{ G}$ and $B_r'^{max} = 332\text{ G/cm}$, we have $\omega_L^{min} = 1.4\text{ MHz}$ and $\omega_z^{max} = 18.7\text{ kHz}$. So we must have $1.4\text{ MHz} > \omega_T > 18.7\text{ kHz}$. Another important consideration is the existence of eddy currents on the chamber induced by the TOP field. They are proportional to the frequency ω_T . These currents will try to oppose the TOP, attenuating its field. An experiment has been done where we have measured the Attenuation $\equiv B_T(\text{no chamber})/B_T(\text{with chamber})$ versus $\omega_T = 2\pi \times f_T$. From Fig. 4.16 we see that it is not interesting to have $\omega_T > 2\pi \times 16\text{ kHz}$. The fit was

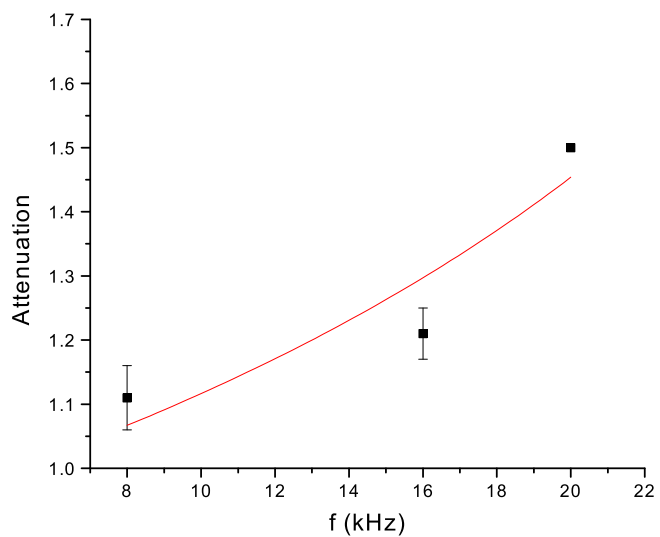


Figure 4.16: Above $f_T = 16$ kHz there is a sharp increase on the field attenuation. It is caused by eddy currents and magnetization of the chamber. The fit parameters for (4.38) are $a = 1.1$ and $b = 2.1 \times 10^{-2}$ s.

obtained by modelling B_T (with chamber) as:

$$B_T(\text{with chamber}) = \mu H - \chi f_T , \quad (4.37)$$

where μ is the chamber magnetic susceptibility, H is the magnetic field without the chamber and χf_T is the field generated by the eddy currents, with χ as a constant. Using Eq. (4.37) with the Attenuation definition we get:

$$\text{Attenuation} = \frac{1}{a - b f_T} , \quad (4.38)$$

where a and b are the fit parameters.

Another reason to have a lower ω_T is that the power dissipated scales as $P_{\text{eddy}} \propto \omega_T^2$. If the chamber heats up too much, the background pressure increases decreasing the trap lifetime. A short lifetime harms the evaporation process, therefore it is better to use a lower frequency to avoid overheating the chamber.

The characteristics of the TOP trap can be summarized as following:

$$B_T^{\max} = 80 \text{ G}, \quad (4.39)$$

$$B_r'^{\max} = 332 \text{ G/cm}, \quad (4.40)$$

$$\omega_T = 2\pi \times 7.4 \text{ kHz}, \quad (4.41)$$

$$\omega_r^{\max} = 6.6 \text{ kHz}, \quad (4.42)$$

$$\omega_z^{\max} = 18.7 \text{ kHz}, \quad (4.43)$$

$$T_{\text{depth}}^{\max} = \frac{1340}{\eta} \mu\text{K}, \quad (4.44)$$

where η is usually 5 when performing evaporative cooling.

The mode matching condition was used to choose the best B_T and B_r' to transfer the atoms from the MOT to the TOP. The radial spring constant for the TOP is obtained from (2.41) and (2.42):

$$\kappa_{\text{TOP}}^r \equiv m\omega_r^2 = \frac{\mu_B(B_r')^2}{2B_T}. \quad (4.45)$$

The mode matching condition is imposed when we equate $\kappa_{\text{MOT}} = 2k_B T_{\text{MOT}}/\bar{\rho}^2$ to (4.45). With the TOP we must also impose that the “circle of death” R_D is bigger than the MOT cloud: $R_D = B_T/B_r' \geq \bar{\rho}$. Using all these conditions and considering

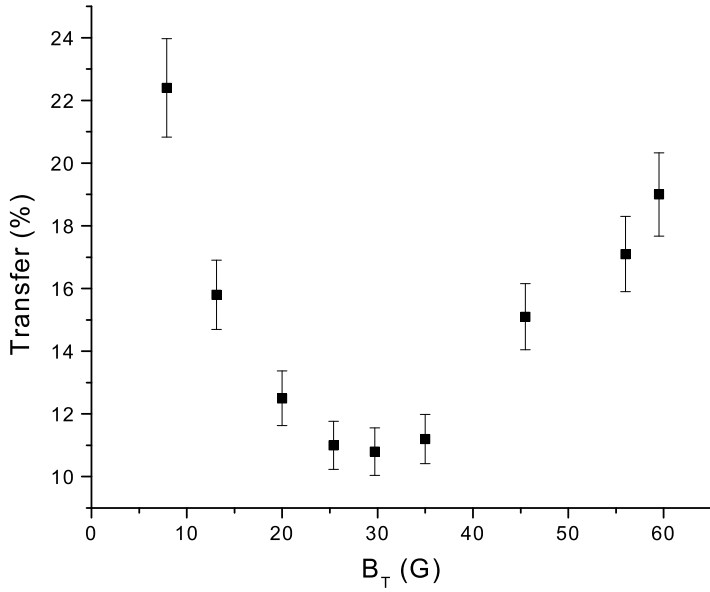


Figure 4.17: Transfer to the TOP at $B'_r = 200$ G/cm. The minimum corresponds to a TOP field where most of the atoms “see” the “circle of death” .

$T_{MOT} = 235 \pm 50$ μK and $\bar{\rho} = 1$ mm, we get:

$$B_T \geq \frac{4k_B T_{MOT}}{\mu_B} = 14 \pm 3 \text{ G} , \quad (4.46)$$

$$B'_r \geq \frac{4k_B T_{MOT}}{\mu_B \bar{\rho}} = 140 \pm 30 \text{ G/cm} . \quad (4.47)$$

Figure 4.17 shows the number of atoms transferred to the TOP versus B_T for $B'_r = 200$ G/cm. At low TOP field more atoms are transferred, but most of them are above the “circle of death”. It is like transferring to a Quadrupole trap. The minimum at $B_T = 30$ G corresponds to $R_D = 30/200 = 1.5$ mm \sim MOT size. For $B_T > 30$ G the number of atoms increases again, since the trap gets deeper and most of the atoms are now below R_D . So the best option is to transfer to a high TOP field to capture as many atoms as possible below the “circle of death”. At $B_T = 80$ G and $B'_r = 200$ G/cm we were able to transfer 30% of the atoms from the MOT, all polarized in the ($F = 2, m = 2$) state.

Chapter 5

Transverse Cooling

5.1 Overview

After transferring the atoms to the TOP we would like to evaporative cool them to reach BEC. This process is only efficient if there are enough elastic collisions to re-thermalize the atoms, otherwise atoms are only lost without any real gain in phase-space density.

A crucial parameter is the number of atoms loaded in the MOT. Using only the comb light 2×10^8 atoms are captured. Considering a transfer efficiency of 30% to the TOP ($B_T = 80\text{ G}$, $B'_r = 200\text{ G/cm}$), there are at most 6×10^7 atoms to start evaporative cooling. The temperature in the TOP is around $300\text{ }\mu\text{K}$ and the radial $1/e^2$ radius is $\sim 1\text{ mm}$. Given these parameters, the maximum elastic collision rate (2.65) is $\Gamma_{el} = 0.5\text{ }s^{-1}$. The trap lifetime is $\tau = 60\text{ s}$, giving a total number of elastic collisions during a lifetime $\Gamma_{el}\tau = 30$. This explains why, after loading the TOP, efficient evaporation was not observed in any of our trials. Also the number of atoms in the trap seems too small when compared to successful BEC experiments [3, 4, 5]. They had usually started evaporation with $N \geq 10^8$ atoms and this is important since a lot of atoms are lost before reaching degeneracy. So we had decided that we needed to increase the number of atoms in the MOT. By gaining a factor of 10, we would have $\Gamma_{el}\tau = 300 > 100$ making it much easier to observe evaporation and eventually reach BEC.

In order to increase the number of atoms in the MOT, a 2D transverse cooling was added on the atomic beam right after it exits the oven. The main objective is to increase

its spatial density, improving the loading rate R . The idea of using transverse cooling to collimate an atomic beam was proposed for the first time in the classical paper of Hänsch and Schawlow [34]. Soon it was proved to be feasible [146, 147] and in the last 10 years it has been used successfully in many experiments.

In 1990 A. Aspect et al. [16] made a theoretical study of the use of transverse cooling to increase the density of a beam of metastable helium. They concluded that the most important parameter is the transverse capture velocity, i.e. the largest initial transverse velocity that can be cooled by the beams. In 1996 W. Rooijakkers et al. [148], using a transverse cooling beam with curved wavefront [149], obtained a gain of 50 in intensity with metastable He. Their interaction length was 180 mm and the laser power was 30 mW. The advantage of a curved wavefront compared to a usual standing wave is that its capture velocity is larger for the same laser power [16]. Also in 1990 the group of H. Metcalf studied the collimation of a Rb beam [19, 20, 21]. By adding a weak magnetic field (~ 0.2 G) perpendicular to the transverse beam, they were able to reach sub-Doppler temperature in the transverse direction. They used a circularly polarized standing wave with a rectangular shape 8 mm x 20 mm with 20 mW. They obtained an increase in beam brightness by a factor of 20. The group of D.E. Pritchard was interested in minimizing the beam spreading after Zeeman cooling [18]. They placed a 2D transverse standing wave inside the Zeeman slower, close to its exit. The density of the Na beam increased by a factor of 6. F. Shimizu et al. modified the curved wavefront method by instead reflecting a beam in a zigzag configuration between two mirrors [22]. The interaction length was longer than a standing wave and it avoided the complicated optics to modify the beam in the wavefront method. The interaction length was 100 mm with 14 reflections in each mirror. They obtained a gain of 30 in intensity with a beam of metastable neon.

The experiment that is most similar to ours was done by the group of M. Leduc [15]. Using a beam of metastable He, they compared the gain in compression between a standing monochromatic light, a curved wavefront, a multi-frequency standing wave and a multi-frequency beam in a zigzag configuration. They noticed that a zigzag beam with frequency spread light gave the best compression. This is the same method that we use. With 90 mm interaction length and 40 mW they had a gain of 4 in beam intensity. The only difference

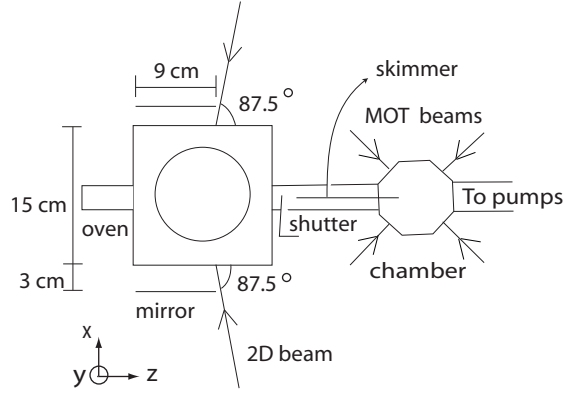


Figure 5.1: Modified setup to implement transverse cooling. A 15 cm^3 cube was added between the oven and the chamber. The skimmer is also longer to provide a better differential pumping. Not shown in the picture are the two mirrors perpendicular to the y direction and the third MOT beam perpendicular to the xz plane.

between their experiment and ours, besides using different atoms, is that they transversally cooled in 1D.

5.2 Experimental Setup and Results

In figure 5.1 the new configuration of our experiment is shown. The ${}^7\text{Li}$ atoms leave the oven at $T \cong 320^\circ\text{C}$ and are transversally cooled inside a 15 cm^3 cube. The oven is attached to the cube through bellows (see Fig. 5.2). The idea is to be able to move the oven to aim the atomic beam better towards the skimmer. Four mirrors were used, each one 9 cm long, paired in two orthogonal axis. A fraction of the comb light (60 mW) was deviated and split equally in four using a combination of polarizing beamsplitter cubes and half-wave plates (see Fig. 5.3). After being cooled, the atoms pass through a 16 cm long skimmer that separates the cube from the trapping chamber.

In Fig. 5.4 the trajectory of the 2D beams and the atoms are shown. The beams are injected with an angle of 87.5° with the symmetry axis z. Not shown are the two other ones that are perpendicular to the figure. The beams and the mirrors were aligned in order to

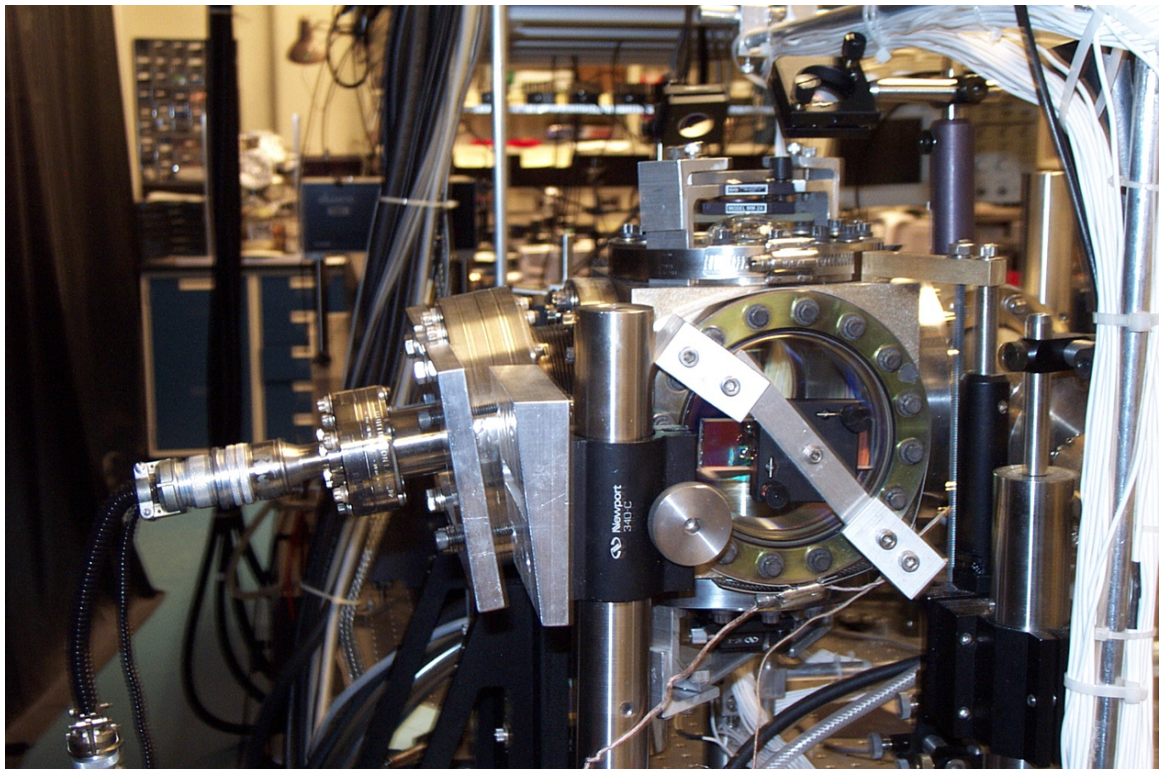


Figure 5.2: Bellows are used to attach the oven to the cube. This allowed us to fine tune the alignment between the atomic beam and the skimmer.

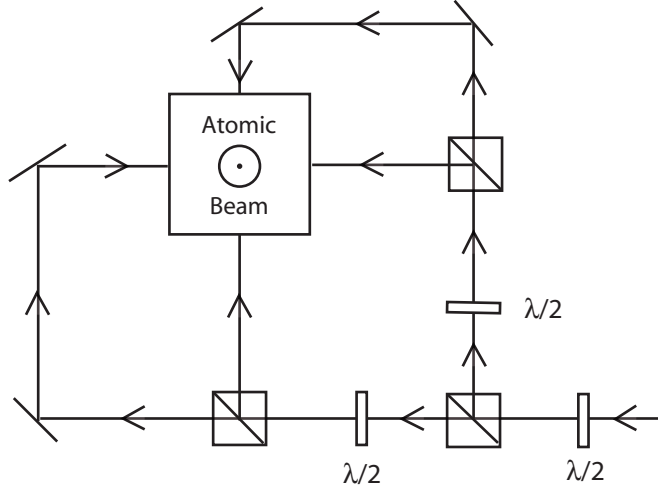


Figure 5.3: Half-wave plates and polarizing beamsplitter cubes were used to split equally the 2D cooling light in four beams.

bounce back and forth the light in a zigzag configuration, covering the whole mirror. This way the atoms had a long interaction length, maximizing their compression. The light is linear polarized with an intensity of 63 mW/cm^2 and a $1/e^2$ diameter of 7.78 mm.

The compression of the atomic beam is limited by the Doppler temperature (2.22). The atoms reach this limit exponentially with a $1/e$ decay time τ_d that is a function of the detuning and intensity of the cooling beam. The mirror length was chosen in order that the atoms had enough time to reach the Doppler limit. This condition can be expressed as $\tau_d \ll T$, where T is the interaction time of the fastest atom captured by the MOT. The velocity of this atom is v_c (the capture velocity of the MOT), giving the following condition:

$$\frac{\tau_d v_c}{L} \ll 1 , \quad (5.1)$$

where $L = l + D$ is the interaction length, l is the mirror length, and D is the beam diameter. Using the same method described in [88], we have estimated $v_c = 127 \text{ m/s}$. The time τ_d can be calculated as being $\tau_d = 285 \mu\text{s}$ (see section 5.4). The interaction length is $L = 10 \text{ cm}$, therefore $\tau_d v_c / L = 0.36 < 1$. That means that the atoms reach transverse Doppler speed

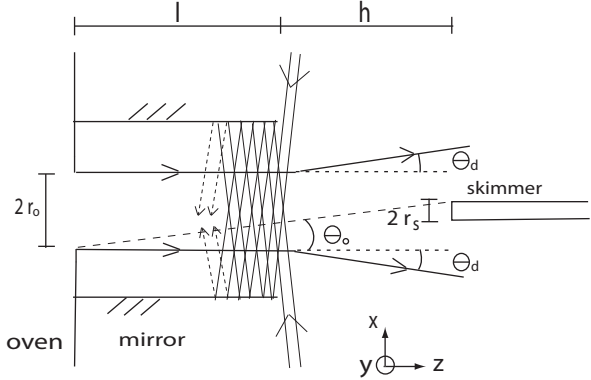


Figure 5.4: The 2D beams have a zigzag trajectory covering the entire mirror length l . After the cooling the atoms still have a transverse expansion due to the Doppler speed. The angle θ_d is given by v_d/v'_l , where v_d is the Doppler speed and v'_l is the longitudinal velocity after cooling. The distance h is 124 mm, the oven radius r_o is 6.35 mm and the skimmer radius r_s is 2.50 mm.

after the first 4 cm inside the cube. Figure 5.5 shows the collimated atomic beam during the 2D cooling.

The loading rate R was measured with a photomultiplier tube. In the first 3 s its behavior is practically linear and we can use $R = \Delta N/\Delta t$. The absolute number of atoms was given by the fluorescence measured with a calibrated CCD camera (4.14). The measured value of the gain in loading rate was $R'/R = 13 \pm 1$, where R' is the loading rate with 2D cooling. The absolute value of R' was $2 \times 10^8 \text{ s}^{-1}$, giving 2×10^9 atoms in the MOT after loading. The transverse cooling ended up giving an increase in the number by a factor of 10. It is interesting to note that this is a very robust technique. It worked since the first time it was turned on without any fine tuning. It is only sensitive to the power division among the four beams. A small unbalance deviates the atomic beam from the skimmer, decreasing the loading rate.

In Fig. 5.6 we show the dependence of R' with the 2D beam intensity when the beam power is changed. The fit was obtained with the phenomenological model presented in section 5.4. At high intensities R' saturates as an indication that the atoms have reached

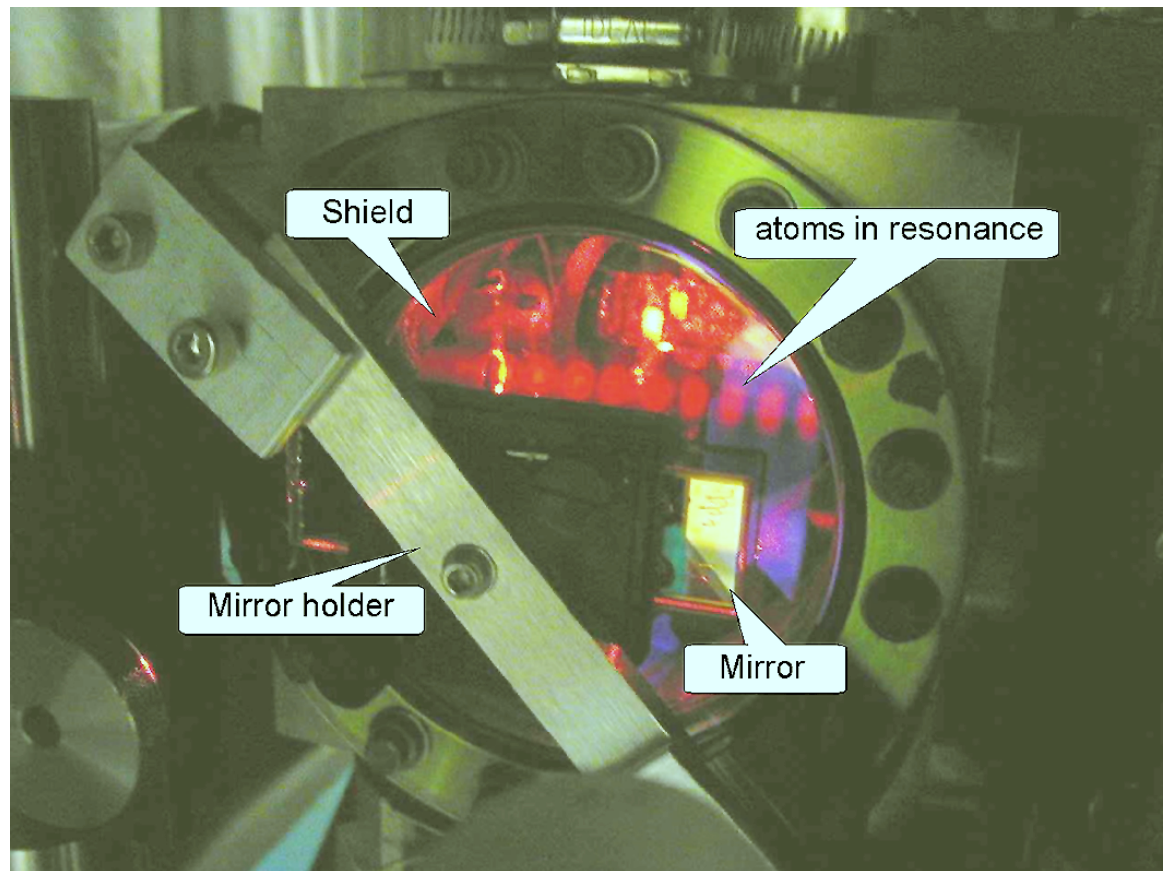


Figure 5.5: Atomic beam during transverse cooling. Notice how it is collimated right after the oven exit. A shield had to be placed in front of the oven to avoid contamination of the windows by lithium.

the Doppler limit. At low intensities it approaches the value with no cooling.

The number of reflections M on each mirror was also changed to see how R'/R varied (Fig. 5.7). The value $M = 10$ corresponds to maximum interaction time while $M = 0$ is the configuration where there are only two retro-reflected beams orthogonal to the atom trajectory. The interaction length is proportional to the number of reflections. Figure 5.7 shows that for $M \leq 5$ the loading rate begins to decrease very fast. This is because the atoms do not interact with the light for enough time to reach the Doppler temperature, limiting its compression. When $M = 0$ the gain is almost none ($R'/R = 1.6 \pm 0.1$). This shows that a long interaction length that satisfies (5.1) is necessary if we want maximum beam compression.

5.3 Doppler Theory applied to Transverse Cooling

The Doppler cooling theory is the simplest one that can be used to study the transverse cooling. It assumes a 2-level atom and it treats multiple laser beams independently [78, 72]. In our experiment, since the 2D beams are travelling waves and there is no magnetic field, the Doppler theory is a good approximation. The total force that the 2D beams exert on an atom is given by [88]:

$$F_t = \frac{\hbar\Gamma k S}{2} \sin \eta \sum_{i=-5}^5 f_i \left[\frac{1}{1 + S + (2\Delta_{2i}/\Gamma)^2} - \frac{1}{1 + S + (2\Delta_{1i}/\Gamma)^2} \right], \quad (5.2)$$

$$\begin{aligned} F_l = & -\frac{\hbar\Gamma k S}{2} \cos \eta \sum_{i=-5}^5 f_i \left[\frac{1}{1 + S + (2\Delta_{1i}/\Gamma)^2} + \frac{1}{1 + S + (2\Delta_{2i}/\Gamma)^2} + \right. \\ & \left. + \frac{2}{1 + S + (2\Delta_{3i}/\Gamma)^2} \right], \end{aligned} \quad (5.3)$$

$$f_i = \{11.7\%, 5\%, 9.6\%, 15.8\%, 10\%, 3.75\%\}, \quad f_{-i} = f_i, \quad i \in \{0, \dots, 5\}, \quad (5.4)$$

$$\delta_i = 2\pi \times (11.7i - 68.6) \text{MHz}, \quad (5.5)$$

$$\Delta_{1i} = \delta_i + kv_t \sin \eta + kv_l \cos \eta, \quad (5.6)$$

$$\Delta_{2i} = \delta_i - kv_t \sin \eta + kv_l \cos \eta, \quad (5.7)$$

$$\Delta_{3i} = \delta_i + kv_l \cos \eta, \quad (5.8)$$

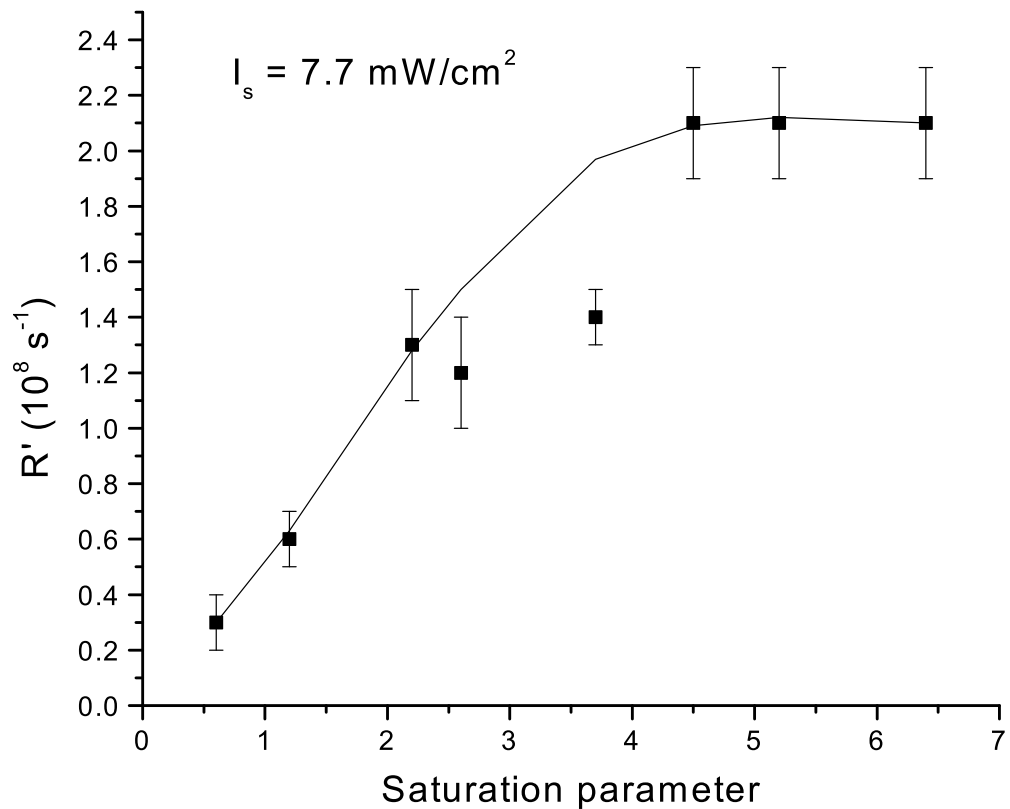


Figure 5.6: The saturation parameter is given by I/I_s . The saturation intensity I_s is calculated from the fit using the χ^2 method, where we have ignored the two points off the curve. For high intensities the loading rate saturates. At this level most of the atoms have reached Doppler temperature in the transverse direction. The fit is given by our model shown in section 5.4.

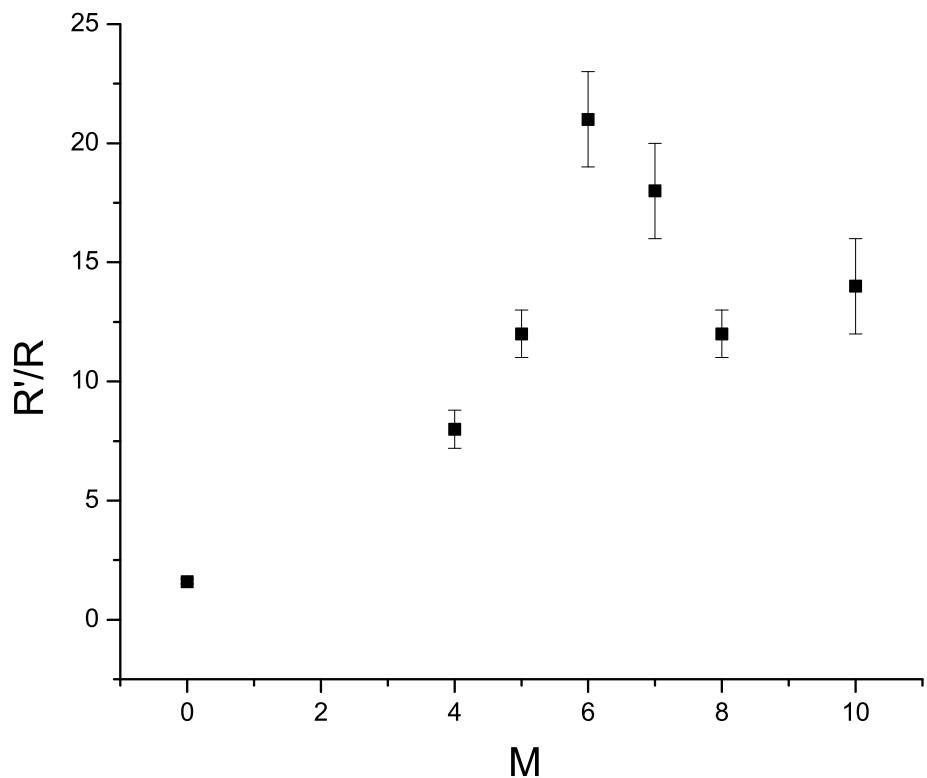


Figure 5.7: A lower number of reflections is equivalent to a smaller interaction length. At $M = 0$ we see that there is almost no gain in loading rate. The larger values around $M = 6$ are caused by fluctuations on the laser beam power from day-to-day measurements.

where the sum is over all comb sidebands, η is the beam angle with the atomic beam (87.5°) and f_i and δ_i are the power fraction and detuning of each sideband. The transverse force F_t is responsible for the beam compression and F_l is the longitudinal cooling force. Because the 2D beams are almost perpendicular to the atomic beam, the compression is the main effect observed. In the low velocity limit, equation (5.2) can be expressed as [78]:

$$\vec{F}_t = -\alpha \vec{v}, \quad (5.9)$$

$$\alpha = -4\hbar k^2 S \sin \eta \sum_i \frac{f_i(2\delta_i/\Gamma)}{[1 + S + (2\delta_i/\Gamma)^2]^2}. \quad (5.10)$$

Equation (5.9) suggests that v exponentially decays to zero. However this does not happen because the atom is constantly heated up by the recoil due to spontaneous emission [72, 78]. It drifts in momentum space with a diffusion constant given by [78] :

$$D_p = \hbar^2 k^2 \gamma, \quad (5.11)$$

$$\gamma = \frac{\Gamma}{2} \sum_i \frac{f_i S}{1 + S + (2\delta_i/\Gamma)^2}, \quad (5.12)$$

where γ is the total photon scattering rate. The result is that the atoms reach a terminal velocity, called the Doppler speed v_d , with a decay time τ_d [78]:

$$\tau_d = m/\alpha, \quad (5.13)$$

$$v_d = \frac{\hbar k}{\sqrt{m}} \sqrt{\gamma/\alpha}, \quad (5.14)$$

where m is the mass of the atom. For $S = 7.6$ (maximum intensity on the 2D beams), equations (5.10), (5.12), (5.13) and (5.14) give us $\tau_d = 285 \mu s$ and $v_d = 1.19 \text{ m/s}$.

5.4 Phenomenological Model

A rigorous theoretical study of the 2D cooling would be very complicated. Using Eqs. (5.2) - (5.14) and some simple physical assumptions, a phenomenological model can be made that explains very well the results. First we will model the gain in loading rate and later its dependence on the intensity of the 2D beams.

The atoms leaving the oven follow an effusion process. This is because the oven aperture is much smaller than the mean-free path p of the atoms in the cube

($r_{oven} = 6.35$ mm $\ll p \sim 10^6$ mm). In this process the velocity distribution of the atoms per unit area, per unit time in spherical coordinates is [77]:

$$\Phi(\vec{v})d^3v = n \left(\frac{m}{2\pi k_B T} \right)^{3/2} v \cos \theta e^{-mv^2/2k_B T} d^3v, \quad (5.15)$$

where n is the atomic beam density, T is the oven temperature, k_B is the Boltzmann constant and θ is the azimuthal angle. Knowing that the MOT can only capture atoms up to a certain velocity v_c and assuming $v_c \ll \sqrt{2k_B T/m}$, equation (5.15) can be integrated, giving an approximate expression for the loading rate:

$$R \propto n v_c^4. \quad (5.16)$$

Using Eq. (5.16) the gain in loading rate can be expressed as:

$$\frac{R'}{R} = \left(\frac{n'}{n} \right) \left(\frac{v'_c}{v_c} \right)^4 \beta, \quad (5.17)$$

where the prime sign means that the parameter is measured with 2D cooling. It is expected that $v'_c > v_c$. The reason is that when there is 2D cooling, atoms with initial velocity larger than v_c can be cooled down and captured by the MOT. The factor β takes into account the difference in size between the atomic beam after cooling and the skimmer aperture. It is given by [16]:

$$\beta = \left(\frac{h \theta_d + r_s}{r_o} \right)^2, \quad (5.18)$$

where h is the distance between the last interaction spot and the skimmer, r_s and r_o are the skimmer and the oven aperture radius and θ_d is the divergence angle of the atomic beam after 2D cooling (see Fig. 5.4). Since the beams are almost perpendicular to the atoms ($\eta = 87.5^\circ$), the main effect of the 2D cooling is the increase in the atomic beam density. Assuming the number of atoms is conserved, the gain in density in the MOT is given by [16]:

$$\frac{n'}{n} = \left(\frac{v_{ct}}{v'_t} \right)^2 \left(\frac{v_c}{v'_l} \right), \quad (5.19)$$

where v_{ct} is the transverse capture velocity and v'_t and v'_l are the atomic transverse and longitudinal velocities after 2D cooling. Using (5.19) in (5.17):

$$\frac{R'}{R} = \left(\frac{v_{ct}}{v'_t} \right)^2 \left(\frac{v_c}{v'_l} \right) \left(\frac{v'_c}{v_c} \right)^4 \beta. \quad (5.20)$$

The value of each parameter in Eq. (5.20) has to be calculated. The MOT capture velocity v_c is estimated using Eq. (5.2) with $\eta = 45^\circ$, $I_s = 7.7 \text{ mW/cm}^2$ and $S = 12$. Equation (5.2) is integrated to calculate the maximum initial velocity an atom can have before it stops inside the MOT [88, 140]. The value of v_{ct} is fixed by the oven-skimmer geometry: $v_{ct} = v_c \tan \theta_0$, where $\tan \theta_0 = (r_o + r_s)/(L + h) = 3.8 \times 10^{-2}$ (see Fig. 5.4) [150]. The transverse velocity v'_t depends on the 2D beam intensity and the interaction length L . Considering that Eq. (5.1) is satisfied at full power, the approximation $v'_t \cong v_d$ is valid, where v_d is the Doppler speed given by (5.14) [16]. The remaining two terms, v'_l and v'_c are calculated using Eq. 5.3 with the following conditions: $v'_l = v_l(L)$ assuming $v_l(0) = v_c$ and $v'_c = v_l(0)$ given $v_l(L) = v_c$. The values are:

$$v_c = 127 \text{ m/s ,} \quad (5.21a)$$

$$v_{ct} = 4.83 \text{ m/s ,} \quad (5.21b)$$

$$v_d = 1.19 \text{ m/s ,} \quad (5.21c)$$

$$v'_l = 122 \text{ m/s ,} \quad (5.21d)$$

$$v'_c = 131 \text{ m/s ,} \quad (5.21e)$$

$$\beta = 0.34 . \quad (5.21f)$$

Applying Eqs. (5.21) in (5.20) we get $(R'/R)_{theory} = 7$. This is close to the experimental result 13 ± 1 . Considering all the approximations that have been made to estimate Eqs. (5.21), it is not a surprise that $(R'/R)_{theory}$ is not within the experimental error of $(R'/R)_{exp}$. Notice that the values (5.21d) and (5.21e) are similar to (5.21a). This supports what has been mentioned before that there is very little cooling in the longitudinal direction. Therefore a good approximation of Eq. (5.20) is:

$$\frac{R'}{R} \cong \left(\frac{v_{ct}}{v'_t} \right)^2 \beta . \quad (5.22)$$

In order to understand the dependence of R' with intensity (Fig. 5.6), it is easier to focus on Eq. (5.22). When the 2D beam intensity varies, v_{ct} is a constant and β varies very little. So we have $R' \propto 1/(v'_t)^2$. Consider now two extreme cases. When $I = 0$, $v'_t = v_{ct}$ and $R' = R$. If I is very large ($S \gg 1$), then v'_t saturates at the Doppler speed. These limits seem to agree with the graph in Fig. 5.6. An equation can be obtained for $\langle (v'_t)^2 \rangle$ by using

the Fokker-Planck equation (2.11) with the normalization condition:

$$\int_{-\infty}^{\infty} \rho(v, t) dv = 1. \quad (5.23)$$

In the demonstration the notation will be simplified by defining $v'_t \equiv v$. Begin with the average $\langle v^2 \rangle$ for an ensemble:

$$\langle v^2 \rangle(t) = \int_{-\infty}^{\infty} v^2 \rho(v, t) dv. \quad (5.24)$$

Taking the derivative of Eq.(5.24):

$$\frac{d\langle v^2 \rangle}{dt} = \int v^2 \frac{\partial \rho}{\partial t}(v, t) dv, \quad (5.25)$$

Using (2.11) in (5.25) and integrating by parts:

$$\frac{d\langle v^2 \rangle}{dt} = -\frac{2D_p}{m^2} \int v \frac{\partial \rho}{\partial v}(v, t) dv + \frac{2}{m} \int v \rho(v, t) F(v) dv. \quad (5.26)$$

Applying (5.9), (5.13) and (5.24) in (5.26):

$$\frac{d\langle v^2 \rangle}{dt} = -\frac{2}{\tau_d} \langle v^2 \rangle - \frac{2D_p}{m^2} \int v \frac{\partial \rho}{\partial v}(v, t) dv. \quad (5.27)$$

Integrating by parts once again (5.27):

$$\frac{d\langle v^2 \rangle}{dt} = -\frac{2}{\tau_d} \langle v^2 \rangle + \frac{2D_p}{m^2} \int \rho(v, t) dv. \quad (5.28)$$

Using (5.11), (5.13), (5.14) and (5.23) in (5.28):

$$\frac{d\langle v^2 \rangle}{dt} = -\frac{2}{\tau_d} \langle v^2 \rangle + \frac{2}{\tau_d} v_d^2. \quad (5.29)$$

Equation (5.29) has a simple physical interpretation. The first term on the right hand side is due to the linear cooling force (5.9) and the second term is due to a constant heating that simulates the effect of the spontaneous emission recoil. Its solution for an atom at $t = T$ and 2D cooling intensity I is:

$$\langle (v'_t)^2 \rangle(I) = v_d^2(I) + [v_{ct}^2 - v_d^2(I)] e^{-2T/\tau_d(I)}, \quad (5.30)$$

where $T = L/v_c$ is the interaction time and the initial condition is $\langle (v'_t)^2 \rangle = v_{ct}^2$ for $T = 0$. Using (5.13), (5.14) and (5.21b) in (5.30), we can fit Fig. 5.6 and estimate the saturation intensity I_s using the χ^2 -method. The value $I_s = 7.7 \text{ mW/cm}^2$ is close to the one previously obtained in [88] (5.2 mW/cm^2). In both cases I_s is only an effective saturation parameter, since the 2-level model is an approximation.

Chapter 6

Evaporative Cooling of ^7Li

Having increased the number of atoms in the MOT by a factor of 10, the cloud in the magnetic trap should now have the right initial conditions to begin the evaporative cooling process.

6.1 RF Evaporative Cooling

The evaporation process was done using RF waves. They were generated by a small, circular antenna (24 mm diameter) placed close to the largest window on the chamber (see Fig. 4.4). The atoms were kicked out from the trap by adjusting the RF frequency to induce transitions from the trapped state ($F' = 2, m' = 2$) to the high-field seeking state ($F = 1, m = 1$) (see Fig. 4.10). Using Eq. (2.81) and the values for g_F and ν_0 given in appendix B, an equation for the RF frequency dependence with magnetic field can be written (see Fig. 6.1):

$$\nu_{RF} = 803.5 \text{ MHz} + 2.1 \times B \text{ (MHz/G)}. \quad (6.1)$$

The forced evaporative cooling is done by scanning ν_{RF} from a high value down to 803 MHz. This should get rid of the hot atoms gradually, and if the elastic collision rate is high enough ($\sim 10 \text{ s}^{-1}$), it should cool down the remaining ones.

One important thing to notice when using RF with TOP traps is that the time-average magnetic field (2.40) can not be used in (6.1). This is because $\nu_{RF} \gg \nu_{TOP}$ ($\nu_{RF} \sim 1 \text{ GHz}$, $\nu_{TOP} \sim 10 \text{ kHz}$), therefore the time scale of the RF-atom interaction is much shorter than

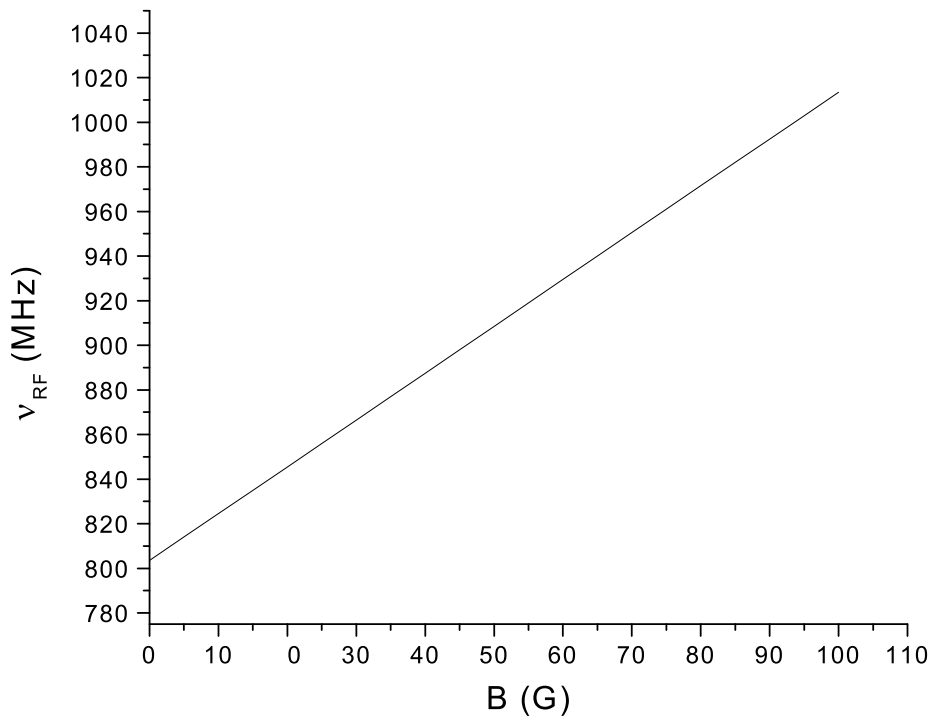


Figure 6.1: Dependence of the RF transition frequency between states $(F' = 2, m' = 2) \leftrightarrow (F = 1, m = 1)$ with magnetic field.

the trap orbit period. That means that the instant TOP magnetic field (2.38) is what has to be used. As a consequence the B field at the “circle of death” varies between $0 \leq B(\rho = R_D) \leq 2B_T$, where B_T is the TOP field at the center of the trap. Since only atoms with $\rho \leq R_D$ remain in the trap, the frequency scan should start at the “circle of death” with $\nu_{max} - \nu_0 = 4.2 \times B_T$ (MHz/G) and finish close to the center with $\nu_{min} - \nu_0 = 2.1 \times B_T$ (MHz/G), where we have defined $\nu_0 = 803.5$ MHz.

An important characteristic of the TOP trap is that it already has a built in evaporation process. By lowering B_T and keeping the Quadrupole gradient B'_r constant, the “circle of death” $R_D = B_T/B'_r$ decreases kicking out the hottest atoms. To make sure that the atoms are being expelled, it can be applied at the same time an RF with frequency $\nu_{RF} = \nu_{max}$ resonant with atoms with $\rho \geq R_D$.

A demonstration of how Eq. (6.1) works can be seen in Fig. 6.2. A total of 3×10^6 atoms were transferred to the TOP with $B_T = 35$ G and $B'_r = 168$ G/cm. A constant RF frequency was then applied for 2 s and the number of atoms left was measured. As we can see there is a minimum around 880 MHz. That is the frequency where all the atoms, even those at the bottom of the trap, are at resonance at some time ($\nu_{min} = 803.5 + 2.1 \times 35 \cong 877$ MHz).

Another important observation is that the optical pumping to the ($F = 2, m = 2$) state is not perfect. It has an efficiency of 80% and the remaining atoms are mostly in ($F = 1, m = -1$). It is important to get rid of them, otherwise they could heat up the ($F = 2, m = 2$) atoms through collisions and generate hyperfine-changing losses. The best way to do this is to evaporate them by scanning the RF frequency to induce a transition to a high-field seeking state ($F = 1, m = -1 \leftrightarrow F = 2, m = -2$) (see Fig. 4.10). The resonance condition for this process is given by $\nu_{RF} = 803.5\text{MHz} - 2.1 \times B$ (MHz/G). The scanning time that we have used is 3 s.

6.2 Measurements using RF Cuts

During the evaporation process it is important to know how some physical variables change. In particular we would like to know what the elastic collision rate and density values are and how they are changing. Also it is important to know if the temperature is decreasing

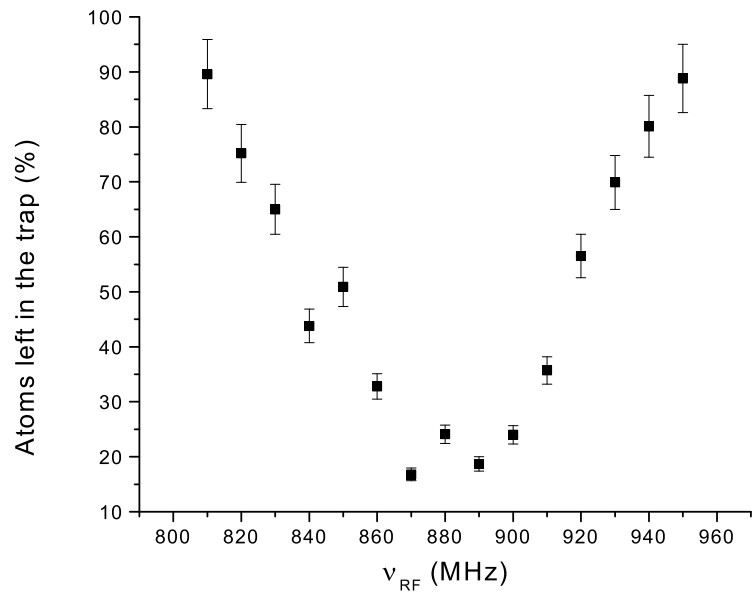


Figure 6.2: RF spectroscopy of ($F' = 2$, $m' = 2$) atoms in a TOP with $B_T = 35$ G and $B'_r = 168$ G/cm. The minimum corresponds to the frequency where the atoms at the center of the trap are on resonance.

and, especially, if the phase-space density is increasing. All these quantities can be derived from only two measurements: the number of atoms and the temperature. For the number of atoms fluorescence was used, as it is described in section 4.4. However free expansion could not be used for the temperature. It is not reliable enough and it is also cumbersome to use it during the evaporation process. We would need to ramp down the magnetic field before shutting it down (to avoid eddy currents), affecting the temperature value. Instead RF cuts were used to estimate the temperature in the trap. It was done by scanning the RF frequency from ν_{max} down to different frequencies ν_{RF} and recording the number of atoms kicked out. When ν_{RF} reaches ν_{min} we should get rid of all the atoms. The graph Fraction of atoms evaporated $\propto (\nu_{RF} - \nu_0)$ gives us information with respect to the average energy of the cloud and, consequently, its temperature.

For the particular case of the TOP trap, the surface where the atoms are kicked out by the RF is defined as [131]:

$$(m'_F g'_F - m_F g_F) \mu_B \max_t |B_{TOP}(\vec{r}, t)| = h(\nu_{RF} - \nu_0), \quad (6.2)$$

where the maximum is taken over a TOP rotation period and h is the Planck constant. Using Eq. (2.38), we get:

$$\max_t |B_{TOP}(\vec{r}, t)| = B_T \sqrt{1 + \frac{\rho^2 + 4z^2}{R_D^2} + 2 \frac{\rho}{R_D}}. \quad (6.3)$$

It is important to find out ρ_0 such that, for a given ν_{RF} , all the atoms with $\rho \geq \rho_0$ are evaporated. The maximum value of ρ is on the xy plane (remember that for the TOP trap $\omega_z^2 = 8\omega_r^2$), so we need to solve Eq. (6.2) with $z = 0$. Using this condition and Eq. (6.3) we have:

$$\rho^2 + 2R_D \rho + R_D^2 \left[1 - \left(\frac{\Delta\nu_{RF}}{\Delta\nu_{min}} \right)^2 \right] = 0, \quad (6.4)$$

where $\Delta\nu_{RF} \equiv \nu_{RF} - \nu_0$ and $\Delta\nu_{min} = (m'_F g'_F - m_F g_F) \mu_B B_T / h$. The only physical solution of (6.4) is the positive root:

$$\rho_0 = R_D \left(\frac{\Delta\nu_{RF}}{\Delta\nu_{min}} - 1 \right) \quad (6.5)$$

Equation (6.5) agrees with what has been said before: when $\Delta\nu_{RF} = 2\Delta\nu_{min} \Rightarrow \rho_0 = R_D$, meaning that atoms are kicked out at the “circle of death” and above. When $\Delta\nu_{RF} = \Delta\nu_{min} \Rightarrow$

$\rho_0 = 0$ and all the atoms in the trap are at resonance at a certain time and eventually are evaporated. Given a frequency ν_{RF} , the minimum energy that an atom needs to have to be evaporated in the TOP is:

$$E_{min} = \frac{1}{2} m \omega_r^2 \rho_0(\nu_{RF}). \quad (6.6)$$

Using (2.42) and (6.5) in (6.6):

$$E_{min} = \frac{|m'_F g'_f|}{4} \mu_B B_T \left(\frac{\Delta\nu_{RF}}{\Delta\nu_{min}} - 1 \right)^2. \quad (6.7)$$

Using the equipartition theorem the temperature of the cloud can be estimated. For a harmonic trap (good approximation for the TOP at low temperatures), we have that $\bar{E} = 3k_B T$, where \bar{E} is the average energy of the cloud. This average can be calculated with RF cuts. A measurement of $f(\nu_{RF}) \times \nu_{RF}$ is done, where $f(\nu_{RF})$ is the fraction of atoms kicked out when the RF frequency is ramped from ν_{max} down to ν_{RF} . Using Eq. (6.7) we create a new graph $f(E) \times E$. The area under this graph gives us \bar{E} and the temperature can be estimated from:

$$T = \frac{1}{3k_B} \int_0^\infty f(E) dE. \quad (6.8)$$

Now that the number of atoms and the temperature are known, the other physical parameters can be calculated. The average size of the cloud can be estimated by using the virial theorem [151]. It says that for a harmonic trap $\bar{E}_k = \bar{U}$, where \bar{E}_k and \bar{U} are the time average of the kinetic and potential energy. Using (2.41) and the equipartition theorem:

$$k_B T = \frac{1}{2} m \omega_r^2 \bar{\rho^2}, \quad (6.9)$$

$$\frac{k_B T}{2} = \frac{1}{2} m \omega_z^2 \bar{z^2}. \quad (6.10)$$

Applying (2.42) and (2.43) in (6.9) and (6.10) the root-mean-square (rms) value of the radial and axial size of a cloud in a TOP can be obtained:

$$\rho_{rms} \equiv \sqrt{\bar{\rho^2}} = \sqrt{\frac{4k_B T}{|\mu|} \frac{B_T}{(B'_r)^2}}, \quad (6.11)$$

$$z_{rms} \equiv \sqrt{\bar{z^2}} = \sqrt{\frac{k_B T}{4|\mu|} \frac{B_T}{(B'_r)^2}}. \quad (6.12)$$

The atomic density of a cloud in a potential $U(\rho, z)$, at thermal equilibrium, is given by:

$$n(\rho, z) = n_p e^{-U(\rho, z)/k_B T}, \quad (6.13)$$

where n_p is the peak density. Using the potential energy for the TOP (2.41) and the definition (6.11) and (6.12), we have:

$$n(\rho, z) = n_p e^{-\rho^2/\rho_{rms}^2} e^{-z^2/2z_{rms}^2}. \quad (6.14)$$

Knowing that the total number of atoms is given by $N = \int n(\rho, z) dV$, n_p is calculated by integrating (6.14):

$$n_p = \frac{2N}{(2\pi)^{3/2} \rho_{rms}^2 z_{rms}} = N(B'_r)^3 \left(\frac{\mu_B}{2\pi k_B T B_T} \right)^{3/2}, \quad (6.15)$$

where we have used the fact that atoms in ($F = 2$, $m = 2$) have $|\mu| = \mu_B$. However the most appropriate density to use in the elastic collision rate (2.65) is the average density. It is defined as:

$$n_{av} \equiv \frac{\int n(\rho, z) e^{-U(\rho, z)/k_B T} dV}{\int e^{-U(\rho, z)/k_B T} dV}. \quad (6.16)$$

Using (2.41) and (6.13) in (6.16), the expression of the average density for the TOP is given by:

$$n_{av} = \frac{n_p}{\sqrt{8}}. \quad (6.17)$$

The average thermal velocity (2.67) can also be expressed in a simpler formula if we input the mass of ${}^7\text{Li}$:

$$v_{th} = 5.5\sqrt{T} \left(\frac{\text{cm}}{\text{s}\sqrt{\mu\text{K}}} \right). \quad (6.18)$$

With Eqs. (6.8), (6.15), (6.17) and (6.18), the values for Γ_{el} (2.65) and the PSD (2.62) can be calculated for a cloud in the TOP trap. This way we can observe their evolution during the evaporation and see if it is working as expected or not.

6.3 Evaporation Results

In this section I will describe the preparation process for evaporative cooling and our first results. The first encouraging signs came from RF evaporation in a Quadrupole trap. An increase in density and PSD has been observed during the evaporation. The next step was to try it in the TOP. We could not get exactly the same behavior and a detailed analysis was done to determine the reason. I will explain this analysis and discuss its consequences for the experiment.

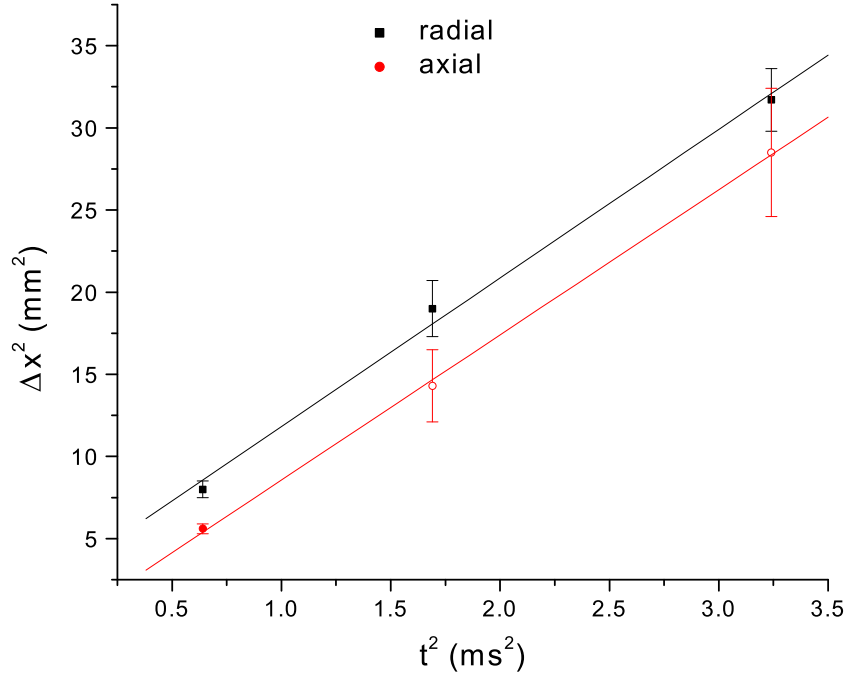


Figure 6.3: Free expansion of a MOT with 2×10^9 atoms. The radial temperature is 1.9 mK and the axial is 1.8 mK.

6.3.1 MOT Temperature

Free expansion was used to estimate the MOT temperature. The cloud $1/e^2$ size was measured using absorption imaging. With a cooling time of 0.5 ms, the slope in Fig. 6.3 gives:

$$T_r = 1.9 \text{ mK} , \quad (6.19)$$

$$T_z = 1.8 \text{ mK} . \quad (6.20)$$

This is much hotter than before when there were only 2×10^8 atoms. The cooling parameters were tweaked and the coldest that the MOT got was 1.2 mK with 1 ms cooling time. The reason for this increase in temperature is the larger number of atoms in the MOT. As I described at the end of section 2.3.2, in the constant density regime $T_{MOT} \propto N^{1/3}$ (2.36).

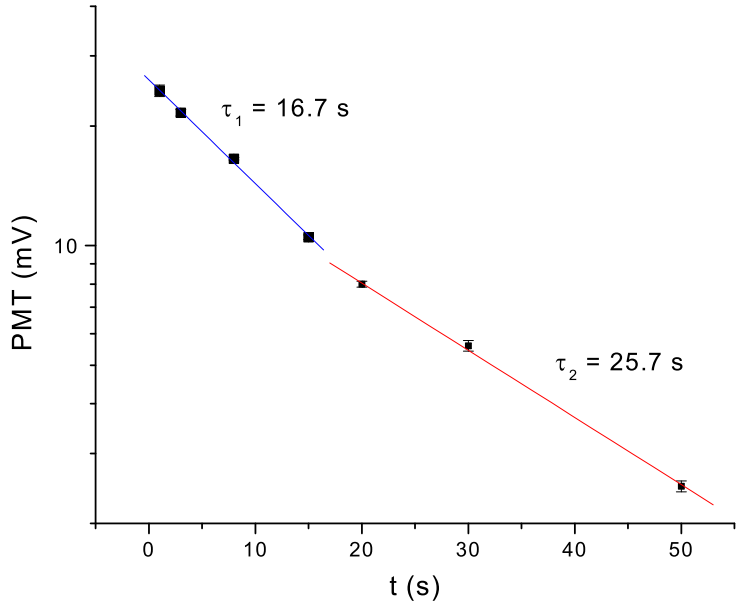


Figure 6.4: Lifetime measurement in a Quadrupole with $B'_r = 88 \text{ G/cm}$. It is characterized by two different decay rates.

This effect has already been observed with other atoms [97, 115], including ^7Li [152]. From our gain of atoms it is expected from the theory an increase in temperature by a factor of $10^{1/3} \cong 2.15$. However the measured increase was $\sim 1000/250 = 4$. The discrepancy is probably due to the uncertainty in temperature estimates with free expansion that can be as high as 50%.

6.3.2 Lifetime in the Quadrupole and the TOP

An important parameter that determines if degeneracy can be reached is the trap lifetime. Assuming that Γ_{el} is large enough to generate efficient evaporation, a long lifetime is needed in order that the total number of elastic collisions obeys $\Gamma_{el}\tau > 100$. Figure 6.4 shows the lifetime measurement in a Quadrupole trap with $B'_r = 88 \text{ G/cm}$ and 2.5×10^7 atoms. It is interesting to note that there are two decay rates. The faster one at $t \leq 15 \text{ s}$ is probably caused by the contribution of hot atoms and atoms in the high-field seeking states leaving

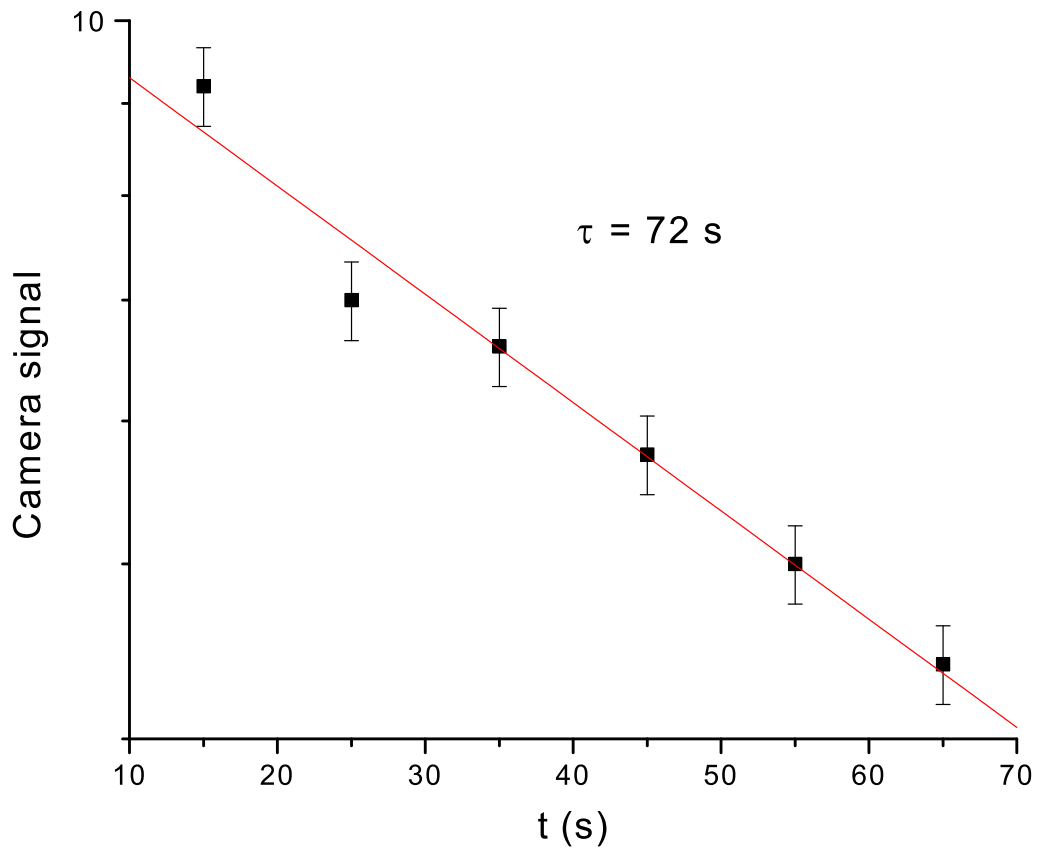


Figure 6.5: Lifetime in a Quadrupole with $B'_r = 168 \text{ G/cm}$ before installing the transverse cooling.

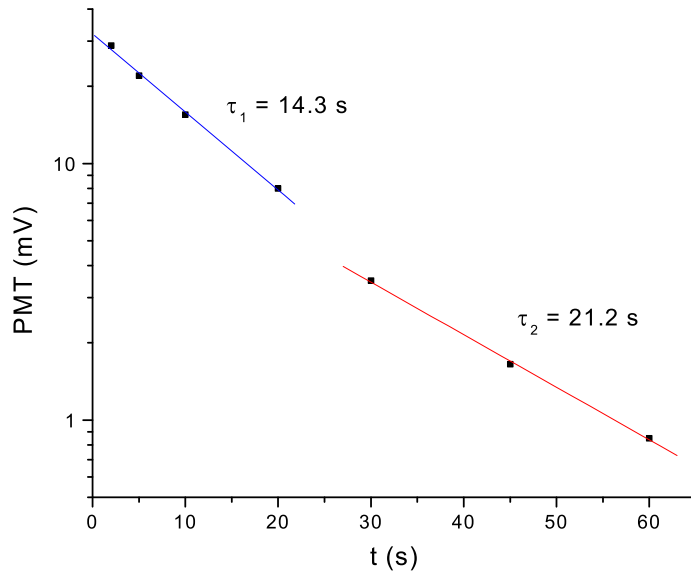


Figure 6.6: Lifetime measurement in a TOP with $B'_r = 88$ G/cm and $B_T = 35$ G. It also has two different decay rates.

the trap. The slower decay rate gives a lifetime of 26 s. This is much shorter than the 70 s that we had before implementing the transverse cooling (Fig. 6.5).

Figure 6.6 shows the measured lifetime in a TOP with $B'_r = 88$ G/cm and $B_T = 35$ G. It also has two different decay rates and is shorter than before the installation of the 2D cooling (Fig. 6.7). The reason for the fast loss of atoms in the beginning is the same as for the Quadrupole. In addition the TOP has the “circle of death” that helps to kick out the hot atoms even faster. This is the reason why the TOP lifetime is shorter than the Quadrupole one.

The vacuum clearly got worse after installing the transverse cooling. Previously we had $\tau \sim 70$ s, while now it is around 20 s. We suspect that the new skimmer has not been cleaned properly and it is outgassing, damaging the trap lifetime. However, instead of breaking up the vacuum and trying to fix the problem, we have preferred to see if evaporative cooling could be observed. The lifetime is not long enough to reach BEC, but

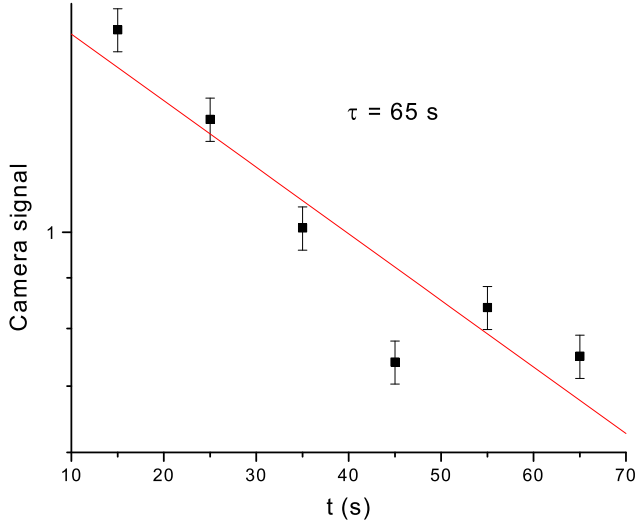


Figure 6.7: Lifetime in a TOP with $B'_r = 168$ G/cm and $B_T = 25$ G before installing the transverse cooling.

the evaporation process only depends on the elastic collision rate and to verify if it works or not became our first priority.

6.3.3 Evaporative Cooling in the Quadrupole

Before trying evaporation in the TOP, we would like to try it first in the Quadrupole. The reason is that it is a simpler trap to work with. There is no “circle of death” radius and only one adjustable parameter: the radial gradient B'_r . It is also very tight, something important to ensure a large atomic density.

First it is important to know the physical properties of the cloud right after being transferred to the Quadrupole. Using fluorescence we measured $N = 5 \times 10^8$ polarized atoms in ($F = 2, m = 2$) state in a Quadrupole with $B'_r = 88$ G/cm. Using RF cuts (1000 MHz $\rightarrow \nu_{RF}$) we estimated their temperature. Following the procedure described in section 6.2, the temperature was obtained from Fig. 6.8. The equations have to be adapted for a Quadrupole field. The condition for ρ_0 is obtained straightforwardly from (6.2) using

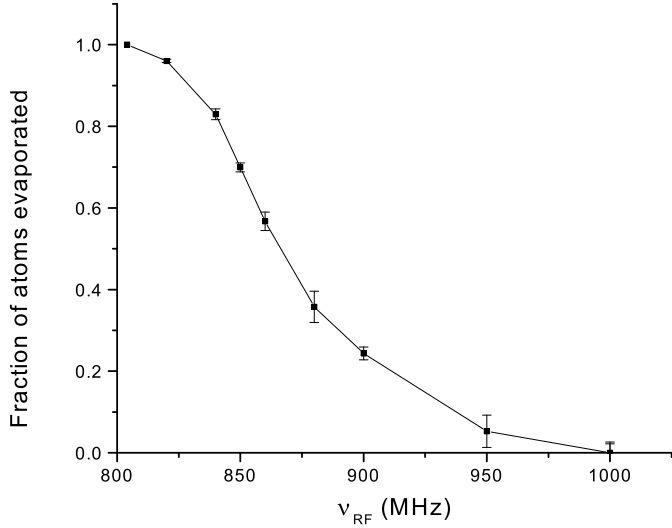


Figure 6.8: RF cut in a Quadrupole trap with $B'_r = 88$ G/cm. The RF ramp started at 1 GHz and lasted for 3 s. This graph gives a temperature of $537 \mu\text{K}$ for the cloud.

equation (2.29):

$$\rho_0 = \frac{2}{3} \frac{h}{\mu_B B'_r} \Delta\nu_{RF} , \quad (6.21)$$

where it was used $m'_F g'_F = 1$ and $(m'_F g'_F - m_F g_F) = 3/2$. The equation for E_{min} is:

$$E_{min} = \frac{2}{3} h \Delta\nu_{RF} . \quad (6.22)$$

The equipartition theorem for a linear trap gives the relation $\bar{E} = 9/2 k_B T$. Using this in (6.22):

$$T = \frac{4}{27} \frac{h}{k_B} \overline{\Delta\nu_{RF}} , \quad (6.23)$$

where $\overline{\Delta\nu_{RF}}$ is obtained from the area under the graph 6.8. Its value is $\overline{\Delta\nu_{RF}} = 75.5$ MHz, and knowing that $h/k_B = 48 \mu\text{K}/\text{MHz}$, we get $T = 537 \mu\text{K}$.

Using the equipartition theorem the average size of the cloud can be found in cylindrical coordinates:

$$\bar{r} = \sqrt{2} \frac{k_B T}{\mu_B B'_r} , \quad (6.24)$$

$$\bar{z} = \frac{1}{2} \frac{k_B T}{\mu_B B'_r} . \quad (6.25)$$

The density in thermal equilibrium obeys (6.13). Using (2.29) and integrating (6.13) over the cloud volume, a relation for the peak density in a Quadrupole is obtained:

$$n_p = \frac{N}{4\pi (\bar{\rho})^2 \bar{z}} . \quad (6.26)$$

The average density, defined by (6.16), is given by:

$$n_{av} = \frac{n_p}{8} . \quad (6.27)$$

All the major parameters for a cloud in a Quadrupole trap with $B'_r = 88$ G/cm can now be calculated:

$$N = 5 \times 10^8 \text{ atoms ,} \quad (6.28)$$

$$T = 537 \mu\text{K ,} \quad (6.29)$$

$$\bar{\rho} = 1.3 \text{ mm ,} \quad (6.30)$$

$$\bar{z} = 0.45 \text{ mm ,} \quad (6.31)$$

$$n_p = 5.2 \times 10^{10} \text{ cm}^{-3} , \quad (6.32)$$

$$n_{av} = 6.5 \times 10^9 \text{ cm}^{-3} , \quad (6.33)$$

$$v_{th} = 127 \text{ cm/s ,} \quad (6.34)$$

$$\sigma = 5.4 \times 10^{-13} \text{ cm}^2 \text{ for } (F = 2, m = 2) , \quad (6.35)$$

$$\Gamma_{el} = 0.63 \text{ s}^{-1} . \quad (6.36)$$

The elastic collision rate (6.36) is very small and this indicates that the evaporative cooling might not work. In our first trial the Quadrupole gradient during the RF ramp was not changed (see Fig. 6.9). Figure 6.10 shows the change of the cloud size, density and PSD with different ν_{RF} . There is no cooling of the cloud and no gain in PSD. There is no evaporative cooling!

The most probable reason why efficient evaporation was not observed is the fact that (6.36) is too small. As I have discussed in section 2.4.3, the Quadrupole gradient can be ramped up to compress the atoms and increase Γ_{el} . The timing sequence is shown in Fig. 6.11 and the compression factor is $\alpha = 332/88 \cong 3.8$. Using this value in (2.77), the elastic collision rate scales as $\Gamma'_{el}/\Gamma_{el} = (3.8)^{4/3} \cong 6$ when $B'_r = 332$ G/cm. Using the value (6.36),

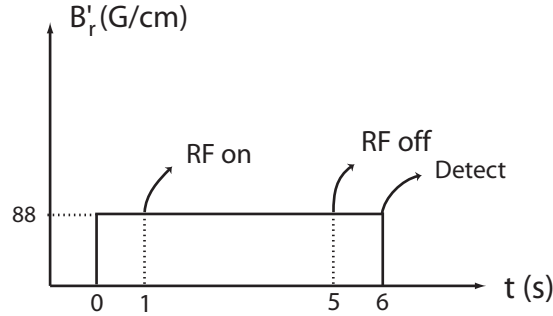


Figure 6.9: Timing for the Quadrupole evaporation without compression. The RF started at 1000 MHz and ramped down to ν_{RF} in 4 s.

Γ_{el} reaches the maximum at $\Gamma'_{el} = 3.8 \text{ s}^{-1}$. This is a much better value than before and we should be able to observe some evaporation. The results are shown in Fig. 6.12. Evaporative cooling clearly happened. The cloud $1/e$ size decreased by a factor of 2, indicating cooling. The density increased by a factor 3 while the PSD increased by a factor of 10. This shows how important it is to have a large value for Γ_{el} and how adiabatic compression can be used to obtain it.

6.3.4 Evaporative Cooling in the TOP

The first thing that is necessary to be done is to optimize the transfer MOT \rightarrow TOP. The objective is to maximize the initial number of atoms in the TOP and the elastic collision rate. Figure 6.13 shows the number of atoms transferred to the TOP as a function of B_T for different radial gradients. It clearly indicates that the best transfer happens at low B'_r and high B_T . It makes sense since this condition maximizes the “circle of death” radius $R_D = B_T/B'_r$, increasing the capacity of the TOP to trap the hottest atoms. The only exception is for $B'_r = 57 \text{ G/cm}$. In this case the MOT is too far from mode matching with the TOP, as we can see from Eq. (4.47), and the transfer is very inefficient.

It is also interesting to study what fraction of atoms is below R_D right after the transfer. That can be done by applying an RF at ν_{max} for 2 s to kick out atoms at $\rho \geq R_D$. The results are shown in Fig. 6.14. As expected, if B'_r is small and B_T is large, all the atoms

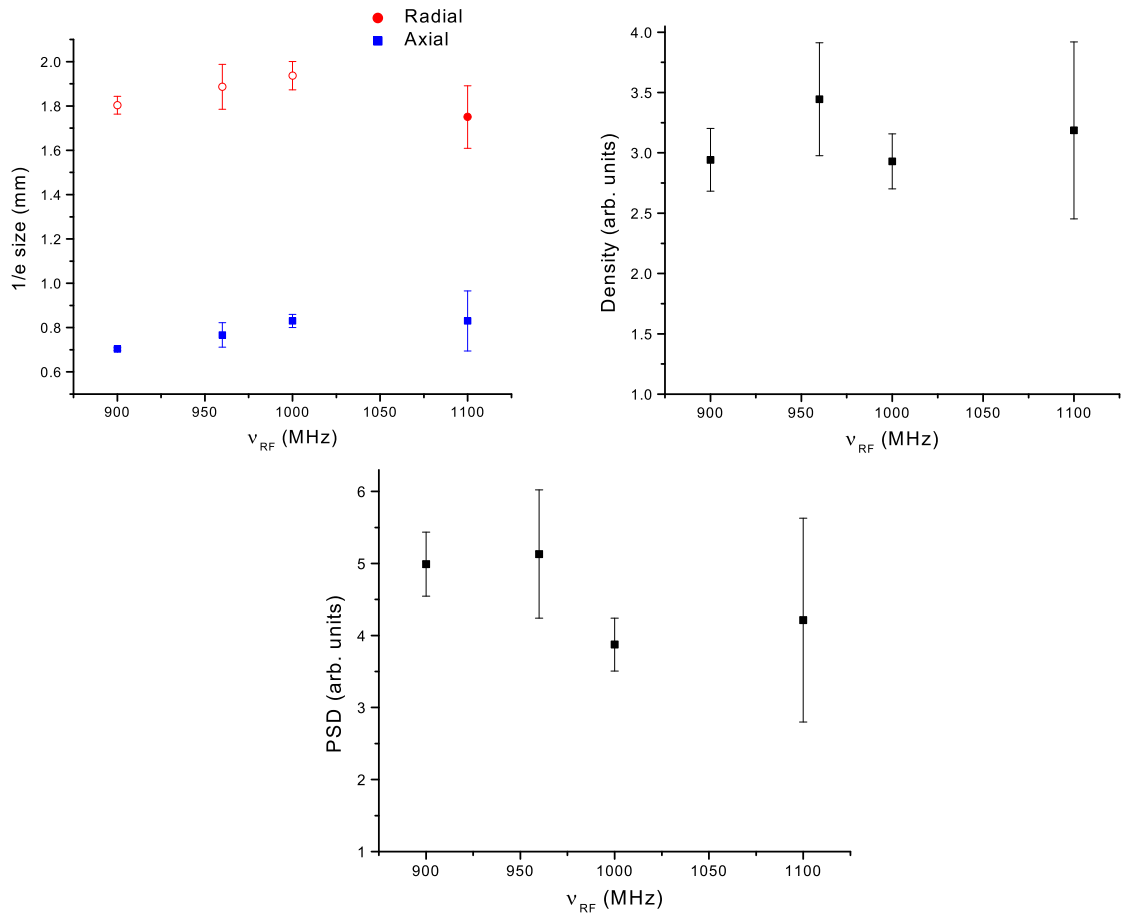


Figure 6.10: Change of the cloud physical parameters during Quadrupole evaporation with no compression. There are no gains in density and PSD, indicating that there is no evaporative cooling. The cloud size also remained the same, a further indication of no cooling. The $1/e$ size was measured with absorption imaging.

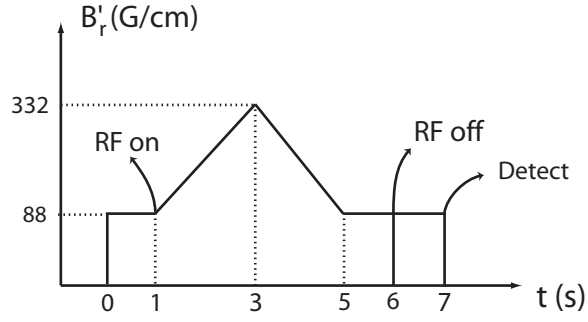


Figure 6.11: Timing sequence for the Quadrupole evaporation with adiabatic compression.

are below R_D . From figures 6.13 and 6.14 we can see that the best TOP configuration for the transfer seems to be $B'_r = 88$ G/cm and $B_T \geq 50$ G.

However maximizing the number of atoms transferred not necessarily maximizes the elastic collision rate. It is also necessary to measure the temperature at different TOP configurations to find out the mode matching condition. Using RF cuts we have measured the cloud temperature for different pairs (B'_r, B_T) . The number of atoms was measured with fluorescence. Care was taken to measure only those below R_D by blasting RF at ν_{max} for 2 s before detection. The other parameters were estimated using the equations from section 6.2. As an example we show in Fig. 6.16 an RF cut in a TOP with $B'_r = 332$ G/cm and $B_T = 50$ G. The experimental procedure is the following: ramp up B'_r to the desired value and after 0.5 s turn on the RF at $\nu_{max} = 1013$ MHz for 2 s. This guarantees that only atoms below R_D remain in the trap. Wait for 0.5 s and turn on the RF ramp from ν_{max} down to ν_{RF} for 2 s. For $B_T = 50$ G we have $\nu_{min} = 908$ MHz. Before detecting the number of atoms left in the trap, ramp down B'_r to 88 G/cm in 0.5 s to shut it down. The idea is to avoid large eddy currents that can distort the fluorescence measurement. Table 6.1 shows all our measurements.

The data from table 6.1 can be better analyzed using the contour graphs 6.17 to 6.21. Figure 6.17 shows what is already known from Fig. 6.13: the maximum number of atoms transferred happens at low gradients and high TOP fields. Figure 6.18 gives the temperature dependence on (B'_r, B_T) . The general trend is $T \propto B_T$. This is expected since a larger B_T

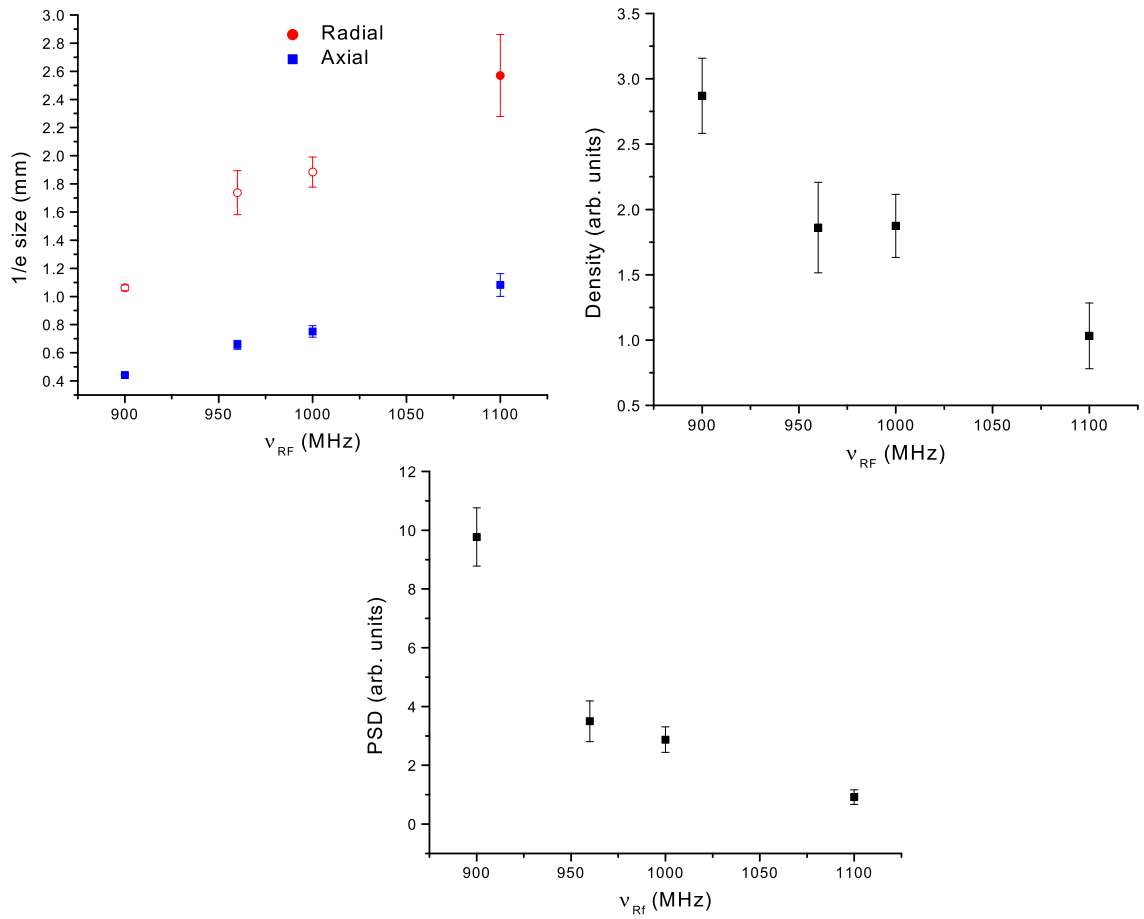


Figure 6.12: Change in the physical properties of the cloud in a Quadrupole during evaporation with adiabatic compression. It is clear the gain in density and PSD and the decrease in cloud size indicating cooling. The $1/e$ size was measured with absorption imaging.

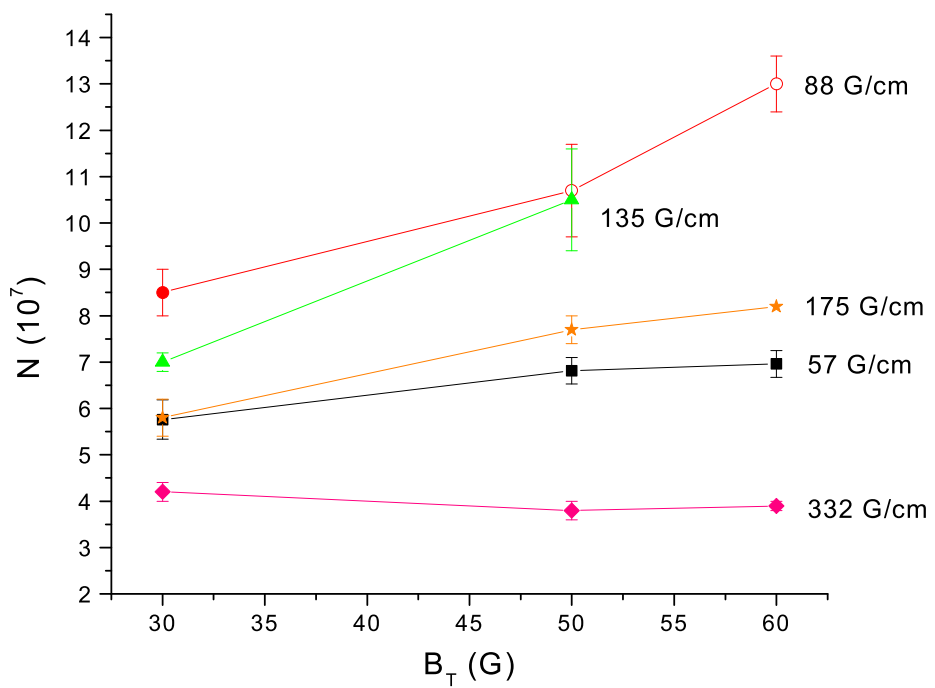


Figure 6.13: Number of atoms transferred from the MOT to the TOP with different radial gradients.

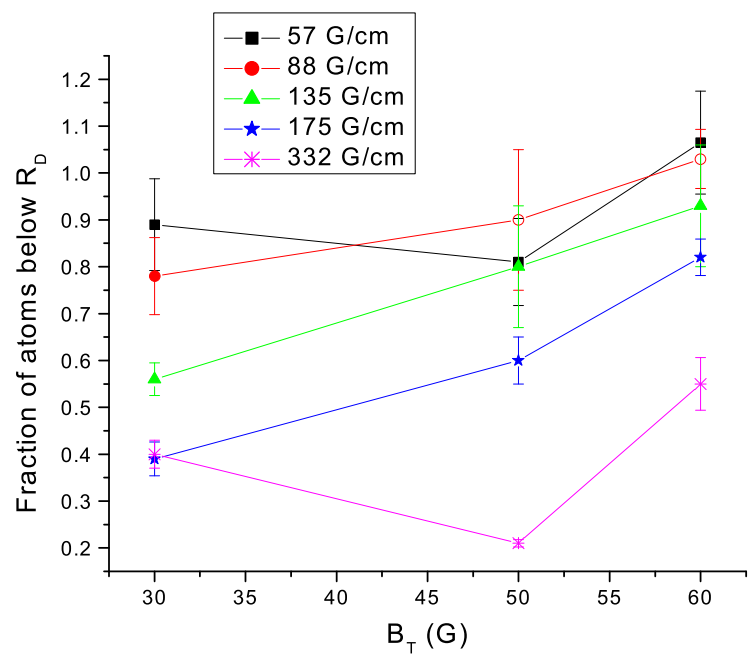


Figure 6.14: Fraction of atoms below the “circle of death” for different radial gradients.

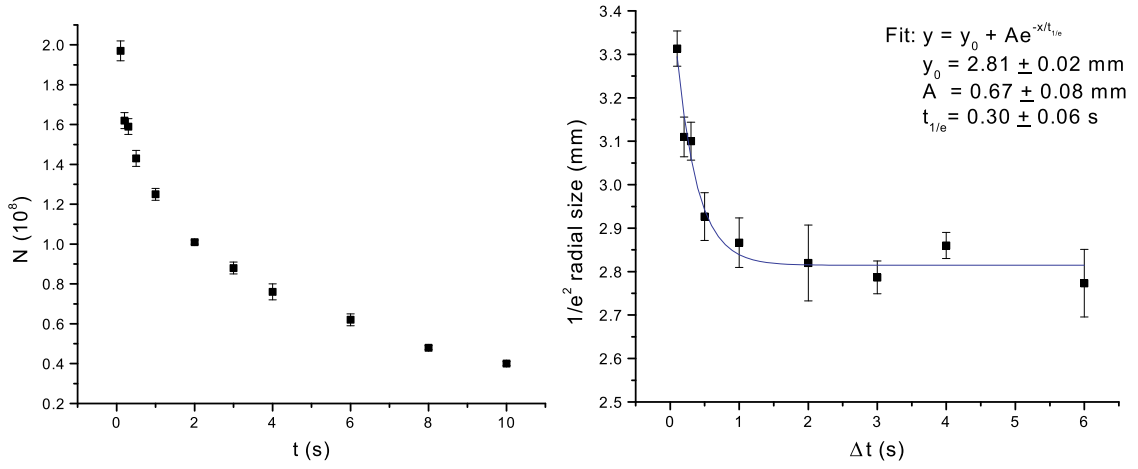


Figure 6.15: In a short time the hot atoms leave through the “circle of death” reducing the cloud radius. The size and number of atoms were measured with fluorescence.

traps more hot atoms, warming up the cloud. The density and elastic collision rate graphs 6.19 and 6.20 are very similar because $\Gamma_{el} \propto n_{av}$. The graph 6.21 for PSD is also similar. These last three graphs show that the region for mode matching the MOT \rightarrow TOP transfer is on the vicinity of (250 G/cm, 42 G).

Only the beginning of evaporation due to the “circle of death” has been observed. Figure 6.15 shows the variation of number of atoms and size of a cloud transferred to the TOP with (88 G/cm, 40G). Knowing that the density scales with size as $n \propto N/\rho^3$ and the temperature as $T \propto \rho^2$ (6.11), it can be obtained from graph 6.15 that in 1 s the PSD increased by a factor of 2. In order to keep it increasing, the “circle of death” radius has to decrease and RF should be applied. However whenever we tried forced evaporative cooling in the TOP, we could not get any results. The TOP field B_T was ramped down for 5 s to evaporate the atoms using the “circle of death”. Atoms were lost without any gain in phase-space density. In many cases the cloud actually got hotter! As an example, in one trial the TOP was at (332 G/cm, 50 G). The cloud initial temperature was $120 \mu\text{K}$ (see Fig. 6.16). After ramping down B_T to 20 G in 5 s (we kept B'_r constant), the number of atoms below R_D and their temperature were measured. Almost 50% of the atoms were above the “circle of

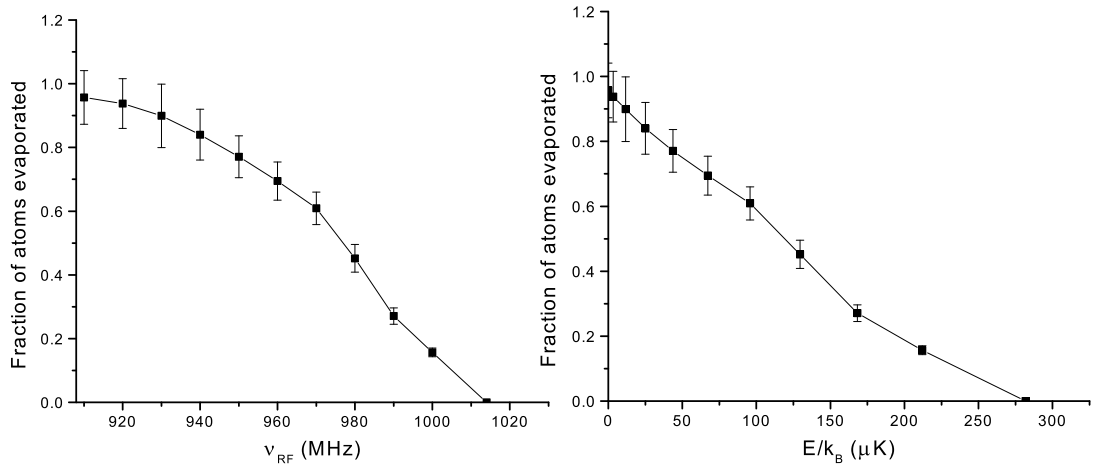


Figure 6.16: RF cuts in a TOP with $B'_r = 332$ G/cm and $B_T = 50$ G after being transferred from the MOT. The temperature estimated from the graph is $120 \mu\text{K}$.

“death” and the temperature measured with RF cuts was $246 \mu\text{K}$.

An indication of why this is happening can be seen in Fig. 6.20. The maximum value for Γ_{el} is 1 s^{-1} at (253 G/cm, 40 G). Even if the cloud is adiabatically compressed to $B'_r = 332$ G/cm (the maximum that can be achieved in our experiment), the new elastic collision rate (2.74) will be only $\Gamma_{el} = (332/253)^2 = 1.7 \text{ s}^{-1}$. This elastic collision rate was able to re-thermalize the atoms in the first second in the TOP, but when forced evaporation started it was not large enough to re-thermalize the remaining atoms at the right pace. Too many atoms were lost, reducing Γ_{el} even more and stopping the evaporation process.

B'_r (G/cm)	B_T (G)	N(10^7)	T (μK)	n_{av} (10^{10} cm^{-3})	R (s^{-1})	PSD (10^{-6})
135	30	3.81	88	0.85	0.31	3.0
214	30	1.25	59	2.03	0.61	13.0
253	30	0.74	59	1.98	0.59	12.7
332	30	0.28	68	1.37	0.44	7.1
135	40	6.6	73	1.27	0.42	5.9
214	40	3.4	71	2.71	0.89	13.1
253	40	2.4	71	3.16	1.04	15.3
332	40	0.75	88	1.62	0.59	5.7
135	50	8.8	61	1.58	0.48	9.6
214	50	5	100	1.71	0.66	4.9
253	50	3.8	86	2.69	0.97	9.8
332	50	1.93	120	1.87	0.80	4.1
135	60	9	106	0.54	0.22	1.4
214	60	6.6	156	0.88	0.43	1.3
253	60	5.2	149	1.23	0.58	2.0

Table 6.1: Physical parameters calculated for the MOT \rightarrow TOP mode matching.

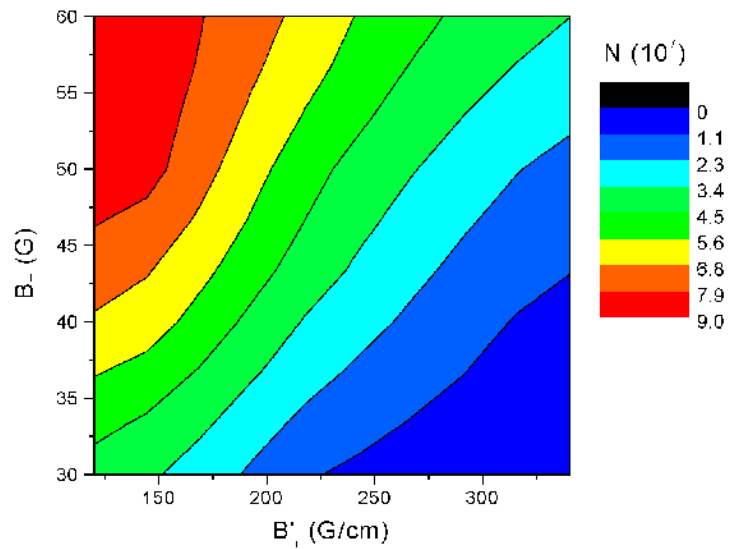


Figure 6.17: Number of atoms

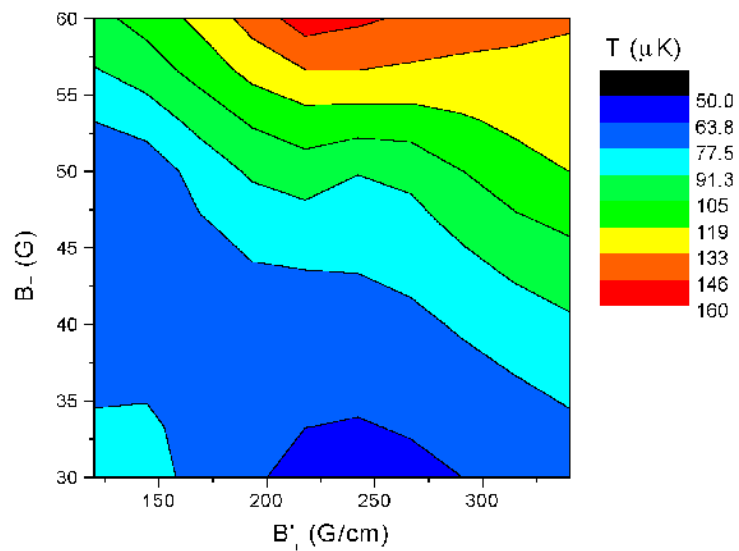


Figure 6.18: Temperature.

Step	N (10^8)	Loss factor
MOT before cooling	20	—
MOT after 0.3 ms cooling	14	1.4
MOT after cooling and pumping to ($F = 2, m = 2$)	10	2
Quadrupole, $B'_r = 88 \text{ G/cm}$, $\Delta t = 0.5 \text{ s}$	2.5	8
TOP (88 G/cm, 40 G), no RF cut at $\rho \geq R_D$, $\Delta t = 0.5 \text{ s}$	1.4	14
TOP (88 G/cm, 40 G), after RF cut at $\rho \geq R_D$, $\Delta t = 1 \text{ s}$	1.2	17
TOP (88 G/cm, 40 G), after RF cut at $\rho \geq R_D$, $\Delta t = 4 \text{ s}$	0.74	27
TOP (253 G/cm, 40 G), after RF cut at $\rho \geq R_D$, $\Delta t = 4 \text{ s}$	0.25	80

Table 6.2: Number of atoms measured with fluorescence at each experimental step. The loss factor is defined as the number of atoms in the MOT before cooling divided by the number measured at each step.

6.3.5 What is the problem with the TOP?

It is important to find out what was the reason for such a small Γ_{el} in the TOP. I believe that the main culprit is that the evaporation started in the TOP with fewer atoms than we expected. A careful study of how many atoms are lost in each step during cooling and trapping has been done. Table 6.2 shows our results. The parameter Δt is the time that the cloud has been in the magnetic trap. Table 6.2 shows that the TOP loses a lot of atoms in a short period of time after the transfer. This is due to hot atoms leaving through the “circle of death”. In the mode matched situation (253 G/cm, 40 G), after 4 s in the TOP (close to the time we start evaporation), there are only 2.5×10^7 atoms left. This is the reason why the elastic collision rate is so small.

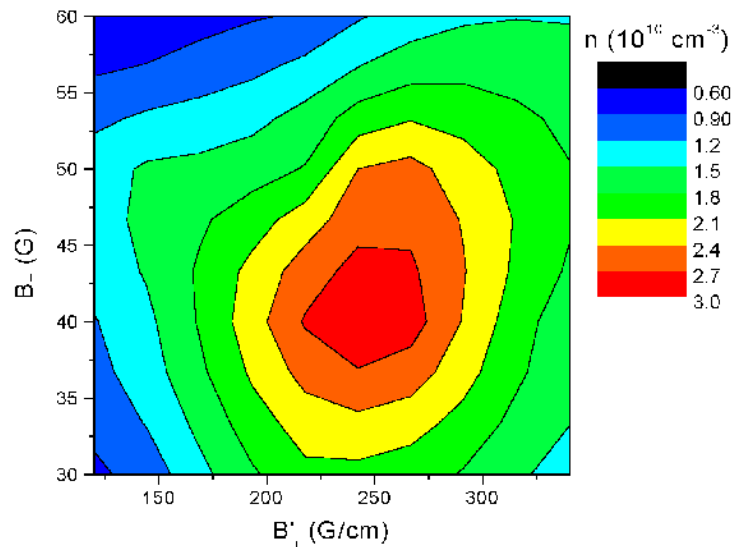


Figure 6.19: Density of atoms.

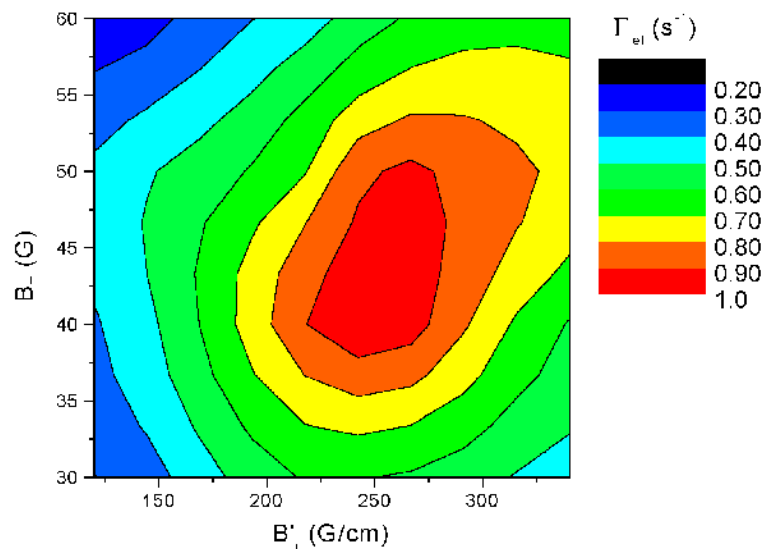


Figure 6.20: Elastic collision rate.

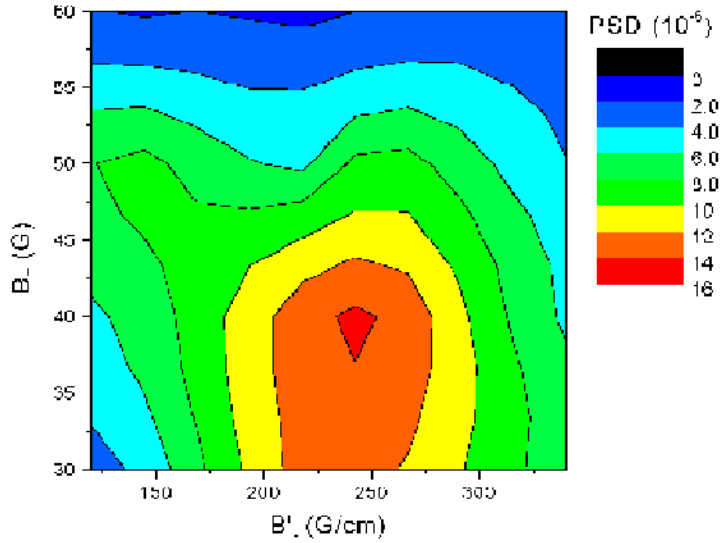


Figure 6.21: Phase-space density.

The origin for so many hot atoms is the MOT. As shown in section 6.3.1, even after cooling its temperature was still at least 1 mK. We could try to cool the cloud even more, however this is not that easy to implement with lithium. That is because sub-Doppler cooling can not be used due to its close-spaced excited states. This limits how cold it can get in the MOT. Another possibility is to use Doppler cooling inside the trap. This has been done before by the group of C. Salomon with ^7Li in an Ioffe-Pritchard trap [153]. However in a TOP this is not that simple. A cloud in a TOP sees the magnetic field varying from 0 to $2B_T$ (see section 6.1). Hence the maximum Zeeman shift inside this trap is $\Delta\nu_{TOP} \propto 2B_T$. The same cloud in an IP trap would see a maximum magnetic field $B_{IP} \sim B_T/4$, where we have used (2.46) and (2.50) with $\Delta U_{TOP} = \Delta U_{IP}$. So the Zeeman shift variation in the TOP is $\Delta\nu_{TOP}/\Delta\nu_{IP} = 8$ times bigger than in the IP trap. As a consequence in the TOP a red-detuned cooling beam will not be on resonance with all the atoms and it might even be blue-detuned with some. Also in the TOP there is not a reference B-field to keep the atoms polarized during the laser cooling. This is the reason why laser cooling would not be easy to implement. And this is a problem because, due to the “circle of death”, the TOP

is an energetic shallow trap when compared to other magnetic ones. Therefore when the cloud is transferred, too many atoms ended up being lost, decreasing the atomic density and the elastic collision rate.

Chapter 7

Conclusion

We have successfully implemented transverse 2D cooling to compress an atomic beam of ${}^7\text{Li}$. Using frequency spread light and a zigzag beam configuration, the loading rate of the MOT was increased by a factor of 13. This gave an increase by a factor of 10 in the number of atoms trapped in the MOT, improving the initial conditions for evaporation. The transverse cooling worked so well because the frequency spread light increased the capture velocity and the zigzag configuration guaranteed a long interaction length.

In the theoretical analysis we showed that the most important parameter when compressing a beam is the ratio $(v_{ct}/v'_t)^2$ in agreement with [16]. The transverse capture velocity v_{ct} is defined by the geometry of the system and the cooling light. The transverse velocity after cooling v'_t is dependent on the 2D cooling and the interaction length. Given enough intensity on the 2D beams ($S \gg 1$), it is important to assure that the interaction length is long enough for the atoms to reach the Doppler speed transversely. However if the light intensity is too low ($S \lesssim 1$), the atoms can not reach v_d and the gain in density is less than maximum (Fig. 5.6). Using the Fokker-Planck equation for 1D laser cooling, a phenomenological equation for $\langle(v'_t)^2\rangle$ was obtained that fits our data well if we assume an effective saturation intensity of 7.7 mW/cm^2 for ${}^7\text{Li}$.

We have also studied the evaporative cooling of ${}^7\text{Li}$ in a Quadrupole and in a TOP trap. We have shown how the temperature inside the trap can be estimated using RF cuts. Doing a series of measurements of number of atoms and temperature we were able to experimentally obtain the mode matching condition for the transfer MOT \rightarrow TOP in the

neighborhood of (250 G/cm, 40 G). Evaporative cooling in the Quadrupole was observed after adiabatic compressing the radial gradient from 88 G/cm to 332 G/cm. The density n increased by a factor of 3 and the PSD by a factor of 10. When there was no adiabatic compression n and PSD did not change, showing the importance of this technique to initiate evaporation. In the TOP the beginning of evaporation through the “circle of death” was observed. In the first second after transferring, the cloud PSD increased by a factor of 2. But when we tried forced evaporation by lowering B_T and applying RF, the increase in PSD stopped and too many atoms were lost. The problem is that the atoms come very hot from the MOT and a large quantity is lost in the TOP due to its small energy depth. This sudden loss decreased the atomic density, affecting the elastic collision rate. Its value ended up being too small ($\Gamma_{el} \leq 2 \text{ s}^{-1}$) to keep up an efficient evaporation process during the ramp down of B_T and ν_{RF} .

Previous successful BEC experiments using the TOP loaded the atoms at a much lower temperature (^{87}Rb with $T \sim 100 \mu\text{K}$) [4, 116, 154]. In the case of ^7Li we can not reach such values in the MOT because sub-Doppler cooling is not possible. Some recent experiments with ^7Li have used 1D laser cooling inside the magnetic trap [153]. However they have used an Ioffe-Pritchard trap that has a strong bias magnetic field. By using a circularly polarized, retro-reflected beam they have avoided optically pumping the atoms to non-trapped states during cooling. The TOP does not have a bias magnetic field, so this technique would not work. Also the Zeeman shift across the cloud is eight times larger than inside an IP trap, making the laser cooling even more difficult. At the end we conclude that there are fundamental limitations to an efficient evaporation of ^7Li in a TOP trap.

The next step in our experiment is to change the magnetic trap to an Ioffe-Pritchard type. This should address the energy depth and the laser cooling problems. Using the transverse cooling to load the MOT, we believe that we will have the right initial conditions to observe evaporation and reach degeneracy in ^7Li in the near future.

Appendix A

^7Li and ^6Li Cooling Properties

Description	Symbol	^7Li	^6Li
Abundance	—	92.5%	7.5%
Mass	m	1.16×10^{-26} Kg	9.96×10^{-27} Kg
Nuclear spin	I	3/2	1
Cooling wavelength	λ	671 nm	671 nm
Doppler temperature	T_D	$140\mu\text{K}$	$140\mu\text{K}$
Doppler velocity	v_d	40 cm/s	43 cm/s
Recoil temperature	T_R	$6.1\mu\text{K}$	$7.1\mu\text{K}$
Recoil velocity	v_r	8.5 cm/s	9.9 cm/s
Excited state lifetime	τ	27.2 ns	27.2 ns
Natural linewidth	$\Gamma/2\pi$	5.9 MHz	5.9 MHz

Table A.1: Important physical properties of ^7Li and ^6Li for laser cooling.

Appendix B

^7Li Hyperfine Structure

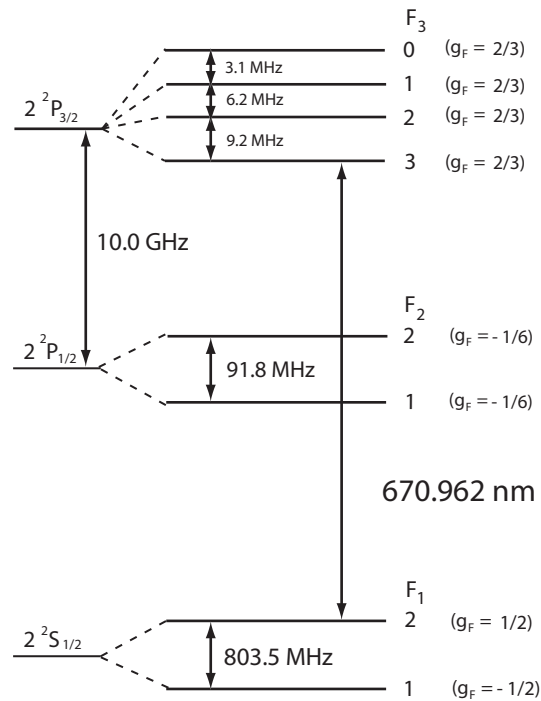


Figure B.1: The cooling transition is between $(F_1 = 2, m = 2) \leftrightarrow (F_3 = 3, m = 3)$ with a lifetime of 27.2 ns and a linewidth of 5.9 MHz. Notice that the separation between the excited levels F_3 is comparable to the linewidth. The Landé g-factor for each level is shown in parenthesis.

Appendix C

Scattering Length

	a_t	a_s	a_-	I
¹ H	1.2	0.41		1/2
⁶ Li	-2160 \pm 250	45.5 \pm 2.5		1
⁷ Li	-27.6 \pm 0.5	33 \pm 2	5.3	3/2
²³ Na	65.3 \pm 0.9	19.1 \pm 2.1	55.4 \pm 1.2	3/2
³⁹ K	-17 \pm 25	140 ⁺³ ₋₆	-20 ⁺⁴² ₋₆₄	3/2
⁴⁰ K	194 ⁺¹¹⁴ ₋₃₅	105 ⁺² ₋₃		4
⁴¹ K	65 ⁺¹³ ₋₈	85 \pm 2	69 ⁺¹⁴ ₋₉	3/2
⁸⁵ Rb	-369 \pm 16	2400 ⁺⁶⁰⁰ ₋₃₅₀	-450 \pm 140	5/2
⁸⁷ Rb	106 \pm 4	90 \pm 1	103 \pm 5	3/2
¹³³ Cs	2400 \pm 100	280 \pm 10		7/2

Table C.1: The scattering length is given in atomic units (Bohr radius = 0.529 Å). It is represented by two components: the triplet a_t and the singlet a_s . The scattering length for the hyperfine state ($F = I - 1/2, m = -F$) is a combination of singlet and triplet and it is given by a_- . The scattering length for the doubly spin polarized state ($F = I + 1/2, m = \pm F$) is equal to a_t . The last column gives the nuclear spin. These values were taken from reference [155].

Bibliography

- [1] C. Adams, M. Siegel, and J. Mlynek, Phys. Rep. **240**, 143 (1994).
- [2] L. de Broglie, Nature **112**, 540 (1923).
- [3] K. B. Davis et al., Phys. Rev. Lett. **75**, 3969 (1995).
- [4] M. H. Anderson et al., Science **269**, 198 (1995).
- [5] C. C. Bradley et al., Phys. Rev. Lett. **75**, 1687 (1995).
- [6] K. Huang, *Statistical Mechanics*, John Wiley & Sons, 2nd edition, 1987.
- [7] A. Einstein, Sitzber. Kgl. Preuss. Akad. Wiss. , 261 (1924).
- [8] A. Einstein, Sitzber. Kgl. Preuss. Akad. Wiss. **1**, 3 (1925).
- [9] T. Gredyak and D. Kleppner, in *New Trends in Atomic Physics, Les Houches Summer School 1982*, edited by G. Grynberg and R. Stora, page 1125, North-Holland, Amsterdam.
- [10] J. Doyle et al., Phys. Rev. Lett. **67**, 603 (1991).
- [11] H. Hess, Phys. Rev. B **34**, 3476 (1986).
- [12] N. Masuhara et al., Phys. Rev. Lett. **61**, 935 (1988).
- [13] D. Pritchard, in *Electronic and Atomic Collisions: invited papers of the XIV International Conference on the Physics of Electronic and Atomic Collisions*, edited by D. Lorents, W. Meyerhof, and J. Peterson, page 593, Elsevier, New York.

- [14] S. Park et al., Opt. Comm. **192**, 57 (2001).
- [15] E. Rasel et al., Eur. Phys. J. D **7**, 311 (1999).
- [16] A. Aspect, N. Vansteenkiste, and R. Kaiser, Chem. Phys. **145**, 307 (1990).
- [17] J. Umezawa and F. Shimizu, Jpn. J. Appl. Phys. I **24**, 1655 (1985).
- [18] M. Joffe et al., J. Opt. Soc. Am. B **10**, 2257 (1993).
- [19] B. Sheehy et al., J. Opt. Soc. Am. B **6**, 2165 (1989).
- [20] B. Sheehy et al., Phys. Rev. Lett. **64**, 858 (1990).
- [21] B. Sheehy et al., Chem. Phys. **145**, 317 (1990).
- [22] F. Shimizu, K. Shimizu, and H. Takuma, Chem. Phys. **145**, 327 (1990).
- [23] R. Brown and R. Twiss, Proc. R. Soc. London A **242**, 300 (1957).
- [24] R. Brown and R. Twiss, Proc. R. Soc. London A **243**, 291 (1957).
- [25] H. T. Stoof et al., Phys. Rev. Lett. **76**, 10 (1996).
- [26] H. S. M. Houbiers, Phys. Rev. A **59**, 1556 (1999).
- [27] R. Combescot, Phys. Rev. Lett. **83**, 3766 (1999).
- [28] J. Maxwell, *A Treatise on Electricity and Magnetism*, Oxford, 1st edition, 1873.
- [29] P. Lebedev, Ann. Phys. (Leipzig) **6**, 433 (1901).
- [30] E. Nichols and G. Hull, Phys. Rev. **13**, 307 (1901).
- [31] E. Nichols and G. Hull, Phys. Rev. **17**, 26 (1903).
- [32] R. Frisch, Z. Phys. **86**, 42 (1933).
- [33] A. Ashkin, Phys. Rev. Lett. **25**, 1321 (1970).
- [34] T. Hänsch and A. Schawlow, Opt. Comm. **13**, 68 (1975).

- [35] D. Wineland and H. Dehmelt, Bull. Am. Phys. Soc. **20**, 637 (1975).
- [36] D. Wineland, R. Drullinger, and F. Walls, Phys. Rev. Lett. **40**, 1639 (1978).
- [37] W. Neuhauser et al., Phys. Rev. Lett. **41**, 233 (1978).
- [38] V. Balykin, V. Letokhov, and V. Mushin, JETP Lett. **29**, 560 (1979).
- [39] V. Balykin, Opt. Comm. **33**, 31 (1980).
- [40] W. Phillips and H. Metcalf, Phys. Rev. Lett. **48**, 596 (1982).
- [41] C. Heer, Rev. Sci. Instrum. **34**, 532 (1963).
- [42] V. Vladimirskeii, Sov. Phys. JETP **12**, 740 (1961).
- [43] V. Letokhov, JETP Lett. **7**, 272 (1968).
- [44] A. Migdall, J. Prodan, and W. Phillips, Phys. Rev. Lett. **54**, 2596 (1985).
- [45] V. Bagnato et al., Phys. Rev. Lett. **58**, 2194 (1987).
- [46] H. Hess, Phys. Rev. Lett. **59**, 672 (1987).
- [47] R. van Roijen et al., Phys. Rev. Lett. **61**, 931 (1988).
- [48] S. Chu et al., Phys. Rev. Lett. **57**, 314 (1986).
- [49] A. Ashkin, Phys. Rev. Lett. **40**, 729 (1978).
- [50] V. Minogin, Sov. J. Quantum Electron. **12**, 299 (1982).
- [51] V. Minogin and J. Javainen, Opt. Comm. **43**, 119 (1982).
- [52] A. Ashkin and J. Gordon, Opt. Lett. **8**, 511 (1983).
- [53] D. Pritchard et al., Phys. Rev. Lett. **57**, 310 (1986).
- [54] E. Raab et al., Phys. Rev. Lett. **59**, 2631 (1987).
- [55] W. Petrich et al., Phys. Rev. Lett. **74**, 3352 (1995).

- [56] M. Mewes et al., Phys. Rev. Lett. **77**, 416 (1996).
- [57] T. Esslinger, I. Bloch, and T. Hänsch, Phys. Rev. A **58** (1998).
- [58] T. Takekoshi and R. Knize, Opt. Lett. **21**, 77 (1996).
- [59] J. Weinstein and K. Libbrecht, Phys. Rev. A **52**, 4004 (1995).
- [60] O. Carnal and J. Mlynek, Phys. Rev. Lett. **66**, 2689 (1991).
- [61] D. Keith et al., Phys. Rev. Lett. **66**, 2693 (1991).
- [62] M. Kasevich and S. Chu, Phys. Rev. Lett. **67**, 181 (1991).
- [63] M. Kasevich and S. Chu, Appl. Phys. **B 54**, 321 (1992).
- [64] C. Oates, K. Vogel, and J. Hall, Phys. Rev. Lett. **76**, 2866 (1996).
- [65] J. McClelland et al., Science **262**, 877 (1993).
- [66] G. Timp et al., Phys. Rev. Lett. **69**, 1636 (1992).
- [67] R. Gupta et al., Appl. Phys. Lett. **67**, 1378 (1995).
- [68] K. Berggren et al., Science **269**, 1255 (1995).
- [69] W. Phillips, Rev. Mod. Phys. **70**, 721 (1998).
- [70] C. Adams and E. Riis, Prog. Quant. Electr. **21**, 1 (1997).
- [71] W. Phillips, J. Prodan, and H. Metcalf, J. Opt. Soc. Am. B **2**, 1751 (1985).
- [72] J. Gordon and A. Ashkin, Phys. Rev. A **21**, 1606 (1980).
- [73] S. Stenholm, Rev. Mod. Phys. **58**, 699 (1986).
- [74] H. Risken, *The Fokker-Planck equation: Methods of solution and application*, Springer, 2nd edition, 1992.
- [75] K. Mølmer, J. Phys. B: At. Mol. Opt. Phys. **27**, 1889 (1994).
- [76] D. Weiss et al., J. Opt. Soc. Am. B **6**, 2072 (1989).

- [77] F. Reif, *Fundamentals of Statistical and Thermal Physics*, McGraw-Hill Book Company, 1985.
- [78] P. Lett et al., J. Opt. Soc. Am. B **6**, 2084 (1989).
- [79] V. Letokhov, V. Minogin, and B. Pavlik, Sov. Phys. JETP **45**, 698 (1977).
- [80] W.D.Phillips and J. Prodan, in *Laser Cooled and Trapped Atoms*, edited by W. Phillips, volume 653, page 137, 1983.
- [81] J. Prodan and W. Phillips, Prog. Quantum Electron. **8**, 231 (1984).
- [82] W. Ertmer et al., Phys. Rev. Lett. **54**, 996 (1985).
- [83] W. Phillips and H. Metcalf, Phys. Rev. Lett. **48**, 596 (1982).
- [84] J. Prodan, W. Phillips, and H. Metcalf, Phys. Rev. Lett. **49**, 1149 (1982).
- [85] W.D.Phillips, J. Prodan, and H. Metcalf, in *Laser Spectroscopy VI*, edited by H. Weber and W. Luthy, page 162, Springer-Verlag, Berlin, 1983.
- [86] H. Metcalf and W. D. Phillips, At. Mol. Phys. **16**, 79 (1985).
- [87] M. Zhu, C. Oates, and J. Hall, Phys. Rev. Lett. **67**, 46 (1991).
- [88] B. P. Anderson and M. A. Kasevich, Phys. Rev. A **50**, R3581 (1994).
- [89] S. Chu et al., Phys. Rev. Lett. **55**, 48 (1985).
- [90] Z. Lin et al., Jp. J. Appl. Phys. **30**, L1324 (1991).
- [91] P. Gould, P. Lett, and W. Phillips, in *Laser Spectroscopy VIII*, edited by W. Persson and S. Svanberg, page 64, Springer-Verlag, Berlin, 1987.
- [92] P. Lett et al., Phys. Rev. Lett. **61**, 169 (1988).
- [93] P. Lett et al., J. Opt. Soc. Am. B **6**, 2084 (1989).
- [94] J. Dalibard et al., in *Proceeding of the 11th Conference on Atomic Physics*, edited by S. Haroche, J. Gay, and G. Grynberg, page 199, World Scientific, Singapore.

- [95] Y. Shevy et al., Phys. Rev. Lett. **62**, 1118 (1989).
- [96] C. Salomon et al., Europhys. Lett. **12**, 683 (1990).
- [97] M. Drewsen et al., Appl. Phys. B **59**, 283 (1994).
- [98] S. Chu et al., in *Proceedings of the 11th Conference on Atomic Physics*, edited by S. Haroche, J. Gay, and G. Grynberg, World Scientific, Singapore, 1989.
- [99] J. Dalibard and C. Cohen-Tannoudji, J. Opt. Soc. Am. B **6**, 2023 (1989).
- [100] A. Aspect et al., Phys. Rev. Lett. **61**, 826 (1988).
- [101] M. Kasevich and S. Schu, Phys. Rev. Lett. **69**, 1741 (1992).
- [102] U. Schünemann et al., Opt. Comm. **158**, 263 (1998).
- [103] J. Chen et al., Phys. Rev. Lett. **69**, 1344 (1992).
- [104] E. Majorana, Nuovo Cimento **9**, 43 (1932).
- [105] P. Giitinger, Zeit. Phys. **73**, 169 (1931).
- [106] J. Schwinger, Phys. Rev **51**, 648 (1937).
- [107] I. Rabi, Phys. Rev **51**, 652 (1937).
- [108] W. Wing, Prog. Quant. Electr. **8**, 181 (1984).
- [109] A. Steane, M. Chowdhury, and C. Foot, J. Opt. Soc. Am. B **9**, 2142 (1992).
- [110] J. Kawanaka et al., Phys. Rev. A **48**, R883 (1993).
- [111] D. Sesko, T. Walker, and C. Wieman, J. Opt. Soc. Am. B **8**, 946 (1991).
- [112] T. Walker, D. Sesko, and C. Wieman, Phys. Rev. Lett. **64**, 408 (1990).
- [113] C. Townsend et al., Phys. Rev. A **52**, 1423 (1995).
- [114] W. Ketterle et al., Phys. Rev. Lett. **70**, 2253 (1993).
- [115] C. Cooper et al., Europhys. Lett. **28**, 397 (1994).

- [116] D. Han et al., Phys. Rev. A **57**, R4114 (1998).
- [117] Y. Gott, M. Ioffe, and V. Tel'kovskii, Nuclear Fusion Supplement **3**, 1045 (1962).
- [118] D. Pritchard, Phys. Rev. Lett. **51**, 1336 (1983).
- [119] T. Bergeman, G. Erez, and H. Metcalf, Phys. Rev. A **35**, 1535 (1987).
- [120] W. Ketterle, D. Durfee, and D. Stamper-Kurn, in *Proceedings of the International School of Physics “Enrico Fermi”*, edited by M. Inguscio, S. Stringari, and C. Wieman, volume 40, page 67, IOS Press, Amsterdam, 1999.
- [121] D. Fried et al., Phys. Rev. Lett. **81**, 3811 (1998).
- [122] U. Ernst et al., Europhys. Lett. **41**, 1 (1998).
- [123] J. Söding et al., Phys. Rev. Lett. **80**, 1869 (1998).
- [124] L. Hau et al., Phys. Rev. A **58**, R54 (1998).
- [125] A. Ashkin, Phys. Rev. Lett. **24**, 156 (1970).
- [126] G. Shivashankar and A. Libchaber, Appl. Phys. Lett. **71**, 3727 (1997).
- [127] S. Henderson, S. Mitchell, and P. Barlett, Phys. Rev. E **64**, 061403 Part 1 (2001).
- [128] T. Takekoshi, J. Yeh, and R. Knize, Opt. Comm. **114**, 421 (1995).
- [129] R. Grimm, M. Weidemüller, and Y. Ovchinnikov, Adv. At. Mol. Opt. Phys. **42**, 95 (2000).
- [130] M. Barrett, J. Sauer, and M. Chapman, Phys. Rev. Lett. **87**, 010404 (2001).
- [131] W. Ketterle and N. V. Druten, Adv. At. Mol. Opt. Phys. **37**, 181 (1996).
- [132] H. Hess, Bull. Am. Phys. Soc. **30**, 854 (1985).
- [133] K. Davis et al., Phys. Rev. Lett. **74**, 5202 (1995).
- [134] J. Gerton et al., Phys. Rev. A **59**, 1514 (1999).

- [135] W. Ketterle and D. Pritchard, Phys. Rev. A **46**, 4051 (1992).
- [136] C. Monroe et al., Phys. Rev. Lett. **70**, 414 (1993).
- [137] V. Letokhov, V. Minogin, and B. Pavlik, Opt. Comm. **19**, 72 (1976).
- [138] V. Letokhov, M. Olshaniî, and Y. B. Ovchinnikov, Quantum Semiclass. Opt. **7**, 5 (1995).
- [139] C. Monroe et al., Phys. Rev. Lett. **65**, 1571 (1990).
- [140] K. Lindquist, M. Stephens, and C. Wieman, Phys. Rev. A **46**, 4082 (1992).
- [141] E. Abraham et al., Phys. Rev. A **53**, R3713 (1996).
- [142] Y. Kagan, A. Muryshev, and G. Shlyapnikov, Phys. Rev. Lett. **81**, 933 (1998).
- [143] A. Eleftheriou and K. Huang, Phys. Rev. A **61**, 043601 (2000).
- [144] C. Bradley, C. Sackett, and R. Hulet, Phys. Rev. Lett. **78**, 985 (1997).
- [145] C. Sackett, H. Stoof, and R. Hulet, Phys. Rev. Lett. **80**, 2031 (1998).
- [146] V. Balykin, V. Lethokov, and A. Sidorov, Pis'ma Zh. Eksp. Teor. Fiz. **40**, 251 (1984).
- [147] V. Balykin and A. Sidorov, Appl. Phys. B **42**, 51 (1987).
- [148] W. Rooijakkers, W. Hogervorst, and W. Vassen, Opt. Comm. **123**, 321 (1996).
- [149] J. Nellessen et al., J. Opt. Soc. Am. B **6**, 2149 (1989).
- [150] M. Prentiss, A. Cable, and N. Bigelow, J. Opt. Soc. Am. B **6**, 2155 (1989).
- [151] H. Goldstein, *Classical Mechanics*, Addison-Wesley, 2nd edition, 1981.
- [152] M. Mewes et al., Phys. Rev. A **61**, 011403 (1999).
- [153] F. Schreck et al., Phys. Rev. A **64**, 011402 (2001).
- [154] B. Anderson and M. Kasevich, Phys. Rev. A **59**, R938 (1999).
- [155] C. Pethick and H. Smith, *Bose-Einstein Condensation in Dilute Gases*, Cambridge Univ. Pres, 1st edition, 2002.